

Trond Andresen

Mathematical modeling of CO₂ based heat pumping systems

New developments for simulation tools to aid the
design of systems for non-residential buildings

Thesis for the degree of Philosophiae Doctor

Trondheim, September 2009

Norwegian University of Science and Technology
Faculty of Engineering Science and Technology
Department of Energy and Process Engineering



Norwegian University of
Science and Technology

NTNU

Norwegian University of Science and Technology

Thesis for the degree of Philosophiae Doctor

Faculty of Engineering Science and Technology
Department of Energy and Process Engineering

© Trond Andresen

ISBN 978-82-471-1756-9 (printed ver.)
ISBN 978-82-471-1757-6 (electronic ver.)
ISSN 1503-8181

Doctoral theses at NTNU, 2009:180

Printed by NTNU-trykk

ABSTRACT

CO₂ based heat pumping systems have in recent years received considerable focus world-wide. Now, attention has been turned toward heating and cooling of larger, non-residential buildings. With plate heat exchanger's now becoming available for CO₂, this natural refrigerant becomes a real alternative for larger applications, considering both efficiency and economy.

However, research and design tools have not been readily available to fully design optimized systems for larger buildings. Simulation-aided design is particularly valuable for CO₂ systems, as existing conventional systems cannot be used with good results. However, the special properties of CO₂ both increase the need for discretization of component models, and require more complex fundamental equations for thermophysical properties. Because of this, circuit simulations with CO₂ are considerably slower compared to simulation of conventional refrigerant systems, to the extent that it is limiting the ability to design optimal CO₂ systems.

In this work, an existing circuit simulation tool, CSIM, has been extended and modified to be suited for efficient design and optimization of heat pumping systems with complex-configuration plate heat exchangers. The modification of CSIM performed in this work includes a versatile and configurable plate heat exchanger model, and a general method to handle more complex fluid stream configurations. The new model can describe the local behavior in individual, parallel flowing, plate channels, including asymmetric heat transfer, pressure drop and mass flow distribution.

Implemented into CSIM, this model can be used to predict the system performance impact due to local behavior in the component. A demonstration simulation case was carried out, comparing the predicted system performance using a simple uniform model, and the new advanced plate heat exchanger model. The results showed that the additional information in the new plate heat exchanger model could have a large impact on the predicted system performance.

A profiling of CSIM simulations on six test cases revealed that approximately 99.85% of the time was consumed calculating thermophysical properties for CO₂. To increase the simulation performance, a new, considerably faster thermophysical library (FTL) for CO₂ has been developed and imple-

mented. FTL is based on linear interpolation in lookup tables containing pre-calculated values of CO₂ properties. Through careful design of extracting functions and table grid, even the highly non-linear properties around the critical point was described with acceptable accuracy.

A test suite was performed, focusing on the accuracy and calculation speed compared to the reference equation of state. Overall, simulation results showed only very minuscule differences, but the simulation time was on average reduced from 945 seconds to 2.2 seconds, a reduction of 99.77%. This considerable reduction in simulation time will facilitate the more advanced component and system models needed to optimize CO₂ system design.

PREFACE

This thesis is submitted in partial fulfillment of the requirements for the academic title *philosophiae doctor* at the Norwegian University of Science and Technology (NTNU). This work was carried out at the Department of Energy and Process Engineering, NTNU, Trondheim, supervised by Professor dr.ing Arne M. Bredesen and co-supervised by dr.ing Geir Skaugen (SINTEF) and dr.ing Kjell Kolsaker (NTNU).

The work has been financed by NTNU through the strategic research area *Energy and Petroleum - Resources and Environment*, and by SINTEF Energy Research.

My colleagues at NTNU/SINTEF all contribute to an interesting and inspirational work atmosphere, but there are a few that deserve special mention for their involvement in this PhD work:

- I would like to thank all my supervisors for their help and encouragement. Geir Skaugen in particular deserves special thanks for introducing me to modeling of heat pumping systems in the first place, in addition to an awe-inspiring technical and thermodynamical insight, guidance and fruitful discussions for the entire duration of this work.
- Thanks to Petter Neksa for his contributions on many levels from the very beginning to the very end.
- Thanks to Jørn Stene for his contagious enthusiasm and direct involvement in the completion of this thesis.
- I am also very grateful to Inge Gran, the SINTEF research director at the Department of Energy Processes, and Professor Trygve M. Eikevik, for providing the financing of parts of this work.
- And finally those closest to me; Camilla, Tobias, Maja and Sofie. Thanks for your endless love and support. Even though you may not always appreciate long rants on selected issues of numerical thermodynamics, you're still the best!

TABLE OF CONTENTS

Abstract	iii
Preface	v
Table of Contents	vii
List of Symbols and Abbreviations	xiii
Definitions	xvii
1. Introduction	1
1.1 Motivation	1
1.1.1 Background	1
1.1.2 CO ₂ as refrigerant for non-residential building systems	2
1.1.3 Plate heat exchangers for CO ₂	3
1.1.4 Improving calculation of thermophysical properties for CO ₂	3
1.2 Aims	4
1.3 Structure of the Thesis	5
2. Simulation tools for heat pumping applications	7
2.1 Background and status	7
2.1.1 Introduction	7

2.1.2	Commercial cycle simulation software	8
2.1.3	In-house simulation tools	9
2.2	Calculation of thermophysical properties in simulation tools	10
2.2.1	Introduction	10
2.2.2	Equations of state for CO ₂	11
2.2.3	Possible methods for improving calculation speed of thermophysical properties	11
2.3	CSIM - Circuit Simulation Tool	12
2.3.1	Introduction	12
2.3.2	Description	13
2.3.3	The NLPQL solver	15
2.3.4	Current thermophysical libraries for CO ₂ in CSIM	16
2.3.5	CSIM data flow to thermophysical libraries	18
2.3.6	Profiling CSIM	20
3.	Fast Thermophysical Library (FTL)	23
3.1	Introduction	23
3.2	Thermophysical property calculation based on linear interpolation	24
3.2.1	Overview	24
3.2.2	Systematical error from linear interpolation	26
3.2.3	Table size	27
3.2.4	Reading from RAM and cache	28
3.3	FTL features and specifications	28
3.3.1	Fast lookup table design requirements	28

3.3.2	Included property functions in FTL	29
3.3.3	Global and native functions	29
3.4	Description of the lookup tables in FTL	32
3.4.1	Thermophysical property base	32
3.4.2	Thermodynamic relations based on Gibb's free Energy	32
3.4.3	Three T-p tables with adapted resolution and coverage	34
3.4.4	Saturation data table	37
3.4.5	Additional data tables	38
3.4.6	Summary of FTL tables	40
3.5	FTL data extraction	41
3.5.1	Calculating table indexes	41
3.5.2	Ensuring valid data points	41
3.6	FTL test suite setup	43
3.6.1	Overview	43
3.6.2	Test computer setup	44
3.6.3	Logging consumed CPU and clock time	44
3.6.4	Saturated property data	45
3.6.5	Validation methods - Individual property function ac- curacy	45
3.6.6	Validation methods - CSIM function profile test suite .	46
3.6.7	Validation method - Simulation test suite	47
3.7	Results	48
3.7.1	Accuracy for saturated gas and liquid property functions	48
3.7.2	Accuracy for continuous region	50

3.7.3	CSIM function profile test suite	59
3.7.4	CSIM simulation test suite	60
3.7.5	Intel and GNU compiler comparison	61
4.	Advanced Plate heat Exchanger Model (APEM)	65
4.1	Background	65
4.1.1	Introduction	65
4.1.2	Plate heat exchanger design	65
4.1.3	Modeling of plate heat exchangers	68
4.2	PHE component model for CO ₂ system simulation	68
4.2.1	Introduction	68
4.2.2	Describing local behavior in channels	69
4.2.3	APEM design criteria	70
4.2.4	Main physical mechanisms	71
4.2.5	Other mechanisms	71
4.3	Mathematical modeling of the plate heat exchanger	73
4.3.1	Overview	73
4.3.2	Variable description	73
4.3.3	Description and model in C	76
4.4	Correlations for pressure drop and heat transfer coefficients	78
4.4.1	Introduction	78
4.4.2	Consistency over phase boundaries	79
4.5	Changes in system calculation and solving	80
4.5.1	Overview	80

4.5.2	Original system solving	80
4.5.3	New system solving	82
4.6	Example-circuit simulation with advanced plate heat exchanger model	83
4.6.1	Overview	83
4.6.2	Test case description	84
4.6.3	Selected correlations for heat transfer coefficient and pressure drop	85
4.7	Results from simulation of demonstration case	88
5.	Discussion	97
5.1	Main findings from the FTL test suite	97
5.1.1	Introduction	97
5.1.2	Analysis of systematic error	97
5.1.3	Accuracy - saturated property data	99
5.1.4	Accuracy - continuous region	101
5.1.5	Impact of near-critical deviation on simulation results .	102
5.1.6	Accuracy - simulation results	104
5.1.7	Calculation performance	105
5.1.8	Usability and versatility	105
5.2	Main findings from simulation with new heat exchanger model	106
5.2.1	Introduction	106
5.2.2	Asymmetric heat transfer	107
5.2.3	Distribution of mass flow in parallel channels	107
5.2.4	Simulation results	108

5.2.5	Usability of model	109
6.	Conclusions and suggestions for further work	111
6.1	Conclusions	111
6.1.1	The Fast Thermophysical Library (FTL)	111
6.1.2	Conclusions - Plate heat exchanger model for complex configurations	112
6.2	Suggestions for further work	113
6.2.1	The Fast Thermophysical Library (FTL)	113
6.2.2	Plate heat exchanger model	113
	References	115
	APPENDICES	118
	A. Results from CSIM function profile performance test	A-1
	B. Description of CSIM cases used for validation of lookup table implementation	B-1
	C. Key simulation result values from CSIM test suite	C-1

LIST OF SYMBOLS AND ABBREVIATIONS

Symbol	Description	Unit
A	Area	m^2
AC	Air-conditioning	
AMTD	Arithmetic Mean Temperature Difference	K
C	Constant	
c_p	Specific heat capacity at constant pressure	$J \cdot kg^{-1} \cdot K^{-1}$
c_v	Specific heat capacity at constant volume	$J \cdot kg^{-1} \cdot K^{-1}$
CFD	Computational Fluid Dynamics	
COP	Coefficient of performance	-
d	Diameter	m
d	Differential operator	-
D	Absolute deviation	
$\frac{dp}{dL}$	Pressure gradient	$Pa \cdot m^{-1}$
DLL	Dynamic Link Library	
∂	Partial differential	-
f	Friction factor	-
f_{obj}	Objective function	
G	Mass Flux	$kg \cdot m^{-2} \cdot s^{-1}$
GUI	Graphical User Interface	
g	Gibb's function	$J \cdot kg^{-1}$
g_T	g 's partial differential of T	$J \cdot kg^{-1} \cdot K^{-1}$
g_{TT}	g 's second order partial differential of T	$J \cdot kg^{-1} \cdot K^{-2}$
g_{TP}	g 's partial differential of T and p	$m^3 \cdot kg^{-1} \cdot K^{-1}$
g_P	g 's partial differential of p	$m^3 \cdot kg^{-1}$
g_{PP}	g 's second order partial differential of p	$m^5 \cdot kg^{-1} \cdot N^{-1}$
h	Specific enthalpy	$J \cdot kg^{-1}$

L	Length	m
\dot{m}	Mass flow	$kg \cdot s^{-1}$
n	Number	-
p	Pressure	Pa
q	Heat flux	$W \cdot m^{-2}$
\dot{Q}	Heat flow, heat load, heating/cooling capacity	W
R	Thermal resistance	$m^2 \cdot K \cdot W^{-1}$
s	Specific entropy	$J \cdot kg^{-1} \cdot K^{-1}$
subhx	sub heat exchanger, see definition	-
T	Temperature	°C
TL	Thermophysical Library	
U	Heat transfer coefficient	$W \cdot m^{-2} \cdot K^{-1}$
v	Specific volume	$m^3 \cdot kg^{-1}$
\dot{V}	Swept volume (Compressor)	$m^3 \cdot s^{-1}$
w	Speed of sound	$m \cdot s^{-1}$
\dot{W}	Work	W
x	Vapor quality	-

Greek Letters

α	Thermal diffusivity	$m^2 \cdot s^{-1}$
β	Surface enhancement factor	-
Δ	Difference	-
η	Efficiency	-
κ	Compressibility	$m^2 \cdot N^{-1}$
λ	Thermal conductivity	$W \cdot m^{-1} \cdot K^{-1}$
μ	Dynamic viscosity	$Pa \cdot s$
ρ	Density	$kg \cdot m^{-3}$
σ	Surface tension	$N \cdot m^{-1}$
ϕ	Corrugation angle	°

Dimensionless Numbers

Nu	Nusselt's number	-
Pr	Prandtl's number	-
Re	Reynold's number	-

Subscripts

0	Evaporator state
Aux	Auxiliary, with auxiliary functions
b	Bulk
co	Compressor
con	Condenser
comb	Combined
crit	Critical
ev	Evaporator
eq	Equivalent
fg	Liquid to gas
g	Vapor phase
gc	Gas Cooler
H	Heating
hyd	Hydraulic
i	Integer number, notation for subhx number
is	Isentropic
j	Integer number, notation for channel number
l	Left side
l	Liquid phase
pitch	Plate pitch
r	Right side
red	Reduced

refr	Refrigerant
sec	Secondary fluid
vol	Volumetric
w	Wall

Superscripts

'	Saturated liquid
''	Saturated gas

DEFINITIONS

Definitions of some phrases frequently used in this work:

APEM - Advance plate heat exchanger model; a new heat exchanger model for circuit simulations capable of calculating local behavior in individual plate channels.

Channel - In context of plate heat exchangers, this phrase describes the flow area between two plates.

Continuous region - The region of temperature and pressure covered by FTL, excluding the two-phase area (one-dimensional in T-p span). It covers liquid, vapor and supercritical areas.

Data point - In the context of interpolation, this refers to one of the 4 (or in some cases 3) table entries used as basis for interpolation.

Explicit functions - In the context of the described lookup tables, this refers to state property functions explicit in T and p ($f(T, p)$), as the main tables are based on Gibb's free energy.

FTL - Fast thermophysical library; an implementation of transport data and a equation of state that calculates considerably faster than the conventional method.

Implicit functions - In the context of the described lookup tables, this refers to state property functions *not* explicit in T and p. Common implicit functions used in this work: $f(h, p)$, $f(s, p)$ and $f(T, h)$

Interpolant - Result of an interpolation.

High-side pressure - In a heat pumping circuit, this is the pressure at the inlet of the expansion valve.

Near-critical - The T-p region in close vicinity to the critical point. Typically $T_c \pm 3^\circ\text{C}$ and $p_c \pm 5$ bar.

Profiling - An analysis of a piece of software (program), typically used to obtain information of frequency and duration of individual procedure calls in specific software operations, e.g a single simulation run. It can be used as basis for further improvement of the software.

Reverse lookup - A method for calculation inverse of implicit functions without resorting to solving. If the relevant function property is consistently increasing or decreasing with respect to either T or p, it is possible to search along that property in the table, and extract the missing T, p or other desired property by interpolation.

Subhx - A heat exchanger can be discretized into smaller parts for simulation; subhx's. It is on this level that local HTC and $\frac{\partial p}{\partial L}$ are calculated, and heat and mass balances performed.

Thermophysical library (TL) - A complete set of functions for calculating the states and transport properties for a fluid.

TL_{Angus} - A thermophysical library based on the equation of state by Angus et. al. Described in chapter 2.3.4.

TL_{Span} - A thermophysical library based on the equation of state by Span and Wagner. Described in chapter 2.3.4.

1. INTRODUCTION

1.1 Motivation

1.1.1 Background

The revival of CO₂ as a working fluid in refrigeration, air-conditioning and heat pump systems was sparked by the Montreal protocol (UNEP, 1987), a treaty to phase out the production of ozone-depleting substances from January 1989. The most common refrigerants at the time had strong ozone-depleting potential. The 2006 assessment report of the refrigeration, air conditioning and heat pumps technical options committee, described the development of the Montreal protocol in more detail (UNEP, 2006).

Ten years later, the Kyoto-protocol (UNFCCC, 1997) was approved, aimed at reducing the emission of greenhouse gases, directly affecting a new range of refrigerants. Searching for environmentally sustainable alternatives, Lorentzen (1994) was of the first to identify CO₂'s potential as an efficient working fluid for modern applications. Pearson (2005) describes the history and revival of CO₂ as refrigerant.

CO₂ used in refrigeration is a waste product from industrial processes, and does therefore not contribute negatively to neither deterioration of the ozone layer nor the greenhouse effect. In addition to its environmental qualities, CO₂ can also be a highly efficient working fluid for many applications. However, CO₂ is very different from other working fluids due to its low critical temperature and high system pressure. Because of these differences, CO₂ needs specially made components as well as different system configurations and control strategies.

CO₂ based heat pumping systems have in recent years received considerable focus world-wide. Consequently, the range of available components is increasing, and the performance is steadily improving as the knowledge and technology improves. Neksa (2002) gave a thorough introduction to the fundamentals of CO₂ as a working fluid, and a range of possible applications.

The first successful commercial product was a heat pump for hot water heating, introduced in 2001 by Denso¹. Today, several manufacturers produce similar models, almost all for the Asian market. With steadily increasing sales for each year, 410,000 of these units were sold in 2007 (R744.com²).

CO₂ for use in mobile air conditioning has also received much focus the last years, but the new technology has so far not caught on among all car-manufacturers. This appears to change soon, as the German Association of the Automotive Industry (VDA) has appointed CO₂ the refrigerant of choice in the next generation of car air conditioners³.

CO₂ is also used in a number of refrigeration applications, particularly in supermarkets. One of the first installations of single-stage CO₂ systems for this application was installed in Italy, and has been in operations since January 2003 (Giroto et al., 2004). In Denmark, a new legislation banning new HFC systems with more than 10 kg of refrigerant (Danish Ministry of the Environment) [2002] went into effect January 1st 2007. Now, CO₂ is the most common refrigerant in new Danish supermarkets, with an estimated 80-100 plants built so far. Other countries also have an increasing number of CO₂ refrigeration systems; Sweden with over 50, and around 15-20 in Norway. This trend is spreading across the world, with installations made in Switzerland⁴, England⁵ and Australia⁶ to name a few. Kauffeld et al. (2008) gave a description of typical solutions and an analysis of environmental impact of commercial refrigeration systems.

1.1.2 CO₂ as refrigerant for non-residential building systems

Now, attention has been turned toward heating and cooling of larger, non-residential buildings. These buildings typically have a high ratio of ventilation air heating. Heating ventilation air is the key to obtain good performance for CO₂ systems, as a high COP requires low refrigerant temperature before the expansion valve. Even with heat recovery from exhaust air, ventilation intake air is usually colder than the return temperature from any hydronic

¹ denso.co.jp

² <http://www.r744.com/articles/2008-09-15-global-heat-pump-market-eco-cute-update.php>

³ <http://www.vda.de/en/meldungen/news/20081020.html>

⁴ <http://www.r744.com/article.view.php?Id=688>

⁵ <http://www.r744.com/articles/2009-01-14-uk-most-energy-efficient-store-uses-co2-refrigeration.php>

⁶ <http://www.r744.com/articles/2008-02-22-industry-visits-australia-first-co2-only-supermarket.php>

system. Therefore, the efficiency of the heat pumping system is greatly affected by the ratio of heating load of ventilation vs. hydronic system. Stene et al. (2007) described concepts for heat pumps in non-residential buildings, with focus on the design of the secondary circuit and serial connection of heat loads at diminishing temperature levels.

However, research and design tools have not been readily available to fully design optimized systems for larger buildings. In this work, an existing circuit simulation tool has been extended and modified to be suited for efficient design and optimization of heat pumping systems with complex-configuration plate heat exchangers.

1.1.3 Plate heat exchangers for CO₂

The plate heat exchanger (PHE) is the first really compact liquid-to-CO₂ heat exchanger type. So far, heat exchangers of the co-axial (tube-in-tube) has been used for these applications. While these heat exchangers are well matched for the heat transfer characteristics of CO₂, they are impractical for larger capacities due to their inherit low compactness and high material costs. With PHE's now becoming available⁷⁸⁹ for CO₂, this natural refrigerant becomes a real alternative for larger applications, considering both efficiency and economy.

However, in order to design efficient systems, there is a need for mathematical models to correctly represent both component and system behavior. The in-house circuit simulation tool developed at NTNU/SINTEF, CSIM (Skaugen et al., 2002), has been used as framework.

The modification of CSIM performed in this work includes a versatile and configurable plate heat exchanger model, and a general method to handle more complex fluid stream configurations.

1.1.4 Improving calculation of thermophysical properties for CO₂

Simulation of CO₂-based heat pumping cycles using the reference equation of state by Span & Wagner (1996) is characterized by high calculation loads,

⁷ <http://www.swep.net/index.php?tpl=news&lang=en&id=306&newsid=1568>

⁸ <http://www.r744.com/articles/2009-03-30-kaori-displays-brazed-plate-heat-exchanger.php>

⁹ <http://www.r744.com/articles/2009-01-19-alfa-laval-adds-series-of-r744-brazed-heat-exchangers.php>

resulting in long simulation times. The high calculation load is indirectly caused by CO₂'s thermophysical properties. Under normal working conditions, a CO₂ heat pump will operate in proximity of the critical point, with large local variations in thermophysical properties. To accurately represent the abrupt variations, the equation of state is more complex than is needed for most other refrigerants. In addition, the local variation of properties requires a high level of discretization in the heat exchangers.

More complex component models, e.g. advanced heat exchanger configurations, will increase the number of variables, and thus the calculation load even further. It is also known that 99.7% of the simulation time is spent calculating thermophysical properties (see chapter 2.3.6) when using the reference equation of state for CO₂. It would therefore be very beneficial if the calculation load of thermophysical properties could be reduced.

The current high calculations times are limiting the ability to efficiently simulate CO₂ circuits using advanced component models with a high level of discretization. However, this is exactly what is required in order to understand and predict the behavior of CO₂ circuits. For example, the use of CO₂ as refrigerant in a HVAC central for non-residential buildings is expected to be a good alternative to conventional refrigerant systems. However, conventional system designs cannot be used with good results.

System configuration and components must be optimized to utilize the specific characteristics of CO₂ in order to obtain competitive, high-efficiency solutions. Better component models and shorter simulation times can contribute to obtaining this goal. Now, when high-pressure plate-type heat exchangers begin to emerge to the market, it's for the first time possible to build compact and efficient CO₂-systems for this application that may be a real alternative for both retrofit and new installations.

1.2 Aims

This work describes the development and implementation of two new contributions for CO₂ circuit simulation and optimization, in order to approach heat pumping systems for non-residential buildings.

The first part aims to identify a method to greatly increase calculation speeds of thermophysical properties for CO₂. This is proposed achieved by replacing a computational demanding equation of state and transport data functions by well-designed lookup table interpolation.

This approach may have a wide range of use, even if it has only been demonstrated for CO₂ in this work. Converting to another refrigerant would only require minor changes. This new, faster implementation of thermodynamic functions will be adapted specifically to one application, the in-house program CSIM, with respect to usability, coverage area of property functions, and accuracy. The framework of the implementation also allows rapid and convenient adaptation of accuracy and coverage area to fit other applications.

The second part aims at developing and implementing a flexible and configurable plate heat exchanger model. The new plate heat exchanger model should be highly configurable, allowing complex stream and plate configurations. The model will be implemented into the in-house simulation and optimization tool, CSIM. This will allow investigations of different plate heat exchanger geometries in respect to optimal system performance, and representative comparisons between systems with different refrigerants.

1.3 Structure of the Thesis

Chapter 2: Brief introduction to characteristics of circuit simulation tools and the calculation of thermophysical properties for CO₂. CSIM is described in more detail, as it is used as a framework for implementing the new plate heat exchanger model and the fast thermophysical library.

Chapter 3: Description of the design, implementation and results of "Fast Thermophysical Library (FTL)".

Chapter 4: Description of the design, implementation and test results of a highly configurable plate heat exchanger model for circuit simulation.

Chapter 5: Analysis and discussion of the results.

Chapter 6: Conclusions and suggestions for further work.

Some material, as more detailed or extensive results and further description of test setup, are included in appendices for reference.

Appendix A: Complete results from the CSIM function profile performance test.

Appendix B: A description of the individual test cases used in the comparison of simulation results.

Appendix C: A larger set of simulation output from the comparison of simulation results.

1. INTRODUCTION

2. SIMULATION TOOLS FOR HEAT PUMPING APPLICATIONS

2.1 Background and status

2.1.1 Introduction

Simulation is very important for research and development of CO₂ heat pumping systems. It allows investigation of the behavior and performance of components and cycles, including optimization of hardware geometry and running parameters. Performing the same tasks exclusively with laboratory measurements will demand almost endless time and resources. Particularly is this the case when it comes to system optimization with many free variables, where simulation tools are essential.

CO₂ is still considered as a "new" refrigerant in modern applications, and requires different systems to realize its full potential. Simulation models that accurately predict the performance of conventional refrigerant systems, may fail completely for CO₂ systems.

Computer simulation with mathematical modeling is a very broad term, including anything from very simple spreadsheet calculations to large network-based groups of computers performing detailed analysis down to a molecular level. An important factor for simulation of heat pumping systems is to include enough details in the models to capture all relevant physical mechanisms present, without making the numerical problem too large to solve efficiently. Identifying the correct level of model detail can be a difficult task. Ding (2007) gave a review of common simulation techniques for refrigeration systems. Winkler et al. (2008) reviewed different algorithms for describing and simulating multi-component systems with respect to computational efficiency and convergence rate.

Simulation tools can be categorized as either "performance-based" or "hardware-based". Performance based simulation tools are suitable for designing complex processes, using more or less generic component models. Typically, a fixed UA-value, LMTD or temperature approach is input for specifying a heat exchanger, in contrast to specifying a real heat exchanger with its full configuration of surfaces and fluid flow patterns.

Hardware-based simulation tools use the geometry of components to calculate the performance. This may include interpretation of configuration parameters and discretization of heat exchangers to calculate local values for heat transfer and pressure drop gradients.

When CO₂ is used as the refrigerant, hardware-based tools should be preferred in order to account for the large span in fluid properties and other CO₂ cycle characteristics. The characteristics of CO₂ as refrigerant has been described and discussed at many occasions, for instance by Neksa et al. (1998), Rieberer (1999) and Cavallini (2004).

2.1.2 Commercial cycle simulation software

For cycle design and research using simulation tools, there are typically two options; acquiring a commercial tool, or building a custom, in-house tool. Important differences between the two will be discussed in the following sections.

There exist a wide range of commercial simulation tools for heat pumping cycles and other process systems.

Pro/II¹ is a steady-state, process design tool, usable for a range of different processes. Typical use is the design of new processes and comparison of different configurations. PRO/II can be categorized as a performance-based simulation tool, and does usually not consider detailed behavior of for instance heat exchangers. This also implies that user-defined heat exchanger configurations are not supported without custom additional software.

FrigoSim² is another cycle simulation tool, specifically aimed at heat pumps and refrigeration plants. FrigoSim includes semi-hardware based models of heat exchangers with generalized configurations and correlations.

While Pro/II and FrigoSim both may be excellent tools for many uses, they will often fail to sufficiently replicate the performance of a hardware-specific cycle. Some commercial cycle simulation software will accept user-made component models which can be very useful in this respect. This may still not be a satisfactory solution, as user-made components must be solved iteratively outside the main system flowsheet. This also impacts convergence of problems, and may cause unreliable solutions to optimizations. Optimization problems should preferably be based on simultaneous solving of all flowsheet

¹ <http://ips.invensys.com/en/products/processdesign/Pages/Pro-II-P004.aspx>

² <http://www.frigosoft.no/frigosim>

variables, including component models. There are great benefits of having full access and modification possibilities of the simulation tool.

Typical drawbacks of commercial simulation software of this type can be linked to lack of control or lack of configurability and customizability. *Control* in this case can be defined as the depth of information about models, correlations, numerics and results. Each of these can be crucial in order to understand the physical behavior of a cycle. The less information available about methods and conditions, the less value does the results have.

Configurability is the options the user has for defining components and the system, and *customizability* is the ability the user has to modify the software by adjusting or adding models. In general, the configurability is limited to a fixed set of features, for instance heat exchanger types, configurations, discretization and calculation method, and the customizability is mostly non-existent.

2.1.3 In-house simulation tools

When commercial software for a specific task is not available, or when an extra level of control or understanding is needed, developing an in-house simulation tool may be the next step. Even quite simple spreadsheet models may yield better understanding than limited output from a commercial software.

Having full control over a simulation tool gives important advantages. In-house simulation tools enable full control over the physical and numerical mechanisms, as well as the ability to add or modify correlations, equations and models when needed. The possibility to use a debugger to follow the numerics and calculation can also be very valuable. This level of control does not exist in commercial software. However, this usually also increases the user-threshold, as more of the tasks of carefully selecting simulation parameters and correlations are left to the user.

For design and research of new components and systems, in-house tools are quite common. In recent years, several research- and academic institutions all over the world have built their own simulation models for CO₂ heat pumping cycles.

Pfafferott & Schmitz (2004) described a transient, hardware-based cycle model with MPE-tubed heat exchangers based on the open programming language *Modelica*³. As an object-oriented language, the inherent modular-

³ www.modelica.org

ity is very well suited for designing e.g. heat exchangers. Further more, all sub-models or modules can be highly encapsulated, allowing convenient implementation of an arbitrary number of cycle designs.

Li & Groll (2005) investigated the theoretical potential for COP improvement in refrigeration cycles by using an ejector to reduce expansion losses. To aid this investigation, a cycle model of the refrigeration ejector-expansion cycle was made, however with very simplified component models.

Sarkar et al. (2006) presented a hardware-based cycle simulation tool with tube-in-tube, counterflow heat exchangers. This tool has the ability to optimize for maximum COP, and solves the equation set by an iterative, Newton-Raphson method.

Richardson (2006) describes in detail the design and development of *VapCyc*, a component-based platform for steady-state cycle simulations. *VapCyc* has the ability to simulate more complex cycles with several heat exchangers in series or parallel, all though limited to air-to-refrigerant heat exchangers. The heat exchanger models use geometry as input, and can be discretized for calculation of local heat transfer coefficient and pressure drop. *VapCyc* has some advanced simulation features, for example calculation of charge inventory, but lacks direct optimization abilities.

2.2 Calculation of thermophysical properties in simulation tools

2.2.1 Introduction

Properties of traditional refrigerants are often fitted to the Martin & Hou (1955) equation of state, which has relatively few parameters. Because of the characteristic properties of CO_2 , heat pumping cycles will often operate in relative proximity to the critical point. In this region, thermophysical properties have large and abrupt variations in value, which can not be correlated well with simple expressions. As a result, accurate equations of state and transport data correlations are quite complex compared to similar functions for other refrigerants, and constitute considerable calculation loads in cycle simulations.

2.2.2 Equations of state for CO₂

While there exist several equations of state for CO₂, there are two in particular that are commonly used for this application:

- The equation of state by Span & Wagner (1996) is widely accepted as the reference equation of state for CO₂, and covers the fluid region from the triple point up to approximately 800°C and 8000 bar. Special focus was given the description of the critical region to ensure good accuracy. This equation of state is also used in the widely referenced thermophysical library Refprop (Lemmon et al., 2007).
- The older EOS by Angus et al. (1976) is also still in use, with the additions from Pitzer & Schreiber (1988). Pitzer re-fitted the coefficients from Angus and added exponential terms for an explicit formulation, avoiding iteration and reducing calculation load. The Pitzer formulation is less accurate further away from the critical region, so a combining function for the two expressions has been used in this work.

Both Span and Angus describe fundamental equations explicit in T and ρ (temperature and density), while the in-house simulation tool CSIM mostly use functions on the form of $f(T, p)$ and $f(h, p)$. This will add to high calculation loads, as the software needs to apply numerical solving routines to calculate the requested properties.

2.2.3 Possible methods for improving calculation speed of thermophysical properties

There are several methods for reducing the calculation load of a CO₂ equation of state. Reducing the complexity of the expressions in the fundamental equation is a common approach, used in many different variants. Pitzer's adaptation of Angus' equation of state described above is one example.

Klaus & van Ness (1967) described a spline fit technique for thermodynamic data. Although before the age of cycle simulations at the level discussed in this PhD work, the described principle is still relevant.

Cleland (1986) proposed curve-fitted equations for rapid calculation of some commonly used thermodynamic properties in a specific operating region. The equations can describe the properties of several refrigerants by using specific coefficient sets for each refrigerant.

Svensson (1994) described a method for making polynomial curve-fits of the main functions and their implicits for a specific operating region. This method can be adaptive, where new polynomial coefficients are generated automatically outside the original operating region.

Ding et al. (2005) described an implicit curve-fitting method for faster calculation of properties for R22 and R407C. This work describes a method where low-order explicit polynomials are generated, and then analytically solved to form explicit equations for thermodynamic properties.

Corbern et al. (2005) presented a method for generating lookup tables and using interpolation to calculate thermodynamic properties. Corberan et al. demonstrated this method for several conventional refrigerants, and achieved considerably reduced calculation time and acceptable accuracy. The interpolation method was compared to property calculation using NIST Refprop v7.0. For a set of 1000 property function calls, the calculation speed increased by a factor ranging from 30 for R22 to a factor of 750 for R407C, while the deviation from Refprop was for the most part kept below 1%.

A well designed lookup table implementation has the advantage of being reasonably simple to implement, very fast to calculate, and is suited for quick modifications to fit other applications and fluid coverage areas. The lookup table can easily be generated to be explicit for any two independent properties, regardless of the equation of state it is generated from.

There can also be a considerable performance leap between different code compilers. This is demonstrated for CSIM in chapter 3.7.5, comparing commercial Intel C and Fortran compilers to the open-source GNU C and Fortran compilers.

2.3 CSIM - Circuit Simulation Tool

2.3.1 Introduction

An in-house developed simulation and optimization suite, CSIM (Skaugen et al., 2002), has the inherent benefits of having the models and mechanics specified in the exact way as desired, while other factors as convergence and stability may be weighted against accuracy and user proficiency requirements. While CSIM requires a relatively high user-threshold to configure flowsheet parameters and initial values, it can optimize complex cases with over 500

system and component (solved) variables and 5-10 degrees of freedom⁴.

The maximum number of variables CSIM can effectively handle is limited by the capabilities of the solver, initial values, level of variable-to-variable dependence, constraint scaling and acceptable simulation time.

In a simulation, the number of variables is identical to the number of describing equations for the flowsheet and components. These equations are programmed in the form of *equality constraints*, meaning each equation should equal zero when the system is in balance. Typical equality constraints are mass and heat balances of heat exchanger elements.

The other form of constraints are *inequality constraints*. These expressions must always be larger than zero, and are used for ensuring numerical or physical behavior, as well as boundary conditions for free optimization variables. Inequality constraints are used to prevent fluid temperature crossing in heat exchangers, and to define e.g. maximum high-side pressure or compressor discharge temperature in an optimization.

Optimizations allow additional free variables, so the total number of variables exceeds the number of equality constraints. The problem solution is then found by minimizing or maximizing an *objective function* in addition to solving all constraints. The most common objective functions for cycle simulations are COP (heating, cooling or combined) and heating and cooling capacity, but anything that can be expressed as a function of the included variables can be used.

2.3.2 Description

CSIM is an advanced, steady-state, cycle simulation and optimization tool developed in-house by the refrigeration technology group at NTNU/SINTEF over some 15 years. CSIM can simulate and optimize a wide range of cycle configurations with detailed component models, from small residential split-type air conditioners to industrial sized heat pump plants. It was specifically designed for analyzing the behavior of transcritical CO₂ cycles, but subcritical cycles with a range of conventional refrigerants can also be analyzed. Water, air and a range of user-configurable coolant mixtures can be used as secondary fluids.

CSIM includes detailed extended-surface heat exchanger models, using actual geometry as input. Local heat balances are calculated for each discretized

⁴ Degrees of freedom refers to the number of extra optimization variables present

heat exchanger element, using local values for heat transfer coefficient, pressure drop and void fraction for both refrigerant and secondary fluids. The discretization of heat exchangers allow very detailed simulation output, for example temperature profiles, heat transfer coefficient and pressure gradient propagations.

CSIM is typically used as a design tool where component geometry and system control strategies are varied to optimize system performance or efficiency within fixed boundary conditions. A system optimization can be performed with several degrees of freedom, such as any combination of the following parameters:

- Evaporator outlet condition
- High-side pressure
- Refrigerant charge
- Heat exchanger geometry parameters (e.g. length of internal HX)
- Compressor speed (rpm)
- Secondary fluids mass flow rates

Several simulation points for on- and off-design can also be performed to estimate seasonal performance or part-load characteristics.

CSIM included the following component models at the start of this work:

- Gas Coolers / Condensers
 - Tube-and-fin (both roundtube and microchannels)
 - Tube-in-tube
 - Shell-and-tube
- Evaporator
 - Tube-and-fin (both roundtube and microchannels)
 - Tube-in-tube
 - Shell-and-tube
- Compressor (single- and two stage)
- Internal heat exchanger

- Intercooler (for two-stage cycles)
- Intermediate pressure heat exchanger (for two-stage cycles)
- Auxiliary gas cooler/condenser in series or parallel to the main gas cooler/condenser
- Water heater gas cooler in series or parallel (single- or two-stage)
- Low pressure receiver

CSIM supports up to three gas coolers in series and two in parallel configuration, in addition to internal heat exchanger, intermediate pressure heat exchanger and intercooler. A cycle in CSIM can contain up to 6 discretized heat exchangers, accounting for most of the total number of variables needing to be solved.

2.3.3 The NLPQL solver

Component models and refrigerant cycle calculations generate a set of simpler constraint equations and an objective function that are solved by using a general optimization package, NLPQL (Schittkowski, 1985). NLPQL is an implementation of a sequential quadratic programming method for non-linear, constrained optimization problems, and uses an iterative gradient method.

Briefly explained, an iterative gradient method is an algorithm to calculate all constraint deviations for the problem, then apply a small increment to one variable and re-calculate the constraints. The change in deviations are stored as gradients in a gradient array. When this has been done for all variables, the solver reads the gradient array and calculates new values for all variables. This procedure is repeated until the sum of the deviations of all equality constraints are below a set threshold, and the objective function is minimized. Because NLPQL minimizes the objective function, an optimization for e.g maximum COP must specify the objective function, f_{obj} , as a negative value:

$$f_{obj} = -COP \tag{2.1}$$

Since the number of variables and the number of constraints change proportionally, the calculated gradient array grows proportional to the number of variables squared. Larger problems are harder to optimize, particularly for higher degrees of freedom.

Table 2.1 shows the simulation time for a gas-cooler with different levels of discretization. Each simulation ran for only 3 iterations, isolating the effect from number of variables. Figure 2.1 shows the correlation between simulation time and the number of variables. From this simple demonstration, it is clear that the simulation time does increase proportional to the number of variables squared. Solving a full CSIM CO₂-cycle with 500 variables can take hours to complete.

Table 2.1: Example simulation time compared to problem size

Number of subhx	Number of variables	Simulation time [s]
18	36	7.06
27	54	15.2
54	108	58.8

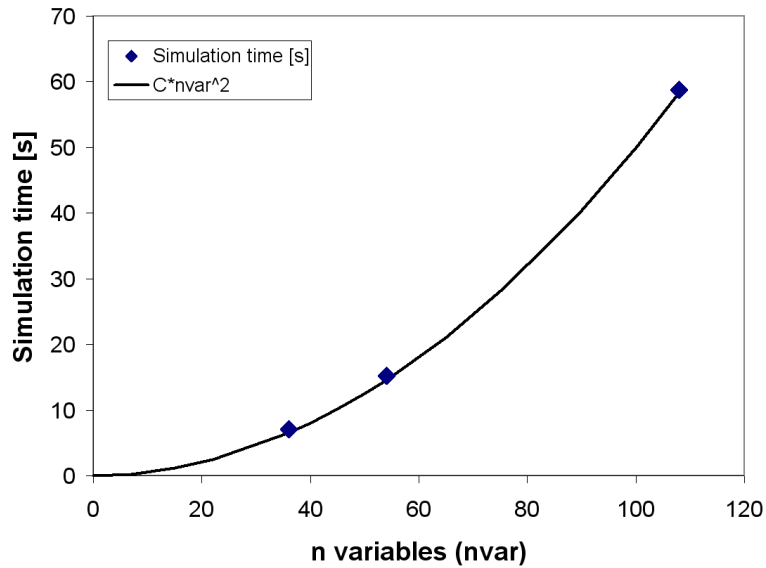


Figure 2.1: Correlation between simulation time and number of variables

2.3.4 Current thermophysical libraries for CO₂ in CSIM

Until now, CSIM has been implemented with two equations of state for CO₂, Angus et al, and Span-Wagner. These equations of state, together with

transport data correlations, form two complete libraries for thermophysical properties for CO₂, as described below:

Thermophysical library with Span-Wagner equation of state - TL_{Span} : TL_{Span} is based on the equation of state by Span & Wagner (1996). Auxiliary functions for saturated properties are not used for full consistency between saturation lines and the continuous region.

For transport data, dynamic viscosity (μ) is based on Fenghour et al. (1998), thermal conductivity (λ) is correlated by Vesovic et al. (1990), and the surface tension (σ) is based on Rathjen & Straub (1977). All transport data functions are programmed in C.

Thermophysical library with Angus et al. equation of state - TL_{Angus} : The TL_{Angus} implementation is based on the equation of state by Angus et al. (1976) with the improvements as suggested by Pitzer & Schreiber (1988) near the critical point. The equation of state is programmed in C with property link features. To improve the calculation speed further, auxiliary functions for saturation pressure and saturated liquid and vapor densities are used.

This equation of state is less computational demanding compared to Span-Wagner, and is frequently used with CSIM because it significantly shortens simulation time. However, the saturation data are not fully consistent with the continuous region, and the overall accuracy is considered to be lower than that of Span-Wagner.

Transport data in TL_{Angus} are identical as in TL_{Span} .

Property link feature: The implementation of Angus et al. features some performance enhancing procedures in addition to the improvements as suggested by Pitzer & Schreiber (1988). The main contributor to lower calculation time is a “property link” procedure, which in essence stores the last calculated values of property functions. If another property at the same fluid state needs to be calculated immediately after the first, the calculation time is much shorter as a full recalculation does not occur.

In CSIM, the program usually requests several properties for the same fluid state. Particularly in the calculation of pressure drop and heat transfer coefficient, property values for c_p , ρ , μ and λ are usually simultaneously requested. If the refrigerant is in a two-phase state, these values are usually calculated for both saturated gas and saturated liquid. As the system components calculation is done on a node-basis, it is possible to stack 10 or more property calls in the same state, and the property link feature significantly reduces the

total calculation time. It is possible to use this technique with Span-Wagner as well, but it has not been implemented so far.

2.3.5 CSIM data flow to thermophysical libraries

CSIM supports a wide range of refrigerants and secondary fluids, and all calculation of thermodynamic properties are handled through a layer of global, generic functions that redirects to the correct equation of state or other correlation for the relevant fluid. This implies that for all fluids, the form of the function call for a particular property is identical, regardless of the form of the relevant equation of state.

CSIM is not optimized for any specific equation of state, and the selection of system variables and the calculation of thermodynamic properties are done according to intuitive practice and numerical stability. For instance, the reference variables in heat exchangers are Δh and p , which are perhaps the most intuitive for the user. The pressure can be tracked through the heat exchangers according to pressure drop, and Δh is proportional to the exchanged heat. Correlations for calculation of pressure drop and heat transfer coefficients commonly use T and p as input arguments, causing relatively frequent use of the function $T(h, p)$.

A schematic representation of the data flow between different modules in CSIM can be seen in figure 2.2.

2. SIMULATION TOOLS FOR HEAT PUMPING APPLICATIONS

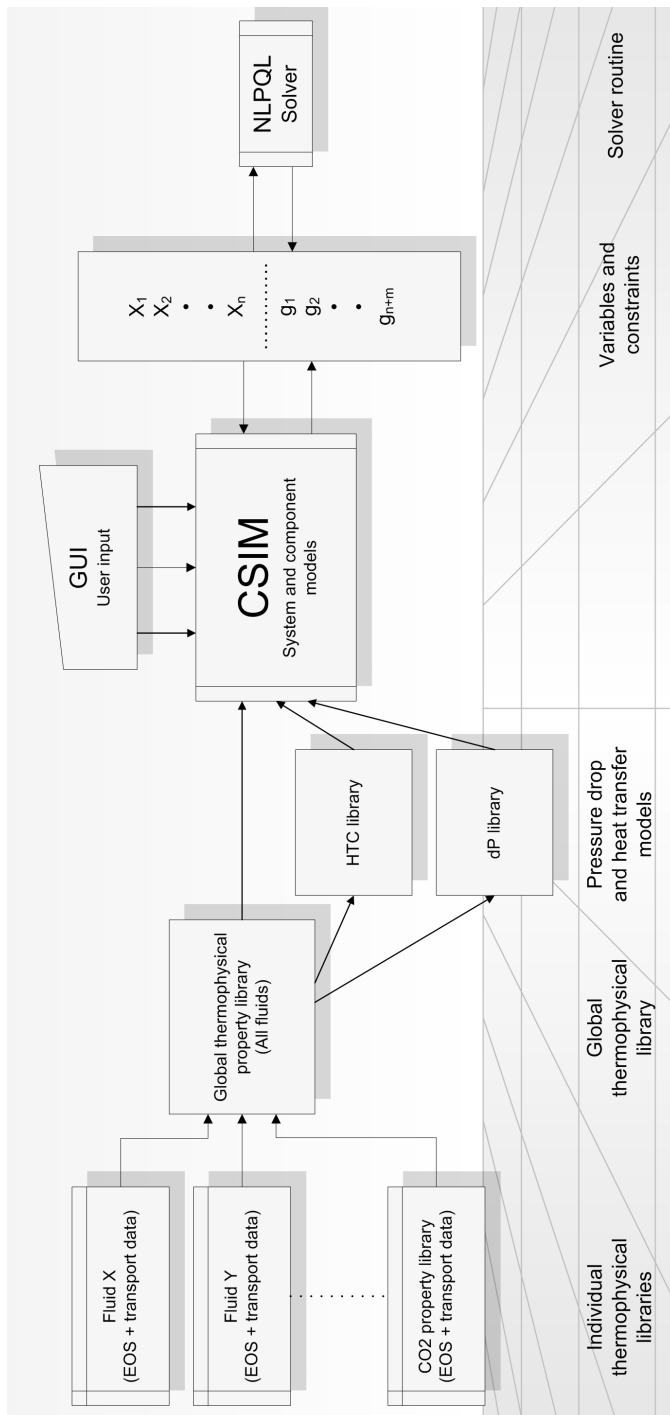


Figure 2.2: CSIM data flow

Both the *Angus* and *Span-Wagner* equations of state use temperature and density as the main property space, but these are not really practical to use directly in the simulation software as describing variables. A new implementation of an equation of state for CO₂ will be in the form most efficient for the current practice in CSIM.

2.3.6 Profiling CSIM

In order to get a better picture of the impact the calculation of thermophysical properties has on simulation time, a simple profiling of CSIM has been performed. The profiling is based on calls made from the component models in CSIM and the libraries for pressure drop, heat transfer and void fraction calculations. That implies that a single logged function call can require several calls to other property functions from within the thermophysical library.

The complete distribution of various property function calls from CSIM will vary depending on the number of components and level of discretization. The distribution in a typical case can be seen in figure 2.3. The total number of calls to thermophysical property functions in a typical simulation run may typically range from 500,000 to 5,000,000 calls, depending on the level of discretization, the number of components, initial values, convergence requirements and operating region.

One commonly used function in CSIM is $x(h, p)$. As long as this state is in the two-phase region, both $h'(p)$ and $h''(p)$ are calculated to find the vapor fraction. $h'(p)$ and $h''(p)$ are implicit functions in both TL_{Angus} and TL_{Span} , which means that numerical solving is used, resulting in many calls to the equation of state.

By logging the cpu time spent calculating thermophysical properties, it is possible to identify the relative calculation load imposed by these functions during a simulation. Table 2.2 shows this ratio for the TL_{Span} and TL_{Angus} implementations in CSIM.

Table 2.2: Relative cpu time consumption for calculation of thermophysical properties, average of three CSIM test-cases.

	TL_{Span}	TL_{Angus}
Total cpu time [% of TL_{Span}]	100.0	5.5
Rel. cpu time thermophys. [%]	99.7	92.5

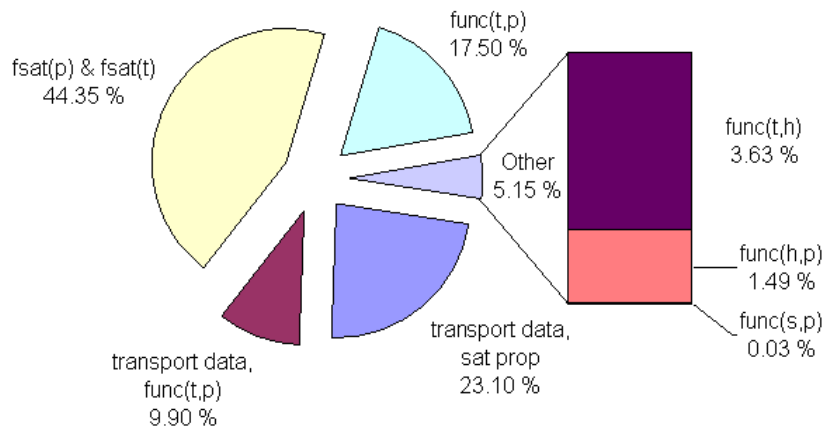


Figure 2.3: Distribution of thermodynamic property calls from a typical CSIM case simulation

From this simple test with a fixed distribution of function calls, several conclusions can be drawn:

- TL_{Angus} is almost 20 times faster than TL_{Span} .
- Of the entire duration of the simulations, 99.7% of the time was consumed by calculation of thermophysical properties when using TL_{Span} .
- There is a great potential for reducing the simulation time if the calculation load of these property functions can be reduced.

2. SIMULATION TOOLS FOR HEAT PUMPING APPLICATIONS

3. FAST THERMOPHYSICAL LIBRARY (FTL)

3.1 Introduction

The constant development of computer hardware results in steadily faster and more advanced computational tools. Still, the computational load of simulation models may grow even faster, as the optimization of system design for CO₂ require more complex models than simulations with other fluids. In addition, CO₂'s reference equation of state has a high calculation load, increasing the challenge of designing optimal CO₂ systems. The implementation of a detailed plate heat exchanger model (see Chapter 4) will increase the calculation load further, due to the high number of variables required to describe the local behavior in parallel channels.

As stated in Chapter 1.1 there is a potential for reducing the calculation time for certain thermophysical properties. In the heat pumping cycle simulation tool CSIM, the calculation of such functions for CO₂ takes up in the order of 99.7 % of the total simulation time when using TL_{Span} . CSIM is typically used as a design tool, where many single simulations are performed on- and off design for each configuration. Very long simulation times will inevitably limit the model resolution, depth of design optimization or time and cost efficiency.

As stated in Chapter 2.1, component models must be able to capture the governing physical behavior with adequate precision. For transcritical CO₂ systems, this usually requires a higher level of detail than systems for conventional refrigerants.

This part of the work investigates whether simple, linear interpolation in lookup tables can replace the calculation of a computational demanding equation of state and transport data in a circuit simulation tool with respect to accuracy and consistency, and achieve a gain in calculation performance that will greatly reduce simulation time. The overall aim for this implementation is to reduce simulation times in CSIM by 99 % (of an approximate theoretical maximum of 99.7 %) compared to the thermophysical library TL_{Span} , and still maintain good accuracy.

Linear interpolation was chosen for this work because it is relatively simple to implement and the quickest to calculate. As increasing calculation speed

of is the main aim of this part of the work, it is sensible to investigate the potentially fastest method first. If linear interpolation yields poor accuracy, it may be improved with e.g. higher-order interpolation. But higher-order interpolation requires more data points, and there will be challenges connected to ensuring the validity of these. Another alternative could be an implementation of splines, but that is more complex to implement, and requires more work to modify for other fluids or areas of coverage.

All design decisions for the Fast Thermophysical Library (FTL) were made to match the designated application, CSIM. This thermophysical library implementation has been performed for CO₂, but is quite general in nature and easily transferable to complex equation of state's for other substances.

3.2 Thermophysical property calculation based on linear interpolation

3.2.1 Overview

The thermodynamics of CO₂ in the operating region of common heat pumping cycles can be described as highly nonlinear, due to the proximity of the critical point. Using linear interpolation to represent these properties well poses several challenges. The most important with respect to accuracy, is the systematical error between a thermophysical property function and the linearly interpolated approximation.

Selecting T and p as grid for the main lookup tables introduces other issues. Close to the critical point, the isotherms and isobars are virtually parallel, describing that pressure and temperature in this area are very closely linked. For a regularly gridded table, this results in a loss of accuracy in this region due to the range of property values a given set of data points will span. Figure 3.1 shows a sketch of a T-p table grid in the pressure-entropy (p-s) space near the critical point. Each blue cross represents a grid point. It is clear that the Δs between each grid point is quite large near the critical point.

Figure 3.2 illustrates a source of error of interpolation close to the critical point. In this situation, the returned value of “h” will be severely underestimated due to the “bad” top-left data point.

3. FAST THERMOPHYSICAL LIBRARY (FTL)

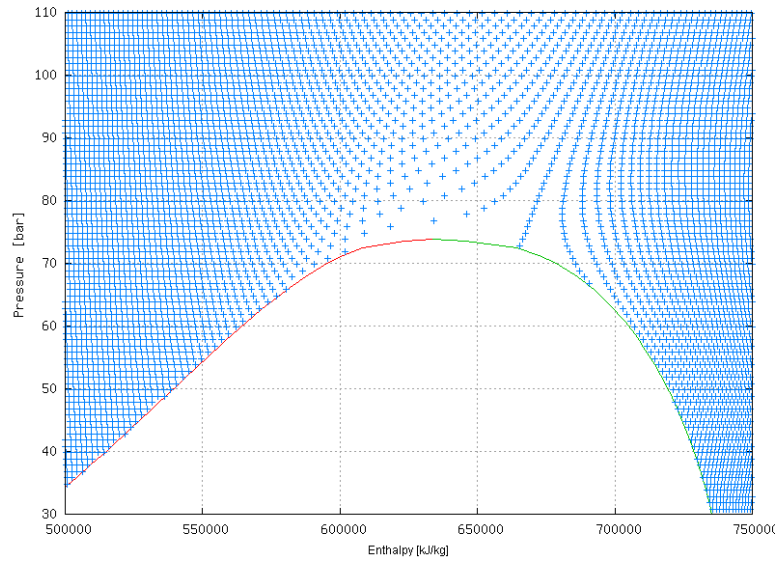


Figure 3.1: Example grid point distribution of a T-p table in the near critical region in the p-h space, using regular grid spacing

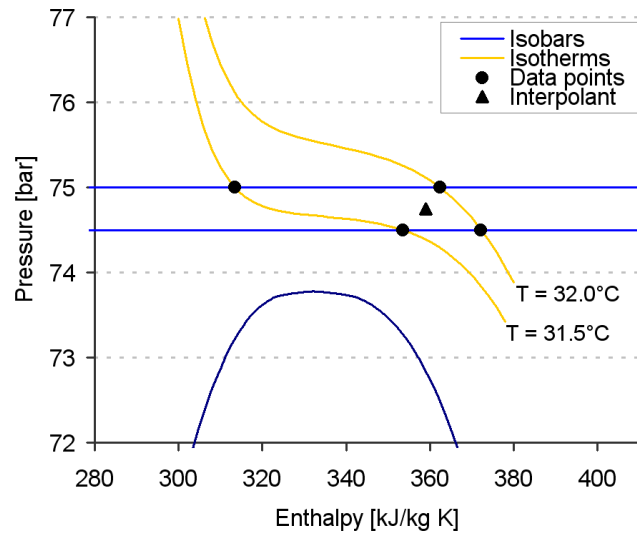


Figure 3.2: Example of interpolation in the near-critical region

3.2.2 Systematical error from linear interpolation

When the curvature of thermophysical properties in the T-p space is not fully replicated with linear interpolation, it is a systematical error. The first example is enthalpy (see Figure 3.3) at 75 bar. On one side of the inflection point, linear interpolation will over-estimate the property value, and underestimate on the other side.

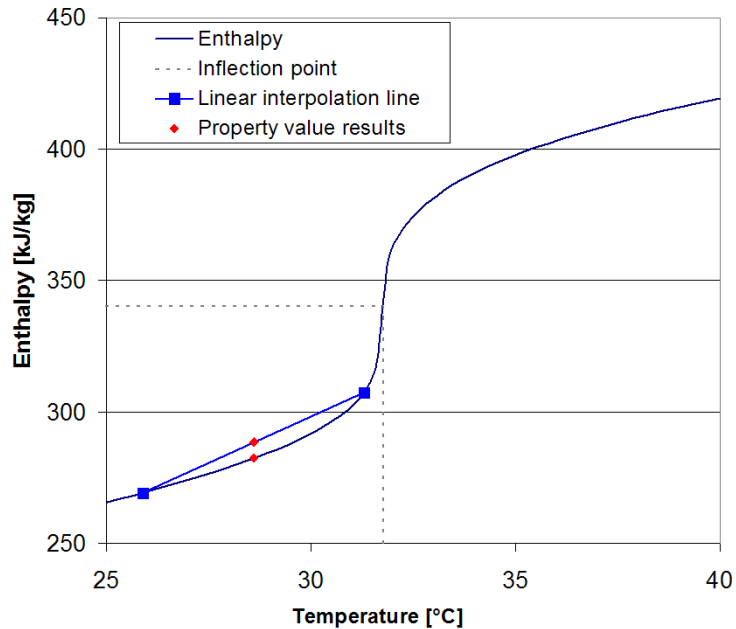


Figure 3.3: Cause of systematic error in linear interpolation. Enthalpy for CO₂ at 75 bar

Properties that have a peak or ridge over the pseudo-critical line, will be over-estimated on both sides. Figure 3.4 illustrates this for the isobaric heat capacity (c_p) at 75 bar.

This systematical error can be reduced by using a tighter grid where the nonlinearities are strongest, but will nevertheless be present. A tighter grid also produces larger tables, which affect calculation performance. A visual analysis of this error is done in chapter 5.1.2.

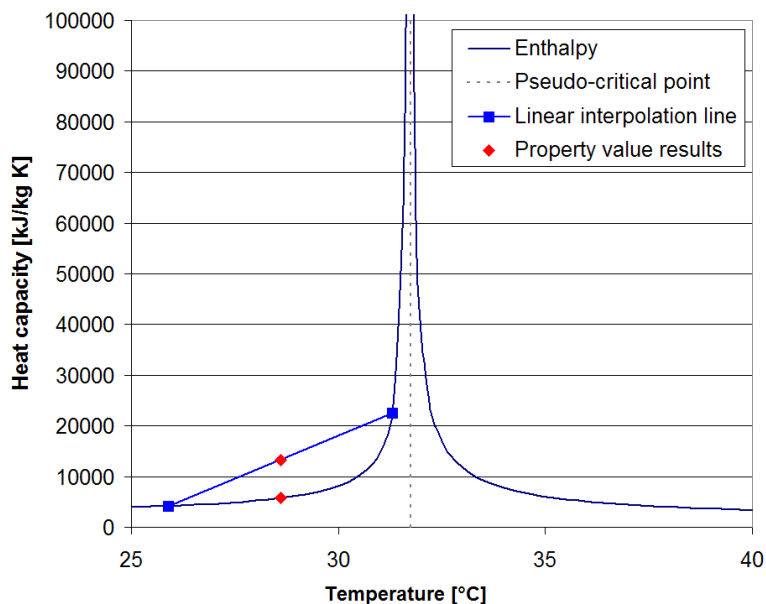


Figure 3.4: Cause of systematic over-estimation in linear interpolation. Isobaric heat capacity (c_p) for CO_2 at 75 bar

3.2.3 Table size

If the lookup table implementation is small enough to fit in the physical memory (RAM) of the computer, there are still at least three factors of table size that have an impact on calculation performance.

- The first is disk read time, the time it takes to read FTL from disk and load it into the RAM. This is matter of fractions of a second up to a couple of seconds depending on the computer speed and FTL size. This is also usually a one-time event. If FTL is used as a DLL in a spreadsheet, it remains in the RAM until the spreadsheet is closed.
- The second concern is how much of the needed table data for one simulation cycle will fit in the CPU cache memory. System simulations in CSIM often calculate the same state points over and over again, particularly in the process of calculating gradients. The difference of reading from RAM or cache is explained further in Chapter 3.2.4.
- The third concern is a numerical one. Larger tables will make operations involving line search slower. Line search is typically used in

reverse-lookup of implicit functions. As most of these searches are binary and not exhaustive, this has only a small impact on calculation time.

All these factors must be considered when programming, compiling and using this implementation. In this work, the goal with respect to table size has been to maintain practical usability. The usability factor is a balance between the accuracy and speed of calculations.

3.2.4 Reading from RAM and cache

Although linear interpolation in tables is a much faster and simpler computational task than calculating large, complex expressions, this method involves repetitive accessing of large data tables. The size and grid spacing of data tables will affect the reading access time directly.

Computer RAM has been cheap and plentiful (for this application) for several years, and the faster, on-die CPU cache has also increased in size. Cache's are smaller memory banks which are integrated into the CPU itself, in contrast to the larger main memory (RAM) that sits on the motherboard and is usually accessible by the slower front side bus (FSB). The cache automatically copies data from frequently used main memory (RAM) locations, and can be accessed with much less latency.

The size of this cache is much smaller than typical RAM sizes. A 2003 Intel Pentium 4 (test computer for this work) has 512 kB of L2 cache, and current (2009) mainstream multi-core CPU's, typically 6-12 MB L2 (and L3) cache. This allows for a considerable amount of data to fit in cache for rapid access.

Detailed analysis and optimization of FTL with respect to cache performance is outside the scope of this work. Nevertheless, this is yet another factor that affects the accuracy-performance balance depending on the size of the tables.

3.3 FTL features and specifications

3.3.1 Fast lookup table design requirements

As previously mentioned, this implementation of FTL is designed for use with CSIM. The requirements are:

- Typical range of coverage for simulations are pressures in the range of 10-140 bar and temperatures in the range of -45 - 140 °C. Internal solving functions may benefit from larger coverage during iterations.
- Must be considerably faster than TL_{Angus} ; the aim is to reduce simulation time by up to 90% (factor of 10).
- CSIM simulations with FTL should yield results as close as possible to TL_{Span} .

In addition to these requirements, it has been attempted to make the lookup table implementation generic for future use with other applications, fluids¹, coverage areas and accuracy requirements. This means following the local NTNU/SINTEF convention for included property functions in thermophysical libraries, even if not all are used by CSIM.

The lookup table data is stored in static array variables for rapid access. The array is implemented into FTL at compile time, as opposed to reading the array from a text file at simulation start. Implementing at compilation level is the fastest with respect to simulation times, and re-compiling FTL for a different region of coverage or grid spacings only takes a few minutes.

3.3.2 Included property functions in FTL

The externally available property functions (global functions, see Figure 3.5) in FTL, are functions that are accessible from outside the library, for example by a simulation tool.

Continuous region property functions included in FTL are listed in Table 3.1, Table 3.2 lists the included functions for the two-phase region and the saturation lines. For the continuous region functions, all functions except $f(T, p)$ are also valid in the two-phase region.

3.3.3 Global and native functions

The global functions in FTL are calculated from a smaller set of local functions, referred to here as native functions. Several native function calls will

¹ In its current form, only a framework for *single property* fluids, mixtures will require additional changes

3. FAST THERMOPHYSICAL LIBRARY (FTL)

Table 3.1: Global property functions in FTL, continuous region

Property	$f(T, p)$	$f(T, v)$	$f(T, h)$	$f(h, p)$	$f(s, p)$	$f(v, h)$	$f(v, u)$	$f(v, p)$
T				X	X	X	X	X
p		X	X					
h	X	X	X					
s	X	X	X	X				
v	X							
u	X	X						
c_p	X	X						
c_v	X	X						
w	X	X						
κ	X	X						X
$\partial p / \partial T$	X	X						
$\partial p / \partial v$	X	X						
λ	X							
μ	X							

Table 3.2: Global property functions in FTL, two-phase region and saturation lines

Property	$f_{sat}(T)$	$f_{sat}(p)$	$f(T, x)$	$f(T, h)$	$f(h, p)$	$f(T, s)$
x				X	X	X
T		X				
p	X					
h	X	X	X			
s	X	X	X			
v	X	X				
c_p	X					
c_v	X					
λ	X					
μ	X					
σ	X					

often be combined to produce the output of a global function call. Some of the global functions are implicit, and require iterative solving of native functions. An example is the function $T(h, p)$. This function is explicit only in a limited region where it is covered by the h-p table. Outside this table, this function is implicit, and calculated by an iterative solution of the explicit function $h(T, p)$.

Another example is the $x(T, h)$ function, in which several native calls are made. First, to check if T is smaller than T_c to ensure that the call is valid. Then $h'_{sat}(T)$ and $h''_{sat}(T)$ is calculated, and x is determined by either interpolation, or a logic check if h is found to be outside the two-phase area.

Figure 3.5 shows the data flow through different modules in FTL. The main modules in CSIM are covered in chapter 2.3.5, and illustrated in Figure 2.2.

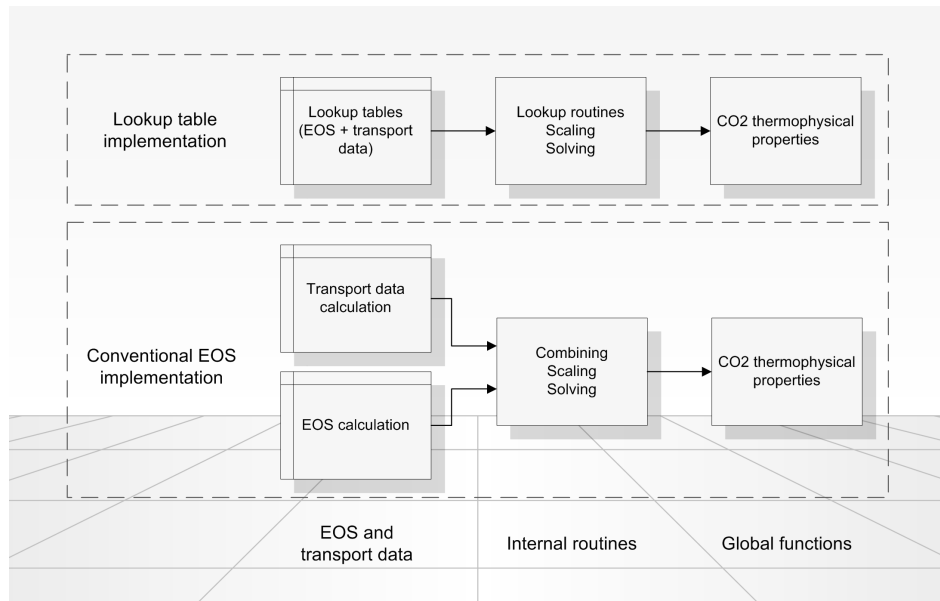


Figure 3.5: CO₂ thermophysical property library data flow

In order to adapt this method for another equation of state or even another single-component fluid, the only thing to really change is the code for generating the tables. Essentially all native and global functions will remain the same.

3.4 Description of the lookup tables in FTL

3.4.1 Thermophysical property base

FTL is using existing implemented equation of state and transport data correlations to generate the lookup tables.

All FTL lookup table data were generated from Span and Wagner's equation of state and transport data from Wakeham et al., Fenghour et al. and Rathjen et al. (TL_{Span}). Span-Wagner's equation of state was used without auxiliary functions for saturation data. While auxiliary functions require less computational time, and are also possibly more accurate than the equation of state, the auxiliary functions are not completely consistent with the equation of state. In this work, a smooth transition from the saturation line to the continuous region has been prioritized.

As a basis for the main tables in the T-p space, Gibb's free energy and the differentials were calculated from the relations shown in Table 3.3. These properties can be combined to form all required thermodynamic properties. Property values in implicit² tables were calculated directly.

3.4.2 Thermodynamic relations based on Gibb's free Energy

While both Span-Wagner and Angus' equations of state for CO₂ describe the Helmholtz function and it's differentials to calculate all properties, the main data tables in FTL contain values for Gibb's free energy and differentials. Gibb's function is explicit in pressure and temperature, which is convenient and desirable for this application.

As can be seen from the profiling of thermophysical property calls from CSIM (see Figure 2.3), approximately 67% of the calls made during a simulation is to saturated property functions of p or T, and an additional 27% is for pure $f(T, p)$ -type functions.

The definition of, and the procedure for calculating Gibb's differentials from Span-Wagner is shown in Table 3.3. The properties of Gibb's function and differentials can then be combined to produce all the other necessary thermodynamical states, as shown in Table 3.4.

² Tables other than T-p space.

3. FAST THERMOPHYSICAL LIBRARY (FTL)

Table 3.3: Definition and relations of Gibb's free energy equation and differentials

Gibb differential	Relation	Notation
g	$h - T \cdot s$	g
$\frac{\partial g}{\partial T}$	$-s$	g_T
$\frac{\partial g}{\partial p}$	v	g_P
$\frac{\partial^2 g}{\partial T^2}$	$-\frac{c_p}{T}$	g_{TT}
$\frac{\partial^2 g}{\partial p^2}$	$\frac{\partial v}{\partial p}$	g_{PP}
$\frac{\partial^2 g}{\partial T \partial p}$	$-\frac{\partial v}{\partial T}$	g_{TP}

Table 3.4: Calculating thermodynamic properties from Gibb's function and differentials

Property	Relation
s	$-g_T$
h	$g - T \cdot g_T$
v	g_P
c_p	$-T \cdot g_{TT}$
c_v	$\frac{T \cdot g_{TP}^2 - T \cdot g_{TT} \cdot g_{PP}}{g_{PP}}$
w	$g_P \cdot \sqrt{\frac{T \cdot g_{TT}}{T \cdot g_{TP} - T \cdot g_{TT} \cdot g_{PP}}}$
$\frac{\partial p}{\partial T}$	$-\frac{g_{PP}}{g_{TP}}$

3.4.3 Three T-p tables with adapted resolution and coverage

In order to obtain better resolution close to the critical point and also add a robust coverage strategy for solving implicit functions, FTL includes three separate tables for the T-p space. The three tables are: a low resolution “background” table covering a very large region, a medium resolution table covering the main operating region for the design application, and a high resolution table for a small area around the critical point. Figure 3.6 shows the coverage area of the T-p tables.

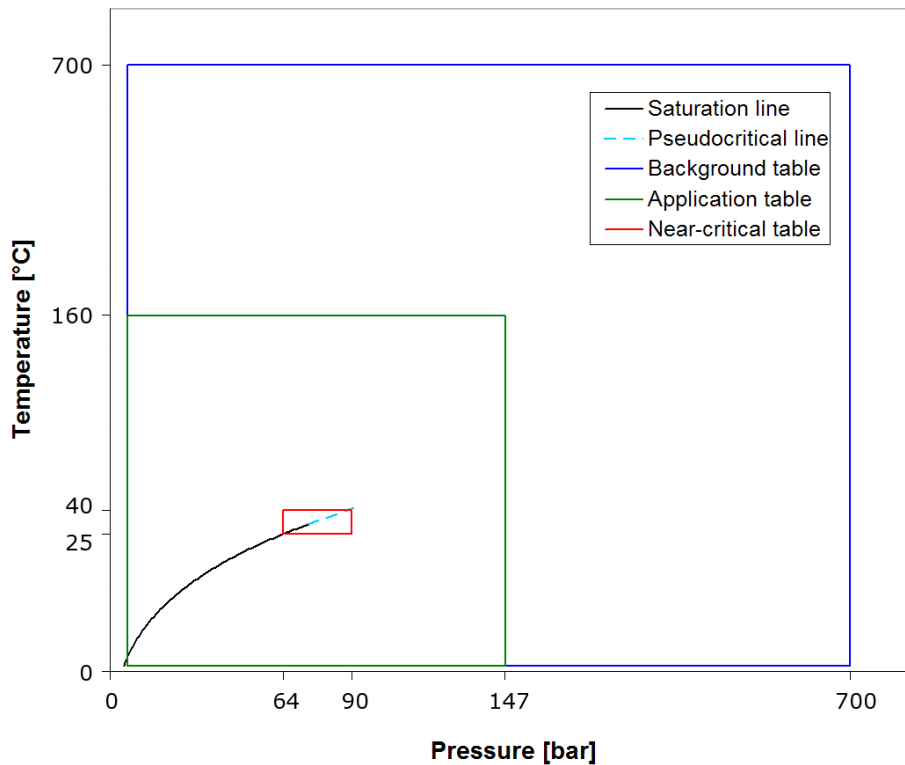


Figure 3.6: Coverage of T-p tables (background table not to scale)

The relevant temperature and pressure range for a heat pumping application are limited upwards by about 150°C and 140 bar. Still, it may be useful to include a larger range for consistency, for example when using implicit (solved) property functions close to the upper limits of the table. This extended region may not require the same accuracy, as no system state should ever actually end up here. With these requirements, a very wide grid can be

used, resulting in a relatively small table for this region.

In this work, the grid spacing for the low resolution table has been set to 5°C and 5 bar, and covers the region up to 700°C and 700 bar. With this range and grid spacing, the extended region, "background" table size is about 1.9 MB in size. The table geometries are described in Table 3.5.

Table 3.5: Specification of low resolution "background" T-p table geometry

	Temperature	Pressure
	[°C]	[bar]
Start	-56.6	6.40
Stop	700	700
Gridspacing	5	5
Number of steps	151	138

Similarly, the region nearest the critical point require the highest grid density. Based on experience, this near-critical region has been localized (for use in this work) in the range of approximately 25 to 40°C and 65 to 90 bar. With a grid spacing of 0.075°C and 0.1 bar, this near-critical table ends up at 4.6 MB in size. The table geometry is described in Table 3.6

Table 3.6: Specification of high resolution near-critical T-p table geometry

	Temperature	Pressure
	[°C]	[bar]
Start	25.1	64.3
Stop	39.9	89.9
Gridspacing	0.075	0.1
Number of steps	199	257

Figure 3.7 shows the impact of implementing the high-resolution table for the near-critical region. The figure maps the deviation from the TL_{Span} in the near-critical region, using a color scale to identify the magnitude of deviation. These map plots are described more closely in Chapter 3.6.5.

For the main table, the grid spacing was set to 0.5°C and 0.5 bar. This resolution in the required coverage area results in a relatively large table of

3. FAST THERMOPHYSICAL LIBRARY (FTL)

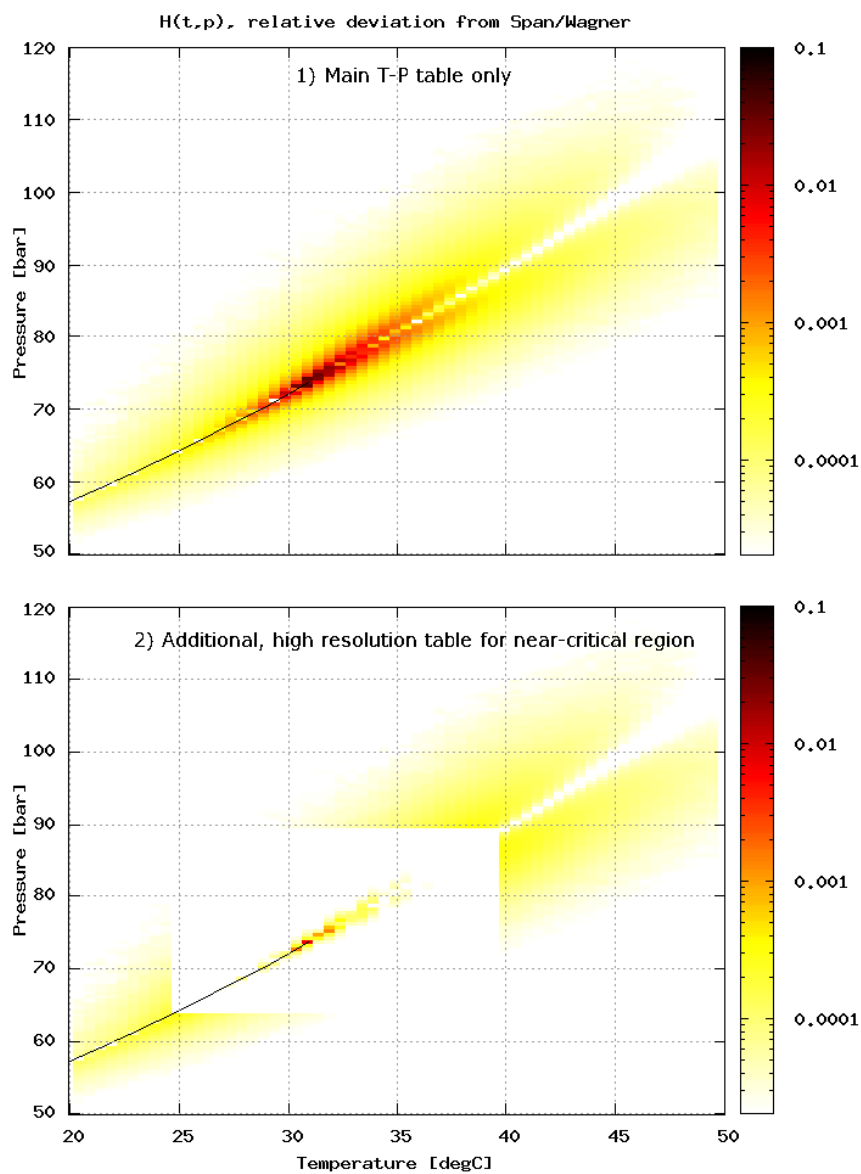


Figure 3.7: Lookup table accuracy for $h(T, p)$, with (bottom) and without (top) higher resolution table for the near-critical region. Relative deviation from TL_{Span}

10.7MB. The table size grows quickly with higher resolution, so this grid was decided upon to balance size, performance and accuracy. The specifications of the geometry can be seen in Table 3.7.

Table 3.7: Specification of main T-p table geometry

	Temperature	Pressure
	[°C]	[bar]
Start	-56.6	6.40
Stop	160	147
Gridspacing	0.5	0.5
Number of steps	435	278

As the three tables overlap in coverage, there are no issues regarding interpolating near boundaries of the inner tables. All three T-p tables contain the same properties: g , g_T , g_{TT} , g_P , g_{PP} , g_{TP} , λ and μ .

3.4.4 Saturation data table

A table for saturation data is generated from the triple point to the critical point. A very small ΔT has been chosen in this table to ensure good accuracy near the critical point. It was not considered necessary to use any form of adapted or irregular grid in this case, as the total table size is fairly small even with the current, high resolution for the entire table.

Table 3.8 shows some key parameters for the saturation lookup table. The number of tabulated properties is relatively high, since it contains transport data, Gibb's function and differential values *and* commonly used thermo-physical properties for both the saturated liquid and -vapor lines. The extra properties were added to simplify calculation at an early stage of development, and are not really required. By only tabulating the strictly required values, the number can be reduced to 15 and the saturation table size correspondingly.

Table 3.8: Specification of saturation data table

T start	T stop	ΔT	N_{steps}	n properties	Disk size [KB]
-56.6	30.9732	0.025	3503	29	1,314

Tabulated saturation data removes the need for inverse-calculation of saturated property functions. As all properties in this table is either consistently increasing or decreasing with a increase in temperature, any property can be used as a function argument to calculate other saturated properties.

The properties included in the saturation data table are: T_{sat} , p_{sat} , h' , h'' , v' , v'' , s' , s'' , c_p' , c_p'' , c_v' , c_v'' , λ' , λ'' , μ' , μ'' , σ' .

In addition, values for Gibb's function³ and differentials for saturated liquid and vapor were added. These are needed when interpolating against the saturation line when the data points are spanning. This actually makes the first values obsolete, as they can just as well be calculated from the Gibb's differentials the same way as for outside the two-phase region. Still, they have remained because they allow slightly quicker calculation of saturated properties, and the impact of the extra table size was considered to be minor.

3.4.5 Additional data tables

In addition to the T-p and saturation data tables, four tables have been generated to improve calculation of otherwise implicit functions. In FTL, implicit functions are calculated by iterative solving or *reverse lookup*⁴. For some properties, both methods occasionally suffered from convergence problems and low accuracy in the near-critical region and the transition over saturation lines. Implementing additional tables that cover most of the two-phase region and extend a bit over the critical point, has removed these issues completely.

The four additional tables are:

- h,p - See Table 3.9 for specification
- T,v - See Table 3.10 for specification
- T,h - See Table 3.11 for specification
- s,p - See Table 3.12 for specification

³ The value of Gibb's function is identical for saturated liquid and saturated vapor, but the values for the differentials vary.

⁴ See definition

3. FAST THERMOPHYSICAL LIBRARY (FTL)

Table 3.9: Specification of h-p table geometry

	Enthalpy [kJ · kg ⁻¹]	Pressure [bar]
Start	125	11.0
Stop	550	95.0
Gridspacing	0.9	0.42

Table 3.10: Specification of T-v table geometry

	Temperature [°C]	Specific volume [m ³ · kg ⁻¹]
Start	-20	0.0014
Stop	40	0.1
Gridspacing	0.25	variable

Table 3.11: Specification of T-h table geometry

	Temperature [°C]	Enthalpy [kJ · kg ⁻¹]
Start	20	125
Stop	50	550
Gridspacing	0.25	1

Table 3.12: Specification of s-p table geometry

	Entropy [J · kg ⁻¹ · K ⁻¹]	Pressure [bar]
Start	900	50
Stop	2100	100
Gridspacing	8	0.33

These tables contain only one or two properties each, but still contribute noticeably to the total size of the FTL implementation. In particular is this the case for the h-p table, which has been designed with relatively high resolution because it contains the most frequently⁵ used implicit function in CSIM, $T(h, p)$.

3.4.6 Summary of FTL tables

Table 3.13 shows a summary of the dimensions of all the tables in FTL.

Table 3.13: List of lookup tables included in the FTL implementation

Table	Grid size	n properties	Disk size [KB]
T-p, main	434 x 278	8	10,727
T-p, near-crit	199 x 257	8	4,740
T-p, background	152 x 139	8	1,930
Sat. table	3503 x 1	29	1,314
h-p	451 x 201	4	3,096
T-v	241 x 42	5	461
T-h	121 x 301	4	1,315
s-p	151 x 151	3	726

As previously mentioned, FTL includes a larger set of thermodynamic property functions than are needed by CSIM, because it follows the local NTNU/SINTEF template for these libraries. Consequently, neither the T-v or T-h (discussed earlier in the chapter) tables are used by CSIM, and could theoretically be removed in an implementation strictly used with CSIM.

In addition to the described tables, FTL also includes property values (the same properties as for other T-p tables) for the pseudocritical⁶ line, which are used to ensure valid data points as described in Chapter 3.5.2.

⁵ The T-h function calls profiled in Chapter 2.3.6 are exclusively used to calculate the vapor quality x , and redirects to saturated function calls: $f_{sat}(T)$

⁶ This is an imaginary line that extends from the critical point along the ridge where c_p has a local maximum

3.5 FTL data extraction

3.5.1 Calculating table indexes

The interpolation procedure is in this chapter shown for $f(T, p)$ functions. Implicit functions use a similar procedure, and saturated functions use a simplified version.

Since there are three separate T-p tables covering the continuous area, $f(T, p)$ functions are first directed to the correct table.

The regularly gridded tables in FTL allows data points to be found directly, without line searching. Using the global static variables for boundaries and grid stepping, the location of the four grid points are calculated as in equations 3.1 to 3.4. These equations return the indexes to T and p coordinates for the data points.

The indexes, i_0 and i_1 , for the temperature grid lines spanning the temperature "T" are found:

$$i_0 = \text{floor}\left(\frac{T - \text{GibbTabTstart}}{\text{GibbTabTstep}}\right) \quad (3.1)$$

$$i_1 = i_0 + 1 \quad (3.2)$$

In a similar manner, the indexes, j_0 and j_1 , for the pressure are found:

$$j_0 = \text{floor}\left(\frac{p - \text{GibbTabPstart}}{\text{GibbTabPstep}}\right) \quad (3.3)$$

$$j_1 = j_0 + 1 \quad (3.4)$$

The "floor function" converts a number to an integer by setting it to the nearest, lower integer value.

3.5.2 Ensuring valid data points

Using the table indexes found in the previous section, the four data points are extracted on the form $g_{i,j}$. These data points are not necessarily valid as basis for interpolation, and must be verified. To ensure validity of the group

of data points, three rules has been set:

1. The data points can not span the phase line
2. For properties that have a peak value in the critical point, the data points for can not span the pseudocritical line for $T_c \leq T \leq T_c + 10^\circ\text{C}$
3. Data points can not span the critical point. This rule only applies to properties not already covered by the second rule

The first rule is intuitive; spanning data points would mean that one or more data points are collected from the far side of the phase line, with property values for a different fluid phase. Naturally, this must be avoided. Figure 3.8 illustrates how this situation may occur.

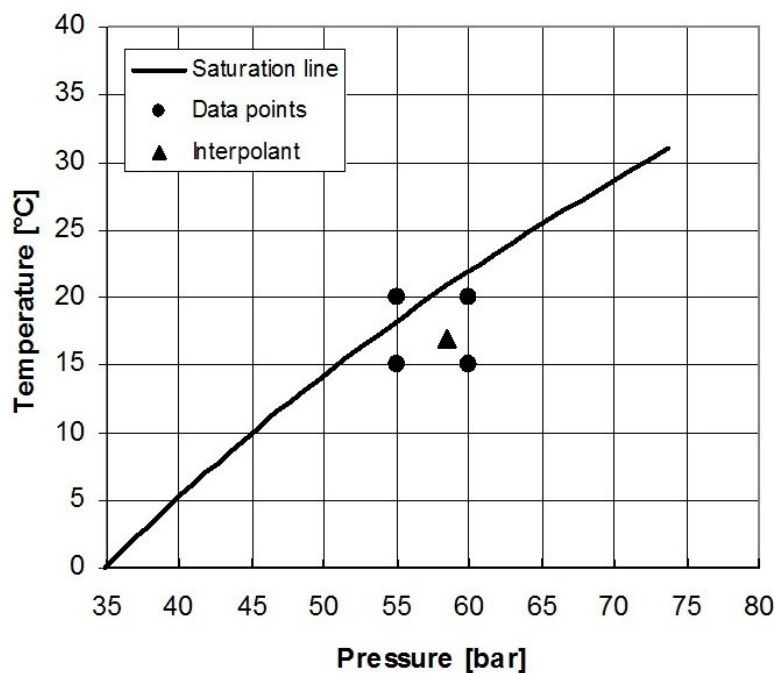


Figure 3.8: Interpolation close to the phase line, data points spanning

The second rule, data points spanning the pseudocritical line, only applies to a few functions relevant to this work, for instance $c_p(T, p)$ and $\lambda(T, p)$. The 10°C range was determined after analysis of the development of c_p along the pseudocritical line.

Conditions for the third rule, data points spanning the critical point, does not occur frequently in normal applications, but should still be enforced to maintain some control of the data points in this situation.

These three simple rules require considerable extra programming. This is the basic structure of the procedure for rule one, and rule two is very similar:

1. Check if T_{i0} or p_{j0} is below the critical point
2. If yes, check if all data points are on the same side of the phase line as the interpolant coordinate (T,p).
3. If no, move invalid data points to the correct saturation line.

In some cases, two invalid points may be moved to the same grid point. That would leave only 3 points for the interpolation, and triangulation⁷ is used instead.

The procedure to enforce the third rule is also quite similar to the first two, but resolves to triangulation with one corner in the critical point. If the data points are not affected by the three rules, the interpolant (i.e. property value) is calculated directly with linear interpolation.

3.6 FTL test suite setup

3.6.1 Overview

With the end focus on CSIM performance and accuracy compared to the TL_{Span} implementation, a series of different tests have been prepared to examine the performance of FTL with respect to accuracy, consistency and calculation speed:

- Validate the accuracy of saturation property functions, equation of state and transport data
- Validate the accuracy of continuous region property functions, equation of state and transport data

⁷ From the three data points a set of linear equations can be established, which again can be represented in matrix multiplication form and solved using Cramer's rule. The programming for solving small matrices is quite efficient. This particular problem could be solved using only 4 lines of code.

- Verify adequate accuracy for simulation output and results
- Document the change in calculation speed for a set of functions distributed to match the function call profile of CSIM
- Document the change in simulation time

In addition to the comparison with TL_{Span} , TL_{Angus} was also included. While the calculation results and simulation output of TL_{Angus} are not directly comparable with Span-Wagner with respect to accuracy, TL_{Angus} is the current default choice in CSIM, due to the shorter simulation times.

3.6.2 Test computer setup

All compiling and testing, unless otherwise noted, were performed with the following setup:

- Dell Precision 360
- Intel P4 3.0 Ghz, 800 Mhz FSB, 512kB L2 cache
- 1 GB DDR RAM
- Windows XP Professional SP2
- Intel C compiler v.10.1.011
- Intel Fortran compiler v.10.1.011

Compilation flags “/O2 /QaxN ” were used for all tests, which translates to “general performance optimizations” and additional “cpu-specific optimizations for the Intel P4 cpu”.

The results for FTL are compared to the results from the two other equations of state; TL_{Span} and TL_{Angus} (see Chapter 2.3.4).

3.6.3 Logging consumed CPU and clock time

All CPU time logging of thermophysical properties were performed using snippets of code that log the number of CPU clock ”ticks” passed while a particular function or procedure was run. Logging of CPU time is supported through the standard C library `time.h`.

Logging CPU time instead of clock time is done in an attempt to isolate the relevant process from all the possible background "noise" on a Windows operating system, as background system processes may be running randomly outside the users control, consuming CPU power. Before starting these tests, other windows programs and certain background processes were shut down to reduce interference on the results.

When logging the CPU time for an entire simulation, the same principles were used.

3.6.4 Saturated property data

The accuracy of saturated properties was tested by statistical comparison of calculated values. From the triple point to the critical point, properties were calculated between table entries to find the maximum expected deviation.

The results of this comparison were summarized for each property in average and maximum deviation. In addition, the summary lists the percentage of sampled value pairs outside a threshold deviation. This is useful in this context, as the deviations tend to be systematical in both location and magnitude. Typically, most properties will show an abrupt increase in deviation near the critical point. As the comparison is made for evenly spaced (in temperature) values, this threshold percentage will tell how many percent of the saturated region the error can be expected to be above the threshold deviation.

In this comparison, two thresholds were set to a relative deviation of 1.0E-3 (% of $D_i > 1.0E-3$), and 1.0E-4. In combination with average and maximum deviation, these numbers are informative with respect to the distribution of deviation magnitude.

The relative deviation for each value pair was calculated by:

$$D_i = \frac{abs(f_{FTL} - f_{TLspan})}{f_{TLspan}} \quad (3.5)$$

3.6.5 Validation methods - Individual property function accuracy

Describing the accuracy of FTL relative to another thermophysical library cannot be well done with common statistical analysis. The region of coverage and the number of compared points are large, and the larger errors are sys-

tematical and confined to much smaller sub-regions that are not well-defined.

The analysis of accuracy is presented as map-plots of the deviation covering the most interesting region of operation. Map-plots give a very clear picture both of the location and the magnitude of the error. The maps consist of one value-by-value comparison for each table grid point in the selected region. As for saturated functions, the comparisons were made mid-way between table entries⁸ in the grid, to show the maximum error that can be expected.

The deviation maps are made up of colored rectangles, where each corner is one of the comparison points. For these map plots, the entire rectangle is colored based on the corner with *maximum* deviation. This is done to further visualize the worst case scenario. Another consequence of this is that for any local maximum deviation, four neighboring squares will be colored accordingly, visualizing a relatively large area as “large deviation” due to this single point.

$f(T, p)$ functions were sampled and compared from the triple point to 120°C and 120 bar, at intervals of 0.5°C and 0.5 bar. In the near-critical region, using the high resolution table, the sample intervals were 0.075°C and 0.1 bar.

$T(h, p)$ and $h(s, p)$ were sampled and compared from -45°C to 120°C, with intervals equivalent to $\Delta p = 1.0$ bar and $\Delta h = 2500$ kJ/(kg K).

3.6.6 Validation methods - CSIM function profile test suite

A more specific combination of functions to emulate a simulation environment was calculated and timed. The functions were calculated with the same frequency as they appear in an actual simulation. This may show theoretical speed benefits for simulation purposes before the complications of a solver are added.

A total of 10 000 000 property function calls were made in this test, distributed into groups of function calls that match the profiling from CSIM. The function profiling of CSIM is described in Chapter 2.3.6. The calculation time of FTL was compared to TL_{Span} and TL_{Angus} .

⁸ Comparing values exactly in the grid points would yield zero deviation. Comparing values mid-way between the table entries, the chosen method here, will identify the maximum deviation.

3.6.7 Validation method - Simulation test suite

To assess the accuracy and performance in a real simulation environment, several test cases were simulated in CSIM, and results and circuit properties compared for the three different EOS implementations. A test case run with a specific implementation is called a subcase.

To compare simulation times on fair and equal terms for all thermophysical libraries, it is important that each subcase has equally good initial values. Experience shows that simulations with TL_{Angus} and TL_{Span} often converge at slightly different system states, due to small differences in calculated thermophysical properties. Therefore, each subcase used initial values from a successfully converged simulation at a slightly different system state.

As an example, each subcase could be simulated at 80 bar high side pressure and a compressor speed at 1600 rpm. This system state would then be the initial values for the actual test at 95 bar high side pressure and 1300 rpm compressor speed for that subcase. This process is repeated for all three EOS implementations.

The test suite consisted of 6 CSIM test cases that span a wide range of operating conditions, simulation modes and configurations. Table 3.14 lists a description of the 6 cases. A more in-depth description of each case can be found in Appendix B.

Table 3.14: Overview of the CSIM test suite

	Mode	Description
Case 1	Sim	Heat pump with plate heat exchangers
Case 2	Opt	Case 1 with 3 optimization variables
Case 3	Sim	Water heater, critical gas cooling process
Case 4	Opt	Air conditioning unit, 1 optimization variable
Case 5	Opt	AC with water heating, very high pressure
Case 6	Sim	Subcritical water-to-water heat pump

3.7 Results

3.7.1 Accuracy for saturated gas and liquid property functions

All properties have been calculated along the saturation lines from the triple point to the critical point, and compared with values from TL_{Span} .

Table 3.15 shows key values from the comparison of state properties, and Table 3.16 shows key values for the transport data. The field “ D_i trend” quotes the sign of the systematical error; “+” for over-estimating and “-” for under-estimating. 3501 evenly spaced (in temperature) value pairs were compared for each property.

Figure 3.9 shows the distribution map of deviation for $c'_{p,sat}(T)$. All properties showed similar patterns, but with different magnitude of deviations.

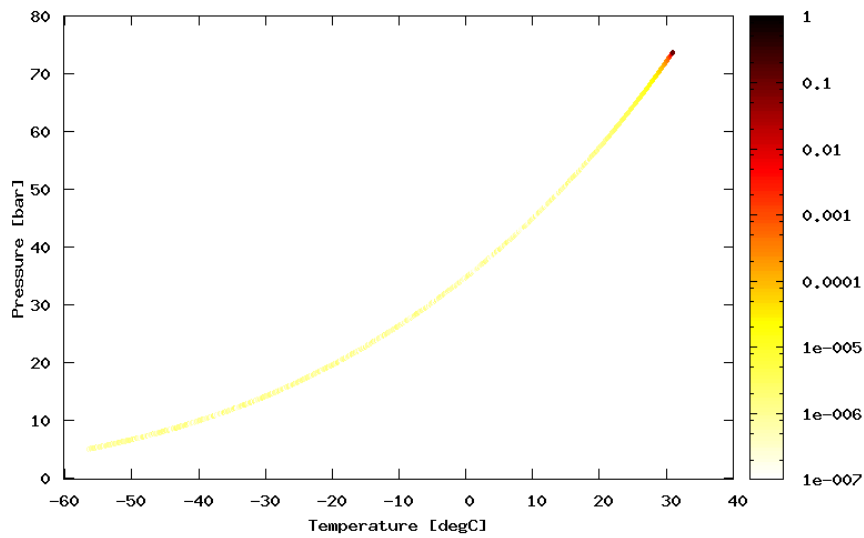


Figure 3.9: Distribution map of deviation compared to TL_{Span} , for $c'_{p,sat}(T)$

Table 3.15: Absolute deviation of state functions for saturated gas and liquid compared to TL_{Span}

D_i trend	$p_{sat}(T)$	$h'_{sat}(T)$	$h''_{sat}(T)$	$s'_{sat}(T)$	$s''_{sat}(T)$	$v'_{sat}(T)$	$v''_{sat}(T)$	$c'_{p,sat}(T)$	$c''_{p,sat}(T)$
Average	6.74E-07	1.72E-06	1.01E-06	2.47E-06	1.33E-06	2.76E-06	2.45E-06	1.25E-04	1.07E-04
Max	4.67E-06	1.38E-03	1.26E-03	1.05E-03	9.66E-04	4.27E-03	3.63E-03	1.69E-01	1.45E-01
% $D_i > 1.0E-3$	0.00	0.03	0.03	0.03	0.00	0.03	0.03	0.03	0.51
% $D_i > 1.0E-4$	0.00	0.09	0.09	0.06	0.09	0.17	0.17	1.57	1.60

Table 3.16: Absolute deviation of transport data functions for saturated gas and liquid compared to Fenghour and Vesovic.

D_i trend	$\sigma'(T)$	$\lambda'_{sat}(T)$	$\lambda''_{sat}(T)$	$\mu'_{sat}(T)$	$\mu''_{sat}(T)$
Average	2.32E-05	4.98E-05	3.46E-05	2.78E-06	3.19E-06
Max	5.09E-02	7.88E-02	4.42E-02	4.29E-03	4.01E-03
% $D_i > 1.0E-3$	0.17	0.26	0.26	0.03	0.03
% $D_i > 1.0E-4$	0.51	0.71	0.83	0.17	0.20

3.7.2 Accuracy for continuous region

Absolute deviation map plots have been produced for all property functions relevant to CSIM.

For explicit $f(T, p)$ type functions, the dimensions of the higher resolution, near-critical table has been designed to ensure that all the highest magnitude deviations are in the near-critical region. Therefore, it is only necessary to examine these deviation samples to identify the maximum deviation for each property function. Still, the larger area deviation map plot is presented for each function. On the following pages, deviation map plots for five relevant equation of state functions are presented.

Table 3.17: Analysis of deviation for FTL thermodynamic properties compared to TL_{Span}

	$h(T, p)$	$s(T, p)$	$v(T, p)$	$c_p(T, p)$	$T(h, p)$	$h(s, p)$
Max. dev	2.3E-02	1.8E-02	7.8E-02	2.9E+0	N/A	4.3E-05
99.9% percentile	2.5E-03	2.0E-03	7.3E-03	1.8E-01	N/A	3.4E-05
99% percentile	2.3E-04	1.7E-04	6.7E-04	1.3E-02	N/A	2.1E-05
Map plot	Fig. 3.10	Fig. 3.11	Fig. 3.12	Fig. 3.13	Fig. 3.16	Fig. 3.17

Table 3.18: Analysis of deviation for FTL transport data functions compared to original correlations

	$\lambda(T, p)$	$\mu(T, p)$
Max. dev	1.0E+0	9.3E-02
99.9% percentile	4.4E-02	7.9E-03
99% percentile	6.2E-04	5.0E-04
Map plot	Fig. 3.14	Fig. 3.15

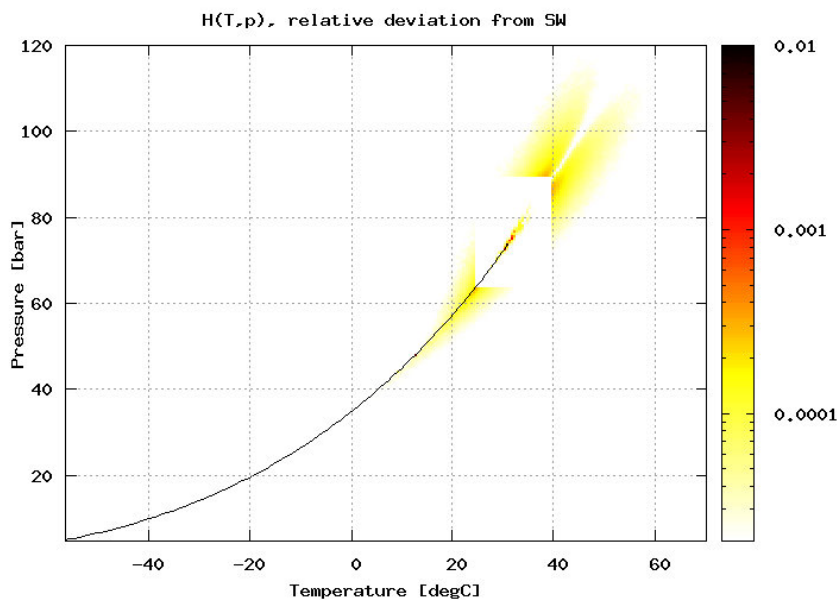
For the two examined implicit functions, $T(h, p)$ and $h(s, p)$, only one sample set was produced as there were no larger deviations near the critical point for these functions.

The map plot for $T(h, p)$ can be seen in Figure 3.16. The accuracy is overall very good, with only minor deviations found. Unfortunately, the implementation of Span-Wagner's equation of state had slight convergence issues around the saturation lines, which can be seen as scattered colored squares. Due to these errors, a maximum error can not be estimated based on the sample data.

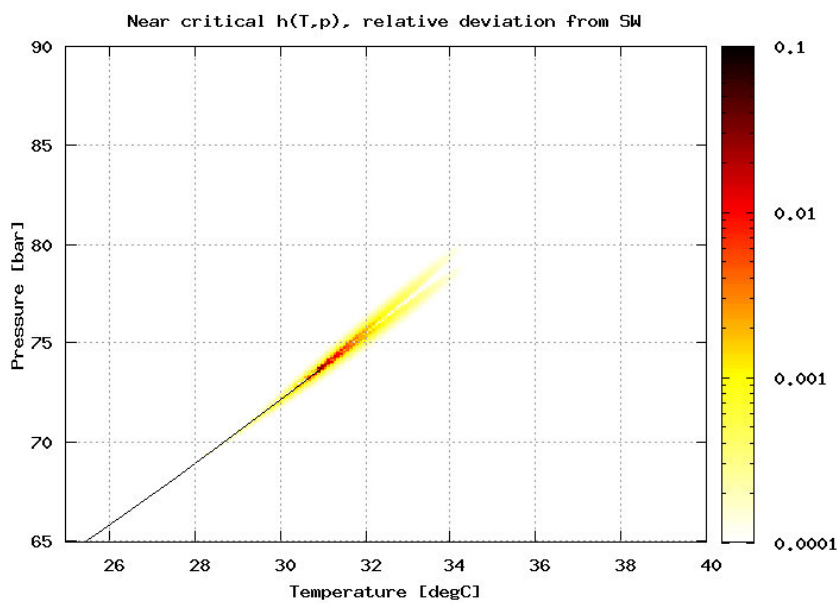
$h(s, p)$ was also well contained, all sampled deviations were relatively consistent in the scale of $1\text{E-}5$, as can be seen in Figure 3.17.

Table 3.17 shows a statistical analysis of the deviation for equation of state functions, and Table 3.18 shows the same information for the two implicit functions.

3. FAST THERMOPHYSICAL LIBRARY (FTL)



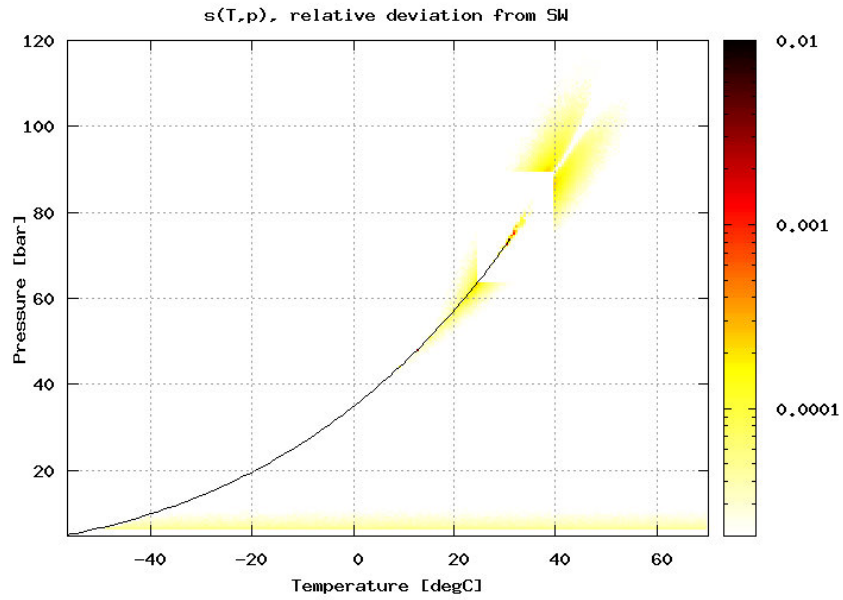
(a) Continuous region, main T-p table



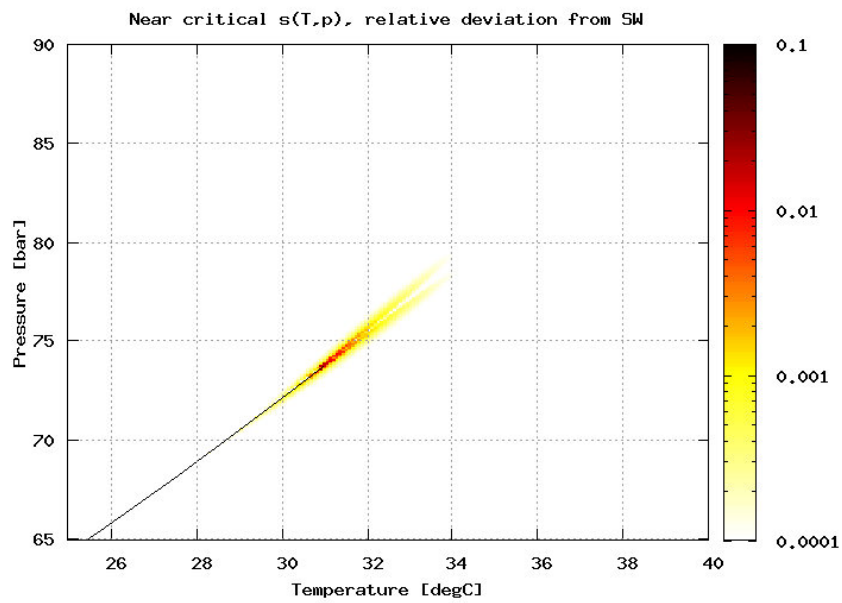
(b) Near-critical region with high resolution table

Figure 3.10: Distribution map of deviation compared to TL_{Span} , for $h(T, p)$

3. FAST THERMOPHYSICAL LIBRARY (FTL)



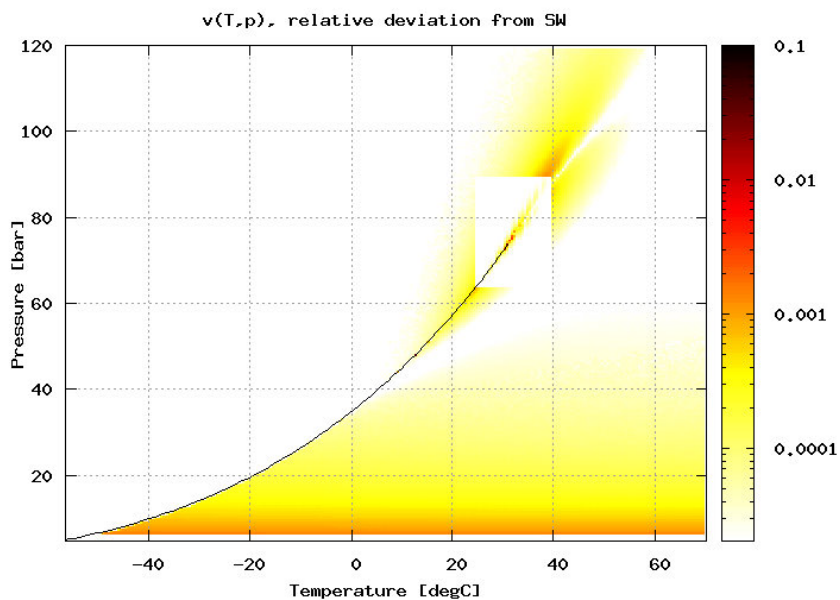
(a) Continuous region, main T-p table



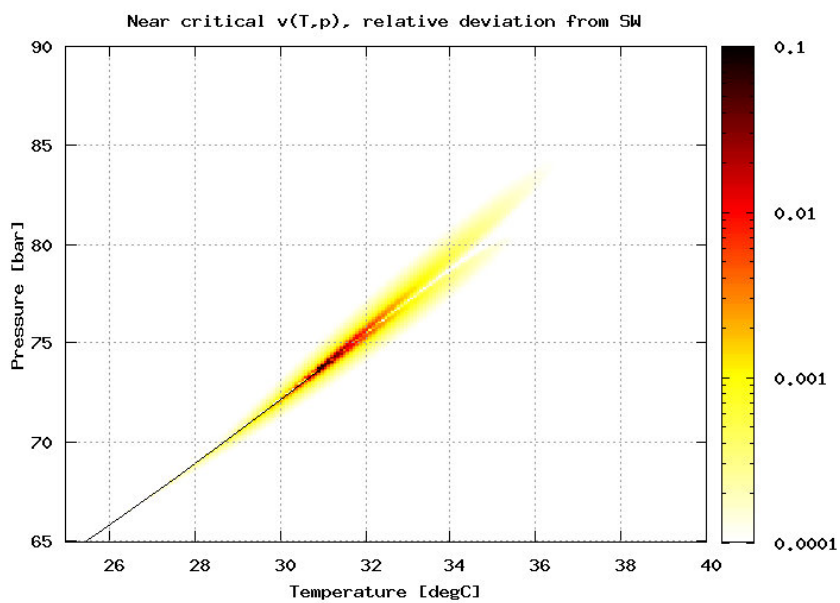
(b) Near-critical region with high resolution table

Figure 3.11: Distribution map of deviation compared to TL_{Span} , for $s(T, p)$

3. FAST THERMOPHYSICAL LIBRARY (FTL)



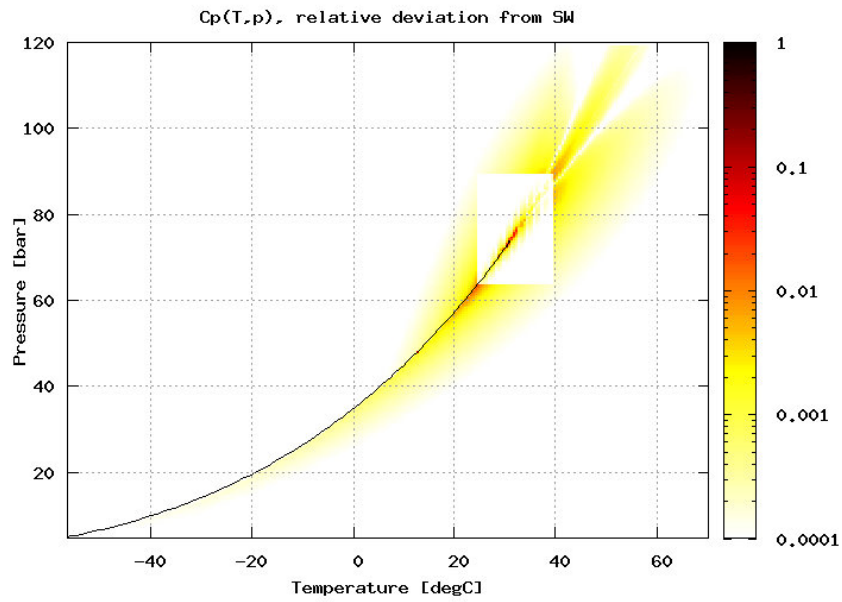
(a) Continuous region, main T-p table



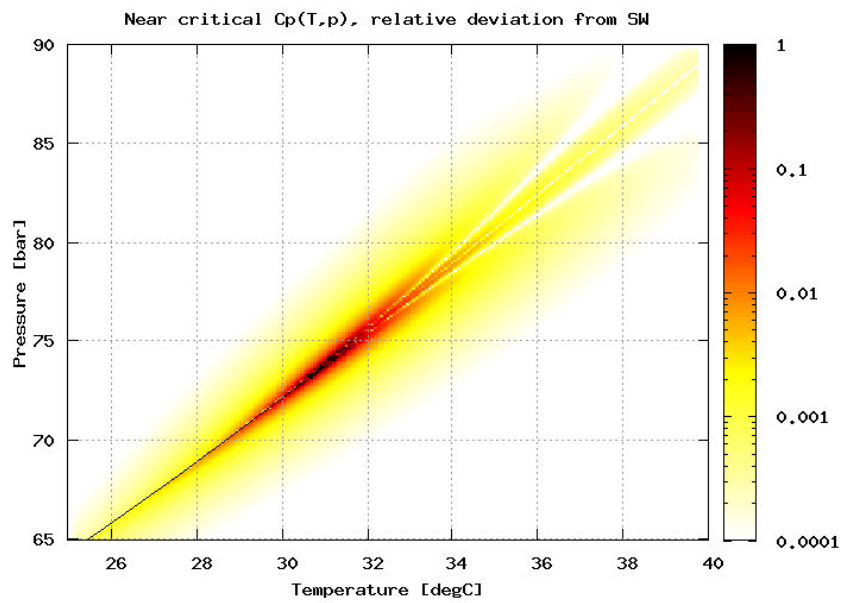
(b) Near-critical region with high resolution table

Figure 3.12: Distribution map of deviation compared to TL_{Span} , for $v(T, p)$

3. FAST THERMOPHYSICAL LIBRARY (FTL)



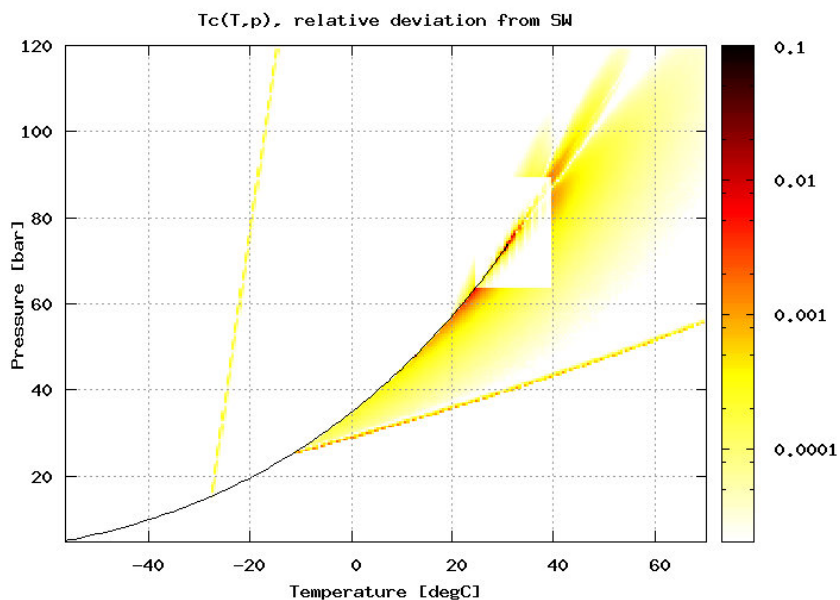
(a) Continuous region, main T-p table



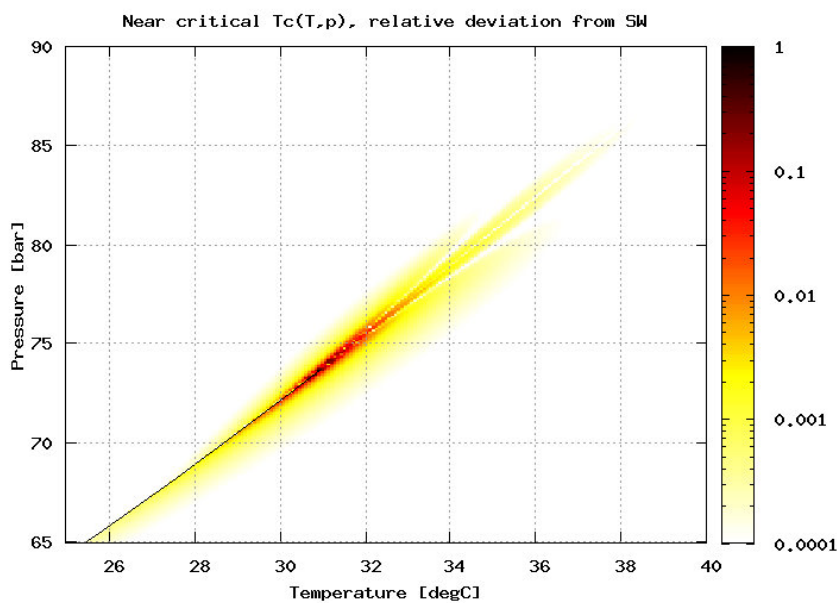
(b) Near-critical region with high resolution table

Figure 3.13: Distribution map of deviation compared to TL_{Span} , for $c_p(T, p)$

3. FAST THERMOPHYSICAL LIBRARY (FTL)



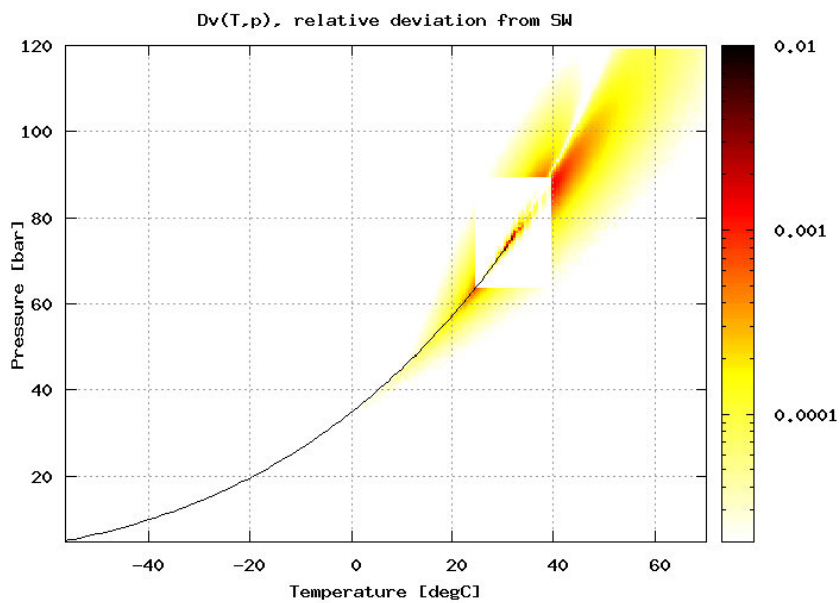
(a) Continuous region, main T-p table



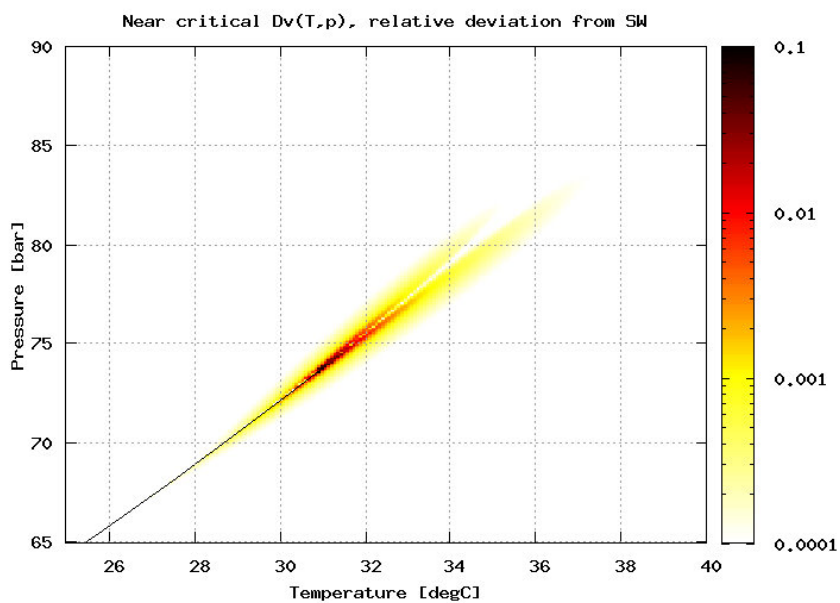
(b) Near-critical region with high resolution table

Figure 3.14: Distribution map of deviation compared to Vesovic et al., for $\lambda(T, p)$

3. FAST THERMOPHYSICAL LIBRARY (FTL)



(a) Continuous region, main T-p table



(b) Near-critical region with high resolution table

Figure 3.15: Distribution map of deviation compared to Fenghour et al., for $\mu(T, p)$

3. FAST THERMOPHYSICAL LIBRARY (FTL)

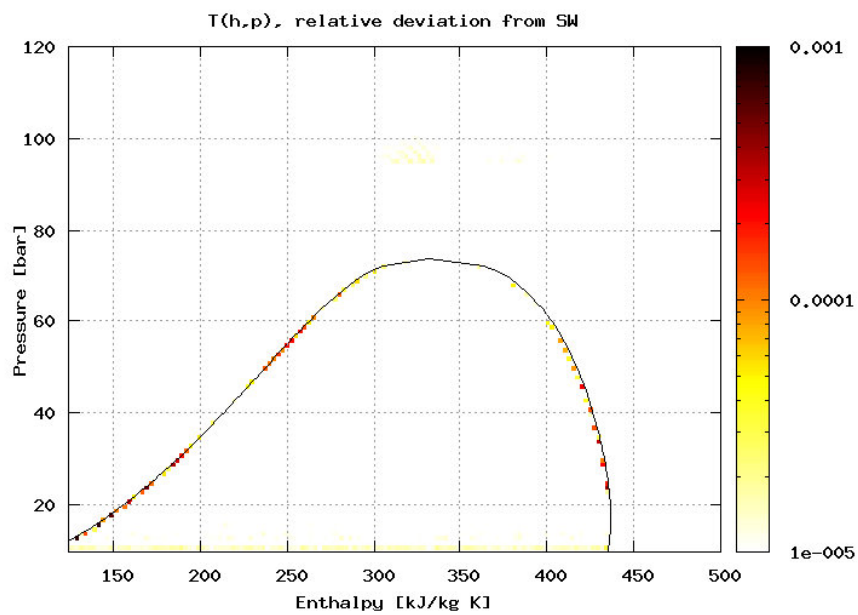


Figure 3.16: Distribution map of deviation compared to TL_{Span} , for $T(h,p)$

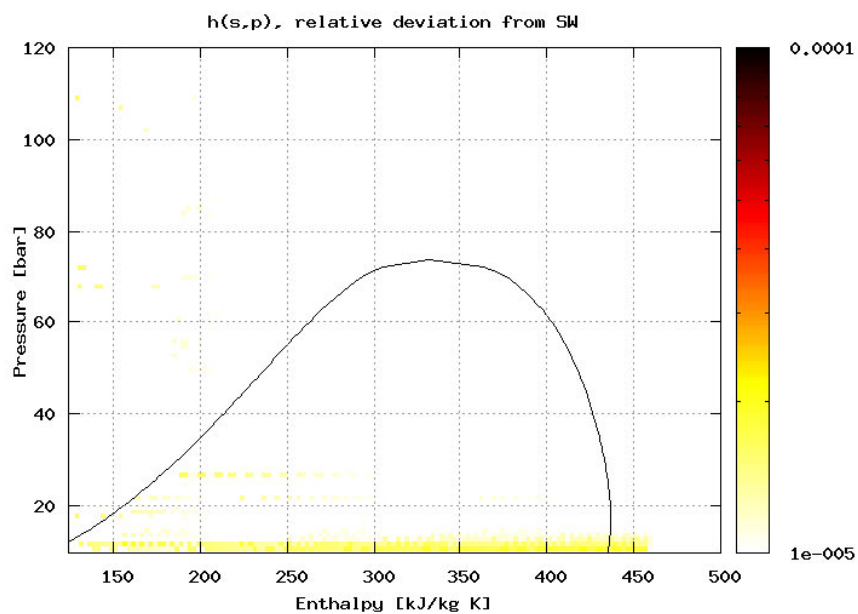


Figure 3.17: Distribution map of deviation compared to TL_{Span} , for $h(s,p)$

3.7.3 CSIM function profile test suite

A total of 10 million property function calls, distributed to match the function call profile of CSIM (see Figure 2.3), were calculated and timed.

Table 3.19: Performance results from CSIM function profile test

	No. Calls	TL_{Span} [s]	FTL [s]	TL_{Angus} [s]
Equation of state				
$f_{sat}(T)$ and $f_{sat}(p)$	4 435 000	3885.74	0.50	15.98
$f(T, p)$	1 750 000	153.68	0.67	31.28
$f(T, h)$	363 000	334.72	0.14	3.40
$f(h, p)$	149 000	639.35	0.20	14.84
$f(s, p)$	3 000	2.12	0.00	0.25
Transport data				
$\lambda(T, p), \mu(T, p)$	990 000	94.5	0.31	16.09
$f_{trans, sat}$	2 310 000	1092.96	0.23	16.42
SUM	10 000 000			

Total calc time [s]		6203.07	2.05	98.26
Relative calc time to TL_{Span}		100.0%	0.03%	1.58%
Relative calc time to TL_{Angus}		6313%	2.09%	100.00%

As can be seen from the results in Table 3.19, FTL reduced the calculation time from 6200 seconds (TL_{Span}) to just over 2 seconds. That amounts to a reduction of 99.97%. Compared to TL_{Angus} , the reduction was 97.9%.

Considered as calculation speed (number of calculations per time unit), FTL is on average approximately 3000 times faster than TL_{Span} , and almost 50 times faster than TL_{Angus} for this property function distribution.

The same test was also run on a different implementation of the Span-Wagner equation of state, using the more rapid auxiliary functions for calculation of some of the saturated properties. This reduced the calculation time with

almost 40% compared to the consistent TL_{Span} . The complete results can be seen in Appendix A.

3.7.4 CSIM simulation test suite

A test suite consisting of 6 test cases, a mix of optimization and simulation problems, were run using the three different thermophysical implementations. The 6 test cases are described in Appendix B, and the simulation output (results) key-values can be found in Appendix C.

Figure 3.18 shows a comparison of key values from the simulation results. For each parameter, both the average and maximum deviations for all cases are shown. Overall, FTL shows only minuscule variation from the TL_{Span} implementation, but using only about 0.2% of the CPU time.

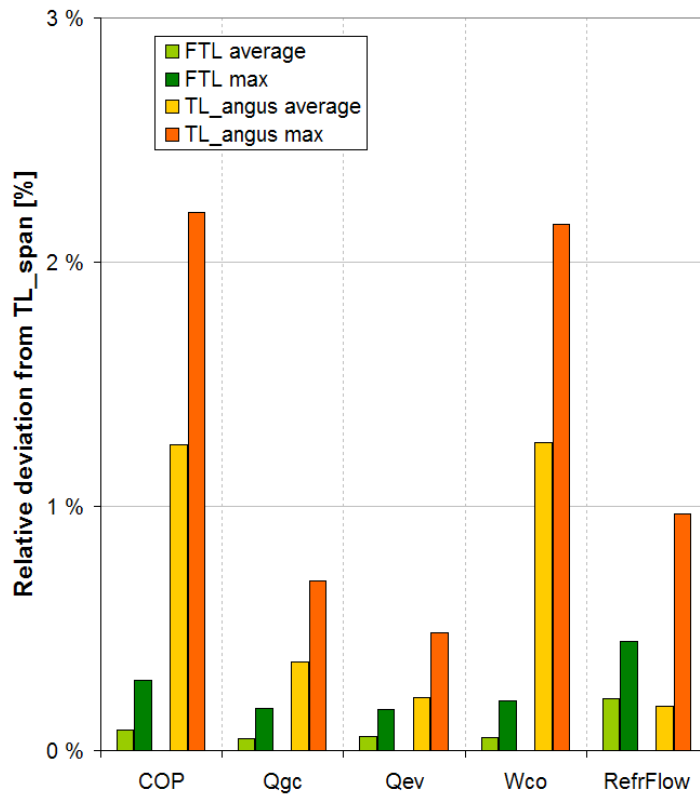


Figure 3.18: CSIM simulations, relative deviation from the TL_{Span} implementation

The results also indicate, as previously mentioned, that the TL_{Angus} implementation converged at slightly different system states. Table 3.20 shows a comparison of key values from the simulation results from case 1.

Table 3.20: CSIM test case 1 key results

Case	COP [-]	\dot{Q}_{gc} [W]	\dot{Q}_{ev} [W]	\dot{m}_{co2} [kg/s]	$\Delta T_{gc,out}$ [K]	T_0 [°C]	CpuTime [s]
TL_{Span}	3.46	49065	36101	0.224	9.02	-0.94	1118.51
FTL	3.47	49081	36116	0.225	9.03	-0.90	2.45
TL_{Angus}	3.41	49406	36166	0.224	9.09	-0.95	29.44
Deviation[%] (FTL vs. TL_{Span})	0.29	0.03	0.04	0.45	0.11	0.01	99.78

Table 3.21: CSIM CPU time analysis, based on 6 test cases

	Sum of CPU time [s]			Ratio TL_{CO2}
	Simulation	CO ₂ properties	Numerical	
TL_{Span}	5668.7	5660.4	8.28	99.9%
FTL	13.24	4.96	8.28	37.1%

Figure 3.19 shows a comparison of the CPU-time for each of the 18 subcases. On average, FTL reduced the simulation time with 99.77% compared to TL_{Span} , and with 90.4% compared to TL_{Angus} .

3.7.5 Intel and GNU compiler comparison

Intel and GNU Fortran/C compilers are both reputable, well established compilers. As all compilers tend to use different strategies and techniques when compiling, the performance of the finished software may vary. Table 3.22 shows a comparison of used CPU time for a simulation case in CSIM. The Intel compiler used the optimization flags `/O2 /QaxN` and the GNU compiler (version 3.4.2) used `-O2`, both compilers were optimizing for high performance. The test computer was the same as described in Chapter 3.6.2.

It is apparent that the Intel compiler reduces the calculation time of the TL_{Angus} implementation by approximately 93%. The FTL implementation shows a reduction of 39%, while the TL_{Span} shows a smaller reduction of 17%.

3. FAST THERMOPHYSICAL LIBRARY (FTL)

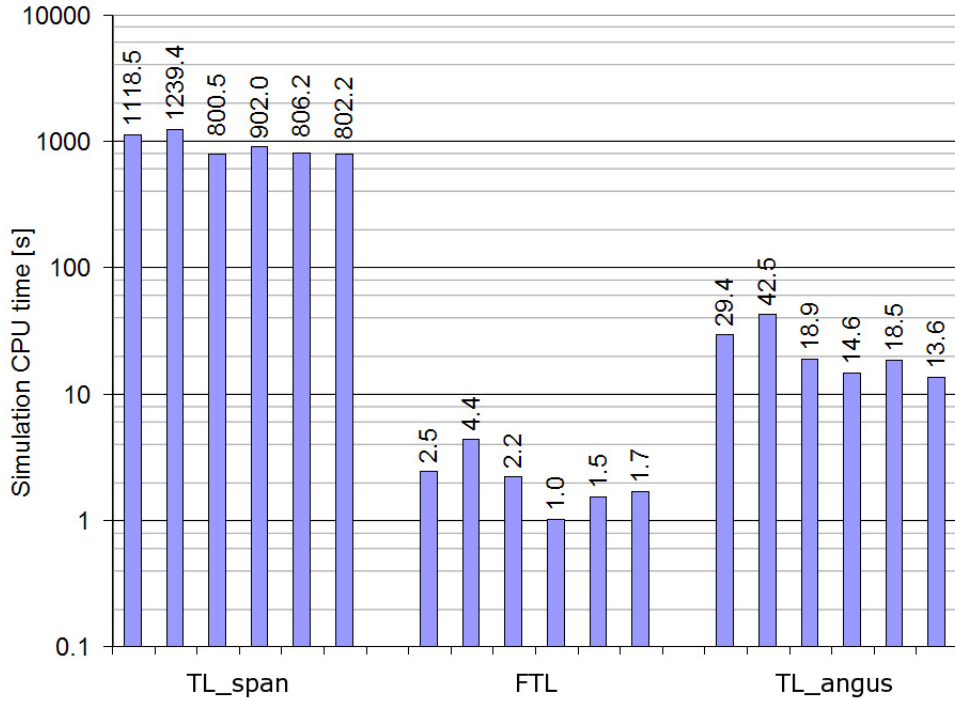


Figure 3.19: CSIM simulation CPU time comparison. NB: logarithmic scale!

TL_{Angus} and FTL are both programmed in pure C, and obviously there is a real gap in compiler performance for this kind of source code. The Span-Wagner equation of state is programmed in Fortran, and it appears that both Intel and GNU produce software with similar performance for the Fortran code.

Table 3.22: Simulation CPU time comparison for GNU C compiler and Intel C compiler suites

	TL_{Span}	FTL	TL_{Angus}
GNU [s]	1166.6	4.4	320.3
Intel [s]	1054.1	2.7	23.0
Intel time reduction	17%	39%	93%

When the work on the FTL implementation first commenced, only the GNU compiler was available for use. The very first calculation speed indicators

3. FAST THERMOPHYSICAL LIBRARY (FTL)

compared to TL_{Angus} were therefore considerably more impressive. With the GNU compiler, CSIM using the TL_{Angus} was 70-90 times slower than the FTL implementation. After the switch to the Intel compiler, this was reduced to a factor of roughly 10.

3. FAST THERMOPHYSICAL LIBRARY (FTL)

4. ADVANCED PLATE HEAT EXCHANGER MODEL (APEM)

4.1 Background

4.1.1 Introduction

The plate heat exchanger (PHE) was the first really compact liquid-to-CO₂ heat exchanger type. So far, heat exchangers of the co-axial type (tube-in-tube) have been used for this application. While these heat exchangers can be well matched for the heat transfer characteristics of CO₂, they are impractical for larger capacities due to their inherent low compactness and high material costs. With PHE's now becoming available for CO₂, this natural refrigerant becomes a real alternative for larger heat pumping applications, considering both efficiency and economy. However, in order to design good systems, there is a need for mathematical models that correctly represent both components and system behavior.

The in-house simulation tool CSIM (see Chapter 2.3) was used as a framework for implementation of the new model. However, the complex pass arrangements possible in PHE's, could not be well represented by the existing system calculation and component description convention.

4.1.2 Plate heat exchanger design

Plate heat exchangers are made up of plates that are clamped together in a frame with rubber gaskets between each plate. Alternatively, the plates are welded or brazed together. The gasket position on each plate determines the flow arrangement through the plates, which allows the heat exchanging fluids to flow in alternate plate channels. In a similar manner, this may also control different pass arrangements. A principle schematic of a plate heat exchanger can be seen in Figure 4.1.

The plates are made from pressed sheet steel, with common thicknesses between 0.4-0.6 mm. The plates are pressed with a pattern, most commonly chevrons. It may be desirable to have contact points between plates to ensure structural rigidity. For chevron-type plates this is often done by stacking

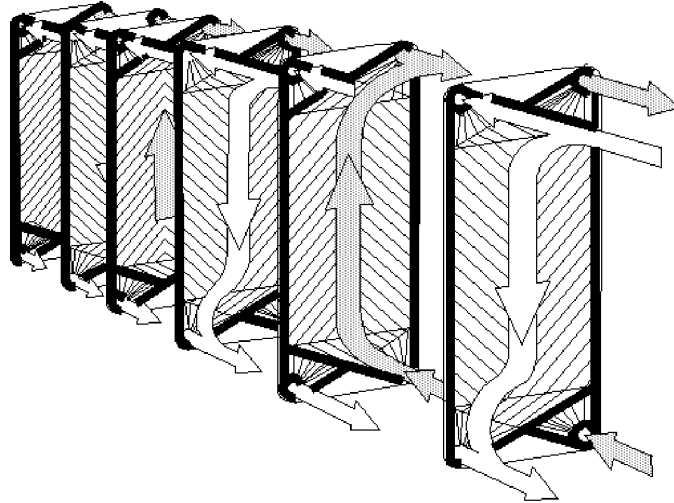


Figure 4.1: Principle schematic of fluid flow in a plate heat exchanger. (From <http://geoheat.oit.edu/>)

alternate plates with reversed chevron angle.

Arrangements of fluid stream passes can be made to enhance the performance. In general, high fluid velocities are desirable with respect to heat transfer characteristics and fouling issues, but will induce higher pressure drop. Figure 4.2 shows a single/single-pass arrangement, and Figure 4.3 shows a two-pass/two-pass arrangement.

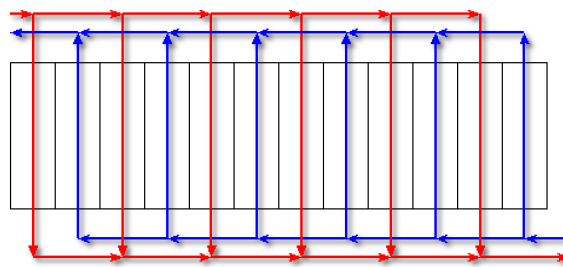


Figure 4.2: Plate heat exchanger with single-/single-pass arrangement

Pass configurations can also be more complex, for instance with an unmatched number of passes for each fluid. Figure 4.4 shows an extreme variant with 10 passes for the refrigerant, and a single pass for the secondary fluid. This may be a solution for streams with very mismatched flow rates.

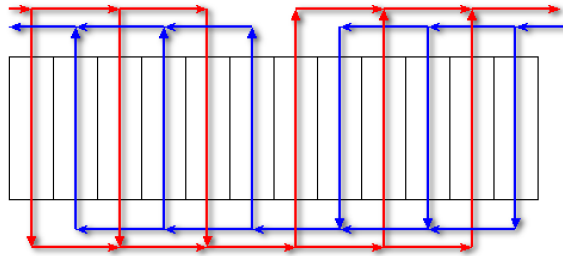


Figure 4.3: Plate heat exchanger with two-/two-pass arrangement

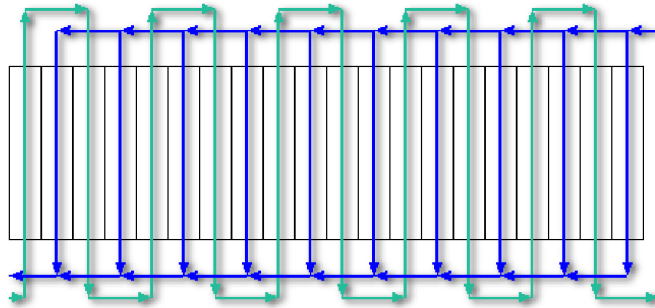


Figure 4.4: Plate heat exchanger with 10-pass/single-pass arrangement

New developments in plate design allows stacking of asymmetric plates to form different flow cross section areas for alternating channels, another option for mismatched fluid flow rates. Figure 4.5 shows a principle sketch of a cross section of stacked asymmetric plates.

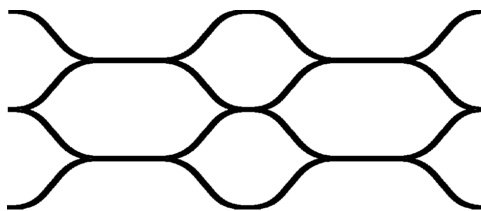


Figure 4.5: Cross section of stacked plates with asymmetric pattern

Plate heat exchangers are used in many applications due to the compactness and cost efficiency, from food processing to district heating plants.

4.1.3 Modeling of plate heat exchangers

Almost all models of plate heat exchangers found in literature are stand-alone, component-only models. Models used in circuit simulations have other requirements, particularly to calculation load. Still, the popularity of these heat exchangers have led to many reports of in-house developed models.

Lyytikainen et al. (2009) described a modeling tool for speeding up CFD simulations of plate heat exchangers for design purposes. The 3-dimensional channels formed by stacked corrugated plates are mathematically reduced to two dimensions, by integrating the flow and energy equations of the channel gap between plates. The overall estimation of pressure drop is quite accurate, but this method is not suitable for system simulations. The described model only covers single-phase flows, and the calculation load is still too high.

Gut & Pinto (2003) described a model for plate heat exchangers with generalized configurations, allowing a very large variation in arrangements. However, this model is for single phase flow only, and it also disregards mass flow distribution between channels.

4.2 PHE component model for CO₂ system simulation

4.2.1 Introduction

As mentioned earlier, the most important criteria for a component model is being able to predict the governing physical behavior. For the new PHE model, this includes the ability to predict local behavior for separate, parallel channel streams. This gives the ability to investigate both the occurrence and effect of asymmetric heat transfer and mass flow distribution between channels. These mechanisms are described further in the next section.

Implemented into CSIM, component and flowsheet equations are simultaneously solved, as opposed to the components being “black boxes” with only inlets and outlets known to the circuit. This is an advantage with respect to rapid and consistent convergence in simulations and, particularly, optimizations. The disadvantage is that very large problems may be difficult for the solver to handle. It can be a difficult task to balance model resolution and level of discretization with simulation time and consistent convergence.

4.2.2 Describing local behavior in channels

A plate heat exchanger is characterized by fluids flowing in parallel channels in one or more passes. In simpler models, all of these parallel channels in the same pass are mathematically considered as one. This simplification ignores important details of mal-distribution of fluid and asymmetric heat transfer in parallel channels, and is not usable at all for configurations with overlapping passes for the two fluids.

The outermost plate channels on each side of the heat exchanger have only half the effective heat transfer area compared to internal channels, and thus a lower thermal efficiency. The lower heat transfer in these channels in turn affect their neighbor channels, and a spread in temperature profiles for parallel channels are observed. This is well documented, for instance by Gut & Pinto (2003).

Figure 4.6 shows temperature profiles for a 13-plate (6+6 channels) single/single-pass gas cooler based on a simulation. In the temperature profile plot, CO₂ at super-critical pressure (95 bar) enters from the top left and cools in the 6 parallel plate channels. Water enters at the bottom right of the plot, flowing in the opposite direction in alternate plate channels. The lower-efficiency channels at each end of the stack are quite pronounced in this plot, and are represented as the top red and the bottom blue lines, for refrigerant and water respectively.

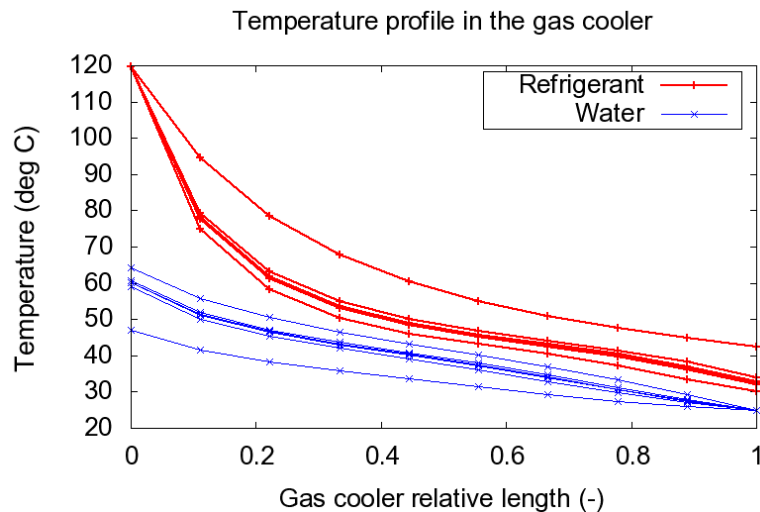


Figure 4.6: Parallel stream temperature profile (CO₂ gascooler, 13 plates)

In multipass heat exchangers, channels adjacent to a pass change also experience lowered thermal efficiency. Depending on the fluid temperatures in the adjacent pass, this can also cause zero- or reversed heat flow, as noted by Bassiouny & Martin (1985).

For two-phase fluids, the asymmetric heat transfer may also cause noticeable maldistribution of mass flow between channels. Fluid channels with higher vapor qualities will have higher friction losses, mainly due to the increased fluid velocity. As channels have asymmetric heat transfer, there will also be a difference in vapor qualities and thereby nominal friction losses. As all channels in a pass must have the same pressure drop, more mass flow will be distributed into channels with lower vapor qualities. In evaporators, more mass flow could be distributed to less efficient channels, further increasing the same effect. This can cause some channel flows to reach superheated vapor states while the mixed fluid outlet state is still two-phase. In addition to affecting heat transfer, this can also cause pinch points in individual channels. Condensers may see the opposite effect, where more mass flow is distributed to the most efficient channels.

Asymmetry in parallel channels in same pass will be a key element for discussion later in the chapter.

4.2.3 APEM design criteria

The development of a new PHE-model was triggered by the need to see how heat exchanger design can impact the entire system performance, more than just the performance of the component itself. This is reflected in how the model is designed, and the included features.

Ideally, the model should be usable for all possible plate and stream configurations. CSIM is primarily a design tool, where several different configurations are investigated and compared in each case. Both simulation time and configuration simplicity and convenience are important.

The level of detail must, as in all similar software, be carefully balanced between realistic predictions of behavior, and being time-efficient and sufficiently simple to use. In this work, only chevron-pattern plates are considered, as these are most common. The design criteria for the PHE model are:

- Configurable plate geometry including asymmetric flow cross section area for the two sides.

- Configurable with respect to channel and pass arrangements.
- Possibility for calculation of parallel channels in same pass separately
 - Compare temperature profiles for different channels in same pass
 - Identify local pinch points, for instance due to local evaporator superheat
 - Compare the relative distribution of mass flow between channels in same pass due to channel pressure drop.
- Model must be suited for use in circuit simulations.
- Selected plate geometry parameters are applicable as variables in system optimization

4.2.4 Main physical mechanisms

The advanced plate heat exchanger model (APEM) accounts for the following physical mechanisms, for each discretized element (*subhx* - "sub heat exchanger").

Heat transfer: Heat transfer between channels is governed by the local heat transfer coefficient from the fluids to the plate wall, as well as the thermal conductivity across the wall itself. The latter has only a very minor effect on thermal resistance due to the small wall thickness found in plate heat exchangers.

Pressure drop in channels and mass flow distribution: The pressure drop is calculated for each *subhx* as a result of the forces from friction, gravitation and acceleration from change in density and void. The total pressure drop in each channel governs the distribution of mass flow between channels in the same pass.

4.2.5 Other mechanisms

Longitudinal heat conduction: Ciofalo (2007) described a model to predict large-scale and local effects of longitudinal heat conduction in plate heat exchangers. He found that longitudinal heat conduction could in fact improve heat transfer over plates with unmatched convective heat transfer coefficient profiles. However, any modeling of local effects require a very high level of discretization to capture the local effects around each chevron. This is not

feasible for a system design application. The effect of longitudinal heat conduction will for almost all conditions be very small, and is not included in this model.

Pressure drop in conduits and inlet and outlet ports: In the current model, pressure drop in ports is not calculated. Instead there is a multiplication factor for increased pressure drop that can be manually set to incorporate a fixed channel-to-port pressure drop ratio.

Due to issues with maldistribution, it's desirable to have governing pressure drop in the channels. Still, calculating at least some of the pressure drop components based on the diameter and length of inlet and outlet tubes/channels is feasible to include in the future. This should include the variable distance of inlet and outlet tubes to each channel. The basis for individual channel pressure drop is already in place.

Bassiouny & Martin (1984a,b) performed a theoretical analysis of flow distribution and pressure drop in Z-type and U-type arrangement plate heat exchangers, all though only for single phase flow. The flow distribution was governed by the pressure distribution in the intake and exhaust conduits, based on the ratio of flow areas in conduits and channels.

Kaka & Liu (2002) described a simple expression for estimating port losses for single phase flows in plate heat exchangers. This could be extended for two-phase flows and used as a simple estimate of port losses in future work. The pressure drop is based on the velocity head of the flow:

$$\Delta p_{port} = 1.4 \cdot \frac{G_p^2}{2\rho} \quad (4.1)$$

D_p is the port diameter and the mass flux G_p is defined as:

$$G_p = \frac{\dot{m}}{\frac{\pi D_p^2}{4}} \quad (4.2)$$

Liquid- and vapor mal-distribution in headers: Calculation of liquid and vapor mal-distribution in headers is not included in this model. Instead, all parallel channels in the same pass have the same inlet conditions, including vapor fraction. It is not clear how a general model of separation in headers could be correlated and implemented at this level.

4.3 Mathematical modeling of the plate heat exchanger

4.3.1 Overview

The following assumptions were made for the heat exchanger model:

- Steady-state operation
- No heat loss to the ambient - end channels have heat transfer to one side only
- No longitudinal heat transfer
- Ideal mixing of fluid at the start of each pass - channels have identical inlet conditions
- Pressure drop in inlet- and outlet ports has neglectable effect on mass flow distribution between channels

The model is specified using real geometry as input. The specification of pass arrangements should be simple and intuitive, yet flexible.

The model is designed to separately calculate individual channels in all passes for both fluids. All channels except in both ends, have two neighbor channels. While other parallel-flow heat exchanger models in CSIM "pair up" one secondary fluid element and one refrigerant element in each heat exchanger element, this is not the case in individual-channel calculation for plate heat exchangers. Instead, the heat balance must be fulfilled simultaneously for each discretized vertical cross-section spanning all channels.

4.3.2 Variable description

During development, there has been a focus on keeping a low number of describing variables, and also trying to continue the variable description convention already present for other heat exchanger types in CSIM. Table 4.1 shows the describing variables for the geometry in the plate heat exchanger model. In addition comes selection of pressure drop (Δp) and heat transfer coefficient (HTC) correlations for single phase, condensation, evaporation and secondary fluid.

4. ADVANCED PLATE HEAT EXCHANGER MODEL (APEM)

Table 4.1: Plate heat exchanger variable description in GUI

Variable name	Variable description	Type
PLATEMAT	Plate material, for instance stainless steel or titanium	choice
FLOWARR	Global heat exchanger flow arrangement, counterflow or co-current	choice
PLATEAREA	Single plate effective heat transfer area	float
CSAREF	Refrigerant channel cross section area, refrigerant	float
CSASEC	Single plate stream cross section area, secondary fluid	float
WALLTH	Plate wall thickness	float
BETA	Plate chevron angle	float
PHI	Surface enhancement factor (due to chevrons)	float
PWIDTH	Single plate width	float
NBI	Number of segments per plate	integer
NCHAN	Total number of channels for each flow	integer
PASSVEC	Vector containing the number of passes for each stream, e.g. 3 passes for the refrigerant and 2 for the secondary fluid	integer
CHANVEC	Vector containing number of parallel channels in each pass going downstream for each fluid. The total number must match NCHAN for each fluid, and the number of passes must match PASSVEC. {2 4 4 5 5} refers to 2+4+4 channels on refr. side, and 5+5 channels on sec. side	integer

4. ADVANCED PLATE HEAT EXCHANGER MODEL (APEM)

Continued...		
Variable name	Variable description	Type
NXCHAN	Number of physical channels per numerical channels. The model can represent several physical channels by a single numerical one to reduce the number of variables.	integer
DPHEADER	Pressure drop in headers and ports can be set to a set fraction of the channel pressure drop	float
GRDISTKEY	Choice to turn on or off distribution of mass flow between channels in same pass based on local ΔP	Choice
Extra optimization variables		
TUNCA	Choice to include CSA for the refrigerant side as an optimization variable	choice
DPVAL	When TUNECAKEY is active, DPVAL is the minimum allowed Δp for the entire heat exchangers refrigerant flow	float
TUNCASEC	Choice to include CSA for the secondary fluid side as an optimization variable	choice
DPVAL	When TUNECAKEY is active, DPVAL is the minimum allowed Δp for the entire heat exchanger secondary fluid flow	float

The option to “merge” channels to reduce total number of variables, is very relevant for heat exchangers with a relatively large number of plates. The parameter NXCHAN represents the number of physical channels per numerical (calculated) channels, meaning that this number must be a denominator of the total number of channels for each fluid.

As described in Chapter 2.3, CSIM uses Δh and ΔT as the free variables when solving the heat exchanger equations, Δh for refrigerant and ΔT for secondary fluid subhx's respectively. Initial values for each subhx can be manually set by the user.

4.3.3 Description and model in C

Based on the geometry variables from the GUI, a 2-dimensional NBI x NCHAN*2 array of nodes is generated. Each node contains the following information:

- Node index number
- Pass index number
- Number of channels in current pass
- Channel index number of current pass
- Fluid (refrigerant or secondary fluid)
- x and y coordinates (channel and segment number, respectively)
- Flow direction (up or down)
- Key to mark inlet element
- Pointers to upstream node or nodes (by node numbers).

An array index is also generated, which returns the node index number for a given x and y coordinate. Much of the included information relates to identification of absolute and relative addresses. This is very useful for the component calculation, as it allows quick and robust access to neighbor channel nodes.

In the heat exchanger calculation routine, the following data are calculated for each node using the current state of the free variables:

- The heat flow: $\Delta \dot{Q}_{fluid}$ ($\Delta h_{refr} \cdot \dot{m}_{refr}$ or $\Delta T_{sec} \cdot c_{p,sec} \cdot \dot{m}_{sec}$)
- Fluid state properties for inlet and outlet, such as T, p and h.
- Local heat transfer coefficients to both left and right side of channel

- Pressure drop: Δp
- Thermal resistance in wall, left and right side

The transferred heat is also calculated;

$$Q_{trans,left} = U_l \cdot A \cdot AMTD_l \quad (4.3)$$

$$Q_{trans,right} = U_r \cdot A \cdot AMTD_r \quad (4.4)$$

where

$$U_l = \frac{1}{R_{htc,i,l} + R_{wall} + R_{htc,neighbor,r}} \quad (4.5)$$

$$U_r = \frac{1}{R_{htc,i,r} + R_{wall} + R_{htc,neighbor,l}} \quad (4.6)$$

Note that within each subhx, the local heat transfer coefficient may differ from the left and right wall depending on the wall temperatures.

The mass flow distribution between channels are decided by the solved variable for “mfac” representing the ratio of channel mass flow to average mass flow. The mass flow for each channel “j”:

$$\dot{m}_j = mfac_j \cdot \dot{m}_{average} \quad (4.7)$$

where the average mass flow $\dot{m}_{average}$ is calculated from:

$$\dot{m}_{average} = \frac{\dot{m}_{tot}}{n_{chan}} \quad (4.8)$$

There must be a set of equality equations to determine the free variables. There is one constraint for each subhx to find the heat balance, and one for each parallel channel in each pass to find the mass flow distribution.

Equality constraints for each heat exchanger element, both secondary fluid and refrigerant nodes:

$$\frac{Q_{fluid_i} - Q_{transLeft_i} - Q_{transRight_i}}{1 + Q_{fluid_i}} = 0 \quad (4.9)$$

Constraints for each channel “j” in pass “k”:

$$\frac{\Delta p_j - \Delta p_{average,k}}{1 + \Delta p_{average,k}} = 0 \quad (4.10)$$

In both these constraints, the denominators are only included for scaling purposes.

4.4 Correlations for pressure drop and heat transfer coefficients

4.4.1 Introduction

As for other types of heat exchangers, there exist a wide and increasing range of general pressure drop and heat transfer correlations. For use in CSIM, correlations should cover a wide range of geometries and load characteristics. Therefore, correlations incorporating describing geometry parameters are preferred over simpler correlations with empirical constants and narrow area of validity.

The review paper by Garcia-Cascales et al. (2007) considered the general-purpose usability of a range of plate heat exchanger correlations for evaporation, condensation and single-phase applications. It is clear that the choice of correlation can have a huge impact on the predicted performance, as many of the reviewed correlations differ considerably in value.

Verifying correlations for CO₂ plate heat exchangers with variable geometry is considered to be outside the scope of this work. However, more general correlations using key geometry parameters such as chevron angle and plate pitch, are preferred over narrower expressions correlated only for a single, fixed plate geometry.

There is currently not a very wide selection for general geometry-based correlations for plate heat exchangers available. Particularly is this the case for two-phase flows. The correlations used for simulation in this work are described in Chapter 4.6.3.

4.4.2 Consistency over phase boundaries

To ensure consistency in calculation of pressure gradients and heat transfer coefficients over phase lines, the implemented correlations were combined asymptotically in the border regions. Without this transition smoothing, there could be a very large step in $\frac{\Delta p}{\Delta l}$ or heat transfer coefficient from one node inside the two-phase area to the next node just outside the saturation line, where a new correlation was set in effect. Such inconsistencies can significantly influence convergence.

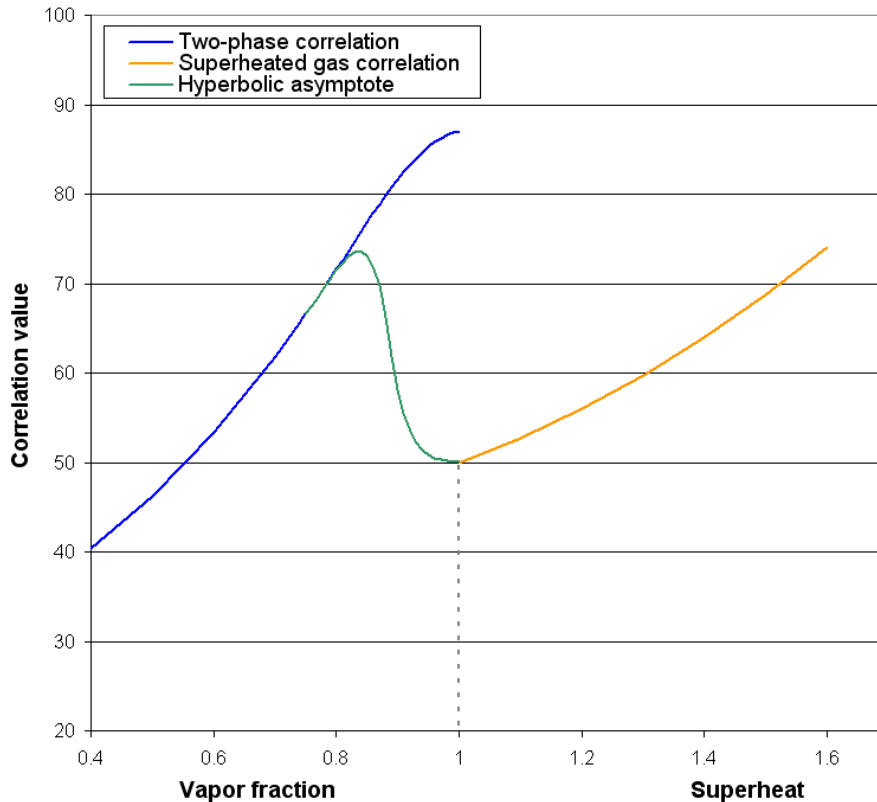


Figure 4.7: Asymptotic combining of two-phase and single-phase correlations in an evaporator using a hyperbolic tangent function

Figure 4.7 shows the principle of this combining function. For evaporation, the combining function was used between 0.8 vapor fraction and the saturated gas line. For condensation, the correlations are smoothed in both ends. The combining function was here used from the saturated gas line to 0.9 vapor quality, and from 0.1 vapor fraction to the saturated liquid line.

4.5 Changes in system calculation and solving

4.5.1 Overview

As mentioned earlier, CSIM had to undergo considerable modifications in order to accept the new plate heat exchanger model. In particular, the direction and sequence of calculation for both system and component models had to be altered.

The main changes are:

- Changed calculation sequence for components in the circuit
- Changed calculation direction for components on the low pressure side, including evaporator
- Changed solved variable for evaporator outlet saturation temperature changed to *inlet saturation temperature* to support calculation of individual channels
- Implementation of an initial value generator for gas cooler and evaporator, to improve convergence with the new, theoretically less favorable control variables in the evaporator
- Removal of "high-side pressure" as a separate solved variable, as it is not needed with the new component calculation sequence

The system solving mechanics both before and after the modification for plate heat exchangers are described below.

4.5.2 Original system solving

A brief look at the mechanics behind the circuit solving in CSIM is necessary to better understand some of the issues around the implementation of the new plate heat exchanger model.

As can be expected in a circuit simulation, the output refrigerant state from one component may become the input state in another component. For instance, the outlet condition of refrigerant from the compressor is identical to the inlet condition in the discharge line, since the two are connected together in the circuit flowsheet. However, the direction and sequence of component calculation does not always follow the same direction as the refrigerant flow.

Instead it is based on engineering knowledge of both thermodynamical sensitivity in the calculations, and the control of real-life heat pumping cycles. In most cases, the most stable system variable is the evaporator outlet state. In both simulations and real-world applications, this state in terms of vapor fraction or superheat, is a very well defined reference. Figure 4.8 shows a principle schematic of the original circuit flowsheet calculation in CSIM.

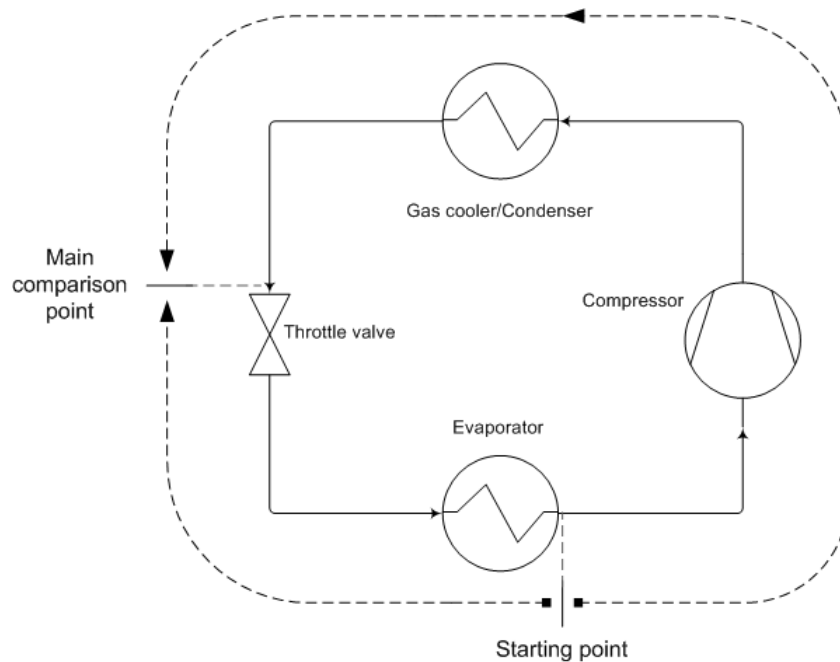


Figure 4.8: Original system calculation procedure in CSIM

From the reference point in the evaporator outlet, the system is calculated downstream through each component until the inlet of the throttling valve. Then jumping back to the evaporator outlet, calculating the evaporator upstream (“backwards”) and continuing through the distributor tubes and the throttle valve. The circuit balance will then be determined by an enthalpy comparison at the inlet (or outlet for that sake) of the throttle valve.

A slightly bad solver guess or initial value for the evaporation temperature¹ will typically cause a relatively minor difference in enthalpy at the comparison point. This is due both to the physics, and the intuitive nature of the evaporation temperature. With some experience, an initial value can usually be estimated within 5 K of error in most cases, by considering the heat

¹ Strictly: the evaporator outlet saturation temperature

exchanger areas, temperature of the secondary fluid, flow rate ratios etc.

4.5.3 New system solving

From the calculation procedure described in chapter 4.5.2, the key differences are new evaporator variables and a new circuit comparison point. System calculation is now performed entirely along the flow direction of refrigerant, starting from the compressor outlet state. This state is not as well defined as the evaporator outlet, but can still be estimated with decent accuracy using either engineering experience, hand calculation or by glancing at a T-s or log p-h diagram.

In addition to balancing all components individually, the flowsheet balance must also be achieved. The balance is fulfilled when the calculated values for the compressor outlet state and mass flow match the solver-guessed initial values for the same iteration. Figure 4.9 shows a principle schematic of the new circuit flowsheet calculation in CSIM.

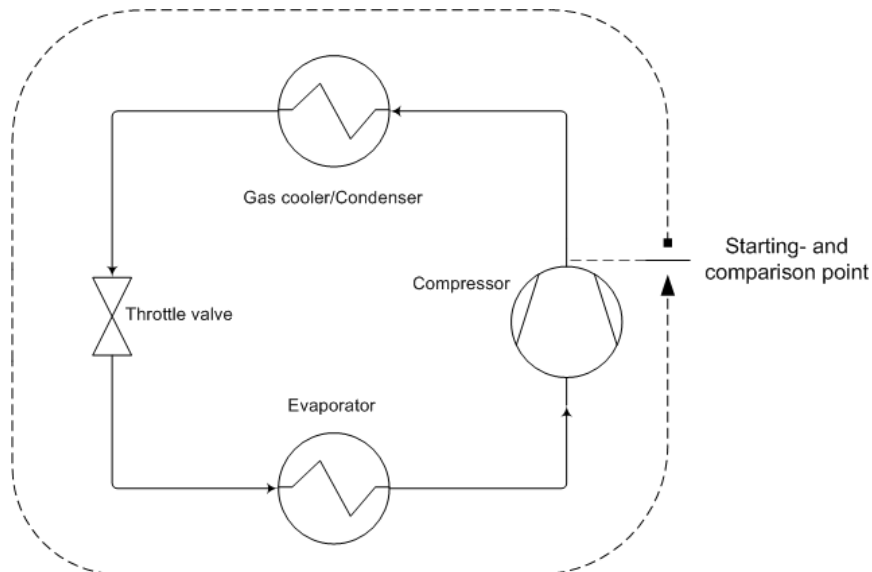


Figure 4.9: New system calculation procedure in CSIM

With the evaporator control variables now being inlet saturation temperature and outlet vapor quality/superheat, the circuit may have become less robust with respect to solver convergence. When setting or changing the evaporator inlet temperature (for initial value or by the solver during simulation), even

a small change may cause a substantial change in the outlet condition and/or cause pinching issues or temperature crossings. These problems are less likely to occur when starting the simulation with good initial values for the evaporator. Ideally, the evaporator's variables (initial values) should be set so all the local heat balances are fulfilled.

A special procedure for balancing the main heat exchangers (evaporator and gas cooler) was implemented by extracting only the necessary information, variables and constraints and using the solver to find the balanced solution. This procedure is implemented as an option in CSIM to be performed before starting the full system simulation. Starting with balanced heat exchangers also considerably reduces the number of iteration needed and the total simulation time. This is expected, as most of a circuit's variables are found in the heat exchangers.

4.6 Example-circuit simulation with advanced plate heat exchanger model

4.6.1 Overview

To demonstrate the capabilities of APEM, a test case has been prepared. The case describes the design point for a theoretical heat pump plant for an office building with heat loads connected in series. The gas cooler heats the water from 25 to 60°C, which covers approximately 70% of the required power in a 80/25°C hydronic heating system. A 25°C return temperature is feasible in buildings with approximately 50% ratio of ventilation air heating in north-European climate. The heat source is water at 6°C.

The system control is simple. The low-pressure is controlled by the a fixed evaporator outlet condition of 93% vapor fraction, and the high side pressure is controlled by the gas coolers heat load requirement. An internal heat exchanger boils off the remaining liquid on the low pressure side, and reduces the high-pressure side temperature before the throttle valve. Figure 4.10 shows a principle sketch of the circuit (low pressure receiver not drawn).

This test case will be simulated several times with the same conditions but with different combinations of heat exchanger models for the evaporator and gas cooler; a simple "uniform" model, and the more detailed "APEM" model. The uniform model assumes uniform distribution of heat transfer, pressure drop and mass flow in all parallel channels, and numerically handles all chan-

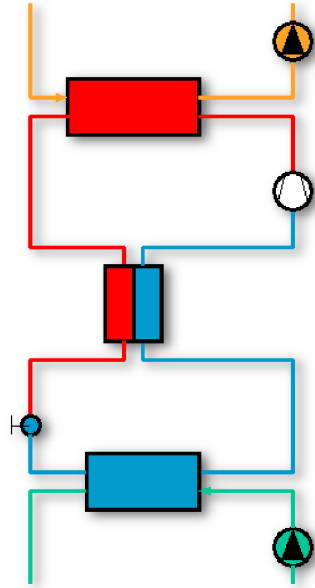


Figure 4.10: CSIM test case circuit

nels as a single channel. APEM calculates all channels separately.

The aim of this simulation was to show the different system performance with uniform and detailed models. Therefore, the system performance was made very dependent of heat exchanger performance, in order to better visualize the differences. Both the gas cooler and the evaporator have only 13 plates, 6 channels for each fluid. This allows a reasonably high level of discretization of each channel, and the output for each channel was distinguishable in the result plots. Both the evaporator and the gas cooler were single-pass, counterflow heat exchangers.

4.6.2 Test case description

The test case was simulated with four combinations of heat exchanger models, as can be seen in Table 4.2. The two main cases to compare were "U/U" and "A/A", but the two intermediate configurations may also yield interesting information.

Figure 4.11 shows the principle flow configuration of the gas cooler. The evaporator was quite similar, but with reversed vertical flow direction, so

Table 4.2: Simulation test matrix

Case name	GC model	EV model
U/U	Uniform	Uniform
A/U	APEM	Uniform
U/A	Uniform	APEM
A/A	APEM	APEM

that the refrigerant was flowing upwards.

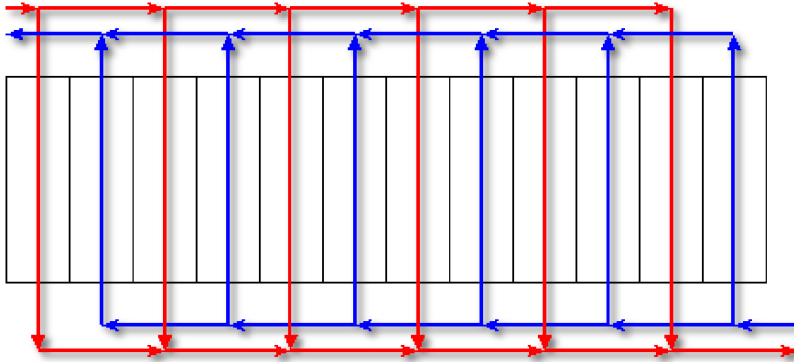


Figure 4.11: Flow configuration of gas cooler, the red stream is refrigerant

The fixed-speed, single-stage compressor used a simple correlation for isentropic and volumetric efficiency depending on the pressure ratio. The evaporator and gas cooler water pumps ran at constant flow rate. The effect of oil in the refrigerant was not taken into account when calculating local heat transfer coefficients in heat exchangers.

4.6.3 Selected correlations for heat transfer coefficient and pressure drop

Single-phase: The correlations proposed by Martin (1996) is a semi-theoretical correlation for single phase flow in chevron type heat exchangers. It uses chevron angle and heat transfer area enhancement ratio due to corrugations as special parameters. This correlation is used for all single-phase flow, for both refrigerant and secondary fluids.

For a given chevron angle, Martin calculates a friction factor as a combination of 0° and 90° angle friction factors, f_0 and f_1 :

$$\frac{1}{\sqrt{f}} = \frac{\cos\phi}{\sqrt{b \cdot \tan\phi + c \cdot \sin\phi + f_0/\cos\phi}} + \frac{1 - \cos\phi}{\sqrt{f_1}} \quad (4.11)$$

where b and c are constants, and f_0 and f_1 are calculated from a combination of simple empirical expressions and other correlations using only the Reynold's number and the surface enhancement ratio (β) as parameters.

The Nusselt number is calculated as:

$$Nu = 0.122 \cdot Prl^{1/3} \cdot \left(\frac{\mu_{bulk}}{\mu_w}\right)^{1/6} \cdot [f \cdot Re^2 \cdot \sin(2\phi)]^{0.374} \quad (4.12)$$

Evaporation: Han et al. (2003b) described correlations for evaporating two-phase flow of R410A, using corrugation pitch and chevron angle as parameters.

$$Nu = C_{ev1} \cdot Re_{eq}^{C_{ev2}} \cdot Prl^{0.4} \cdot Bo_{eq}^{0.3} \quad (4.13)$$

where C_{ev1} and C_{ev2} are functions of heat exchanger geometry:

$$C_{ev1} = 2.81 \cdot \left(\frac{L_{pitch}}{d_{hyd}}\right)^{-0.041} \cdot \left(\frac{\pi}{2} - \beta\right)^{-2.83} \quad (4.14)$$

$$C_{ev2} = 0.746 \cdot \left(\frac{L_{pitch}}{d_{hyd}}\right)^{-0.082} \cdot \left(\frac{\pi}{2} - \beta\right)^{0.61} \quad (4.15)$$

The "eq" subscript refers to parameters calculated with equivalent mass flux, G_{eq} .

$$G_{eq} = G \cdot \left(1 - x + x \cdot \sqrt{\frac{\rho_l}{\rho_g}}\right) \quad (4.16)$$

The equivalent mass flow is also used to calculate the pressure gradient due

to friction:

$$\frac{dp}{dL} = -f \cdot \left(\frac{G_{eq}^2}{d_{hyd} \cdot \rho_l} \right) \quad (4.17)$$

The friction factor is here correlated on a similar form as the Nusselt number:

$$f = C_{ev3} \cdot Re_{eq}^{C_{ev4}} \quad (4.18)$$

where

$$C_{ev3} = 64710 \cdot \left(\frac{L_{pitch}}{d_{hyd}} \right)^{-5.27} \cdot \left(\frac{\pi}{2} - \beta \right)^{-3.03} \quad (4.19)$$

$$C_{ev4} = -1.314 \cdot \left(\frac{L_{pitch}}{d_{hyd}} \right)^{-0.62} \cdot \left(\frac{\pi}{2} - \beta \right)^{-0.47} \quad (4.20)$$

Condensation: Han et al. (2003a) also proposed correlations for condensing flow. It is on a similar form as for evaporation, but with other coefficients:

$$Nu = C_{con1} \cdot Re_{eq}^{C_{con2}} \cdot Pr_l^{1/3} \quad (4.21)$$

where

$$C_{con1} = 11.22 \cdot \left(\frac{L_{pitch}}{d_{hyd}} \right)^{-2.83} \cdot \left(\frac{\pi}{2} - \beta \right)^{-4.5} \quad (4.22)$$

$$C_{con2} = 0.35 \cdot \left(\frac{L_{pitch}}{d_{hyd}} \right)^{0.23} \cdot \left(\frac{\pi}{2} - \beta \right)^{1.48} \quad (4.23)$$

The pressure gradient is calculated in the same manner as for evaporating flow, but using different coefficients in the expression for the friction factor:

$$C_{con3} = 3521.1 \cdot \left(\frac{L_{pitch}}{d_{hyd}} \right)^{4.17} \cdot \left(\frac{\pi}{2} - \beta \right)^{-7.75} \quad (4.24)$$

$$C_{con4} = -1.024 \cdot \left(\frac{L_{pitch}}{d_{hyd}} \right)^{0.0925} \cdot \left(\frac{\pi}{2} - \beta \right)^{-1.3} \quad (4.25)$$

Void correlation: The correlation by Kowalczewski (1966) was used to calculate the volume of liquid and vapor in heat exchanger elements. It describes the slip between phases in horizontal and upwards vertical flow. For downwards vertical flow, a homogeneous model is used.

4.7 Results from simulation of demonstration case

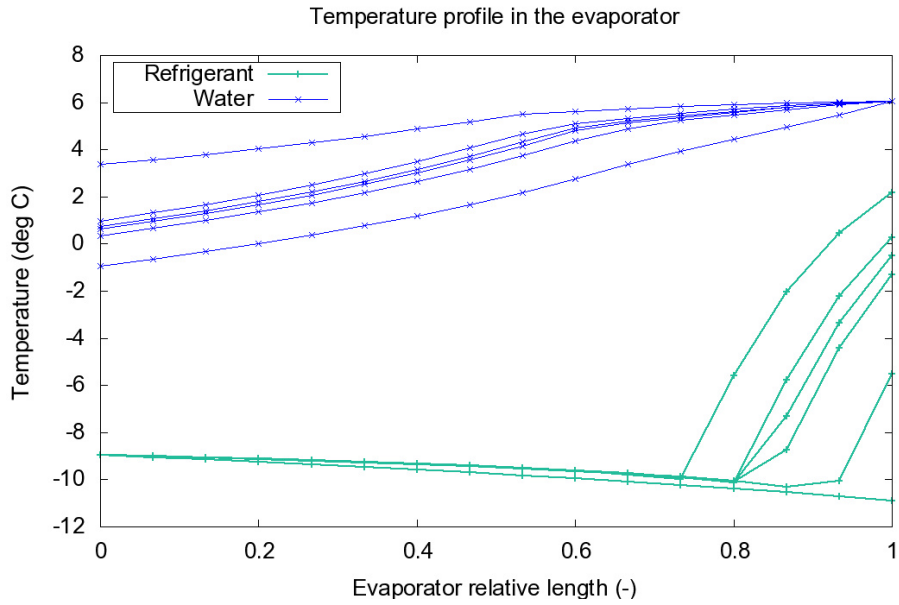
A simulation test cases was run with different combinations of uniform ("U") and APEM ("A") heat exchanger models in the gas cooler and the evaporator. As an example, the case name "U/A" refers to uniform gas cooler model and APEM evaporator model.

A comparison of key values from the simulation of the four configurations can be seen in Table 4.3. For graphical comparison, only the "U/U" and "A/A" cases are included.

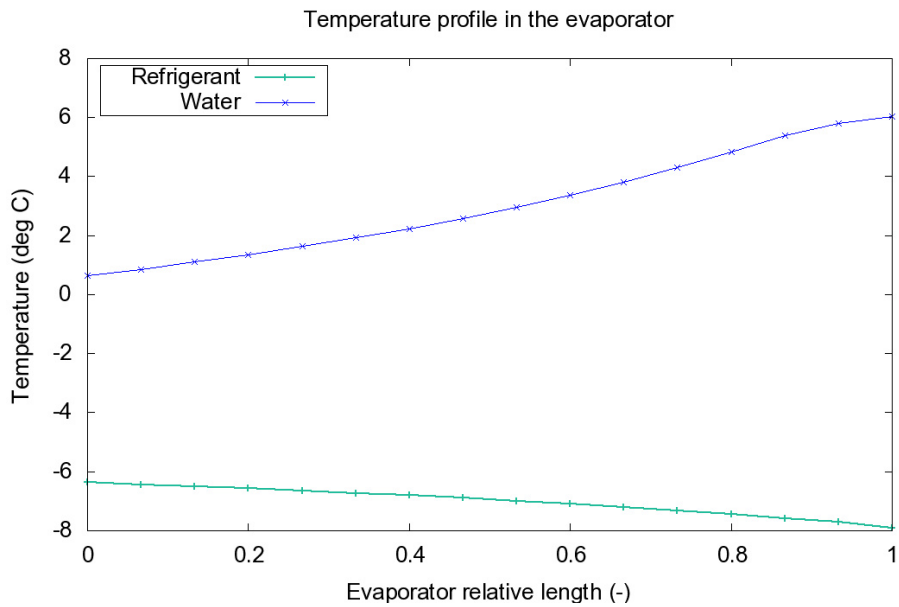
Figure 4.12 shows a comparison of temperature profiles in the evaporator for case "U/U" and "A/A", Figure 4.13 shows the heat transfer coefficient profiles and Figure 4.14 shows the pressure drop profiles.

In these figures, the x-axis shows the relative location within the channel; "0" marks refrigerant inlet, and "1" marks refrigerant outlet and secondary fluid inlet.

4. ADVANCED PLATE HEAT EXCHANGER MODEL (APEM)



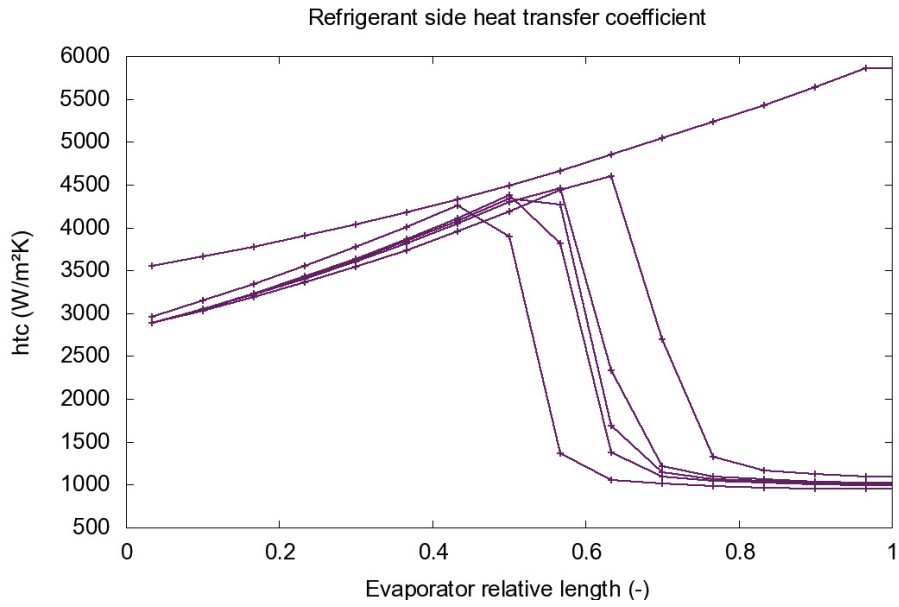
(a) Simulation with APEM heat exchanger models ("A/A")



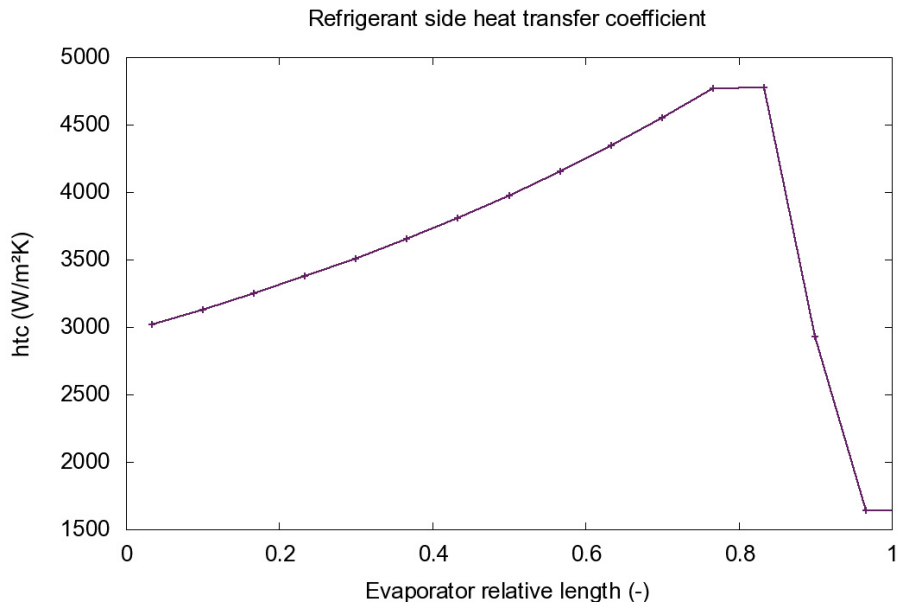
(b) Simulation with uniform heat exchanger models ("U/U")

Figure 4.12: Temperature profiles of the evaporator, comparison of case "U/U" and "A/A"

4. ADVANCED PLATE HEAT EXCHANGER MODEL (APEM)



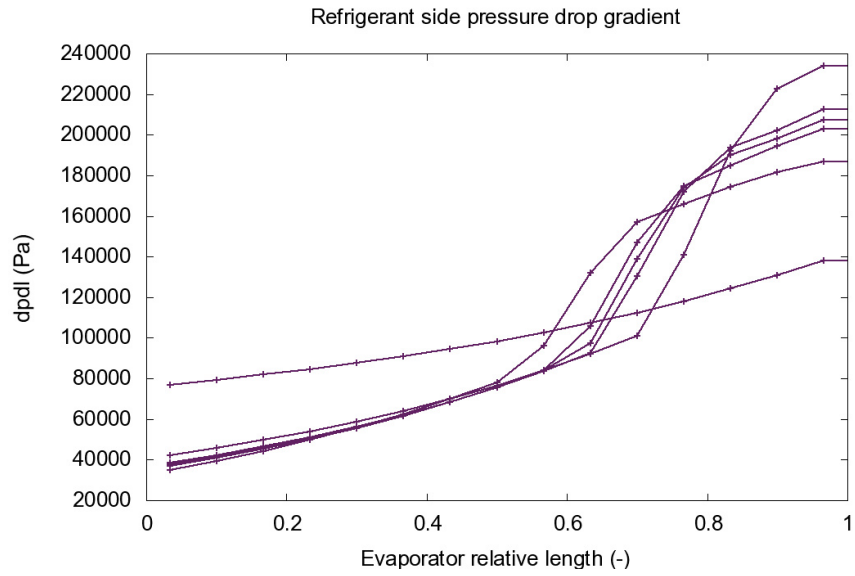
(a) Simulation with APEM heat exchanger models ("A/A")



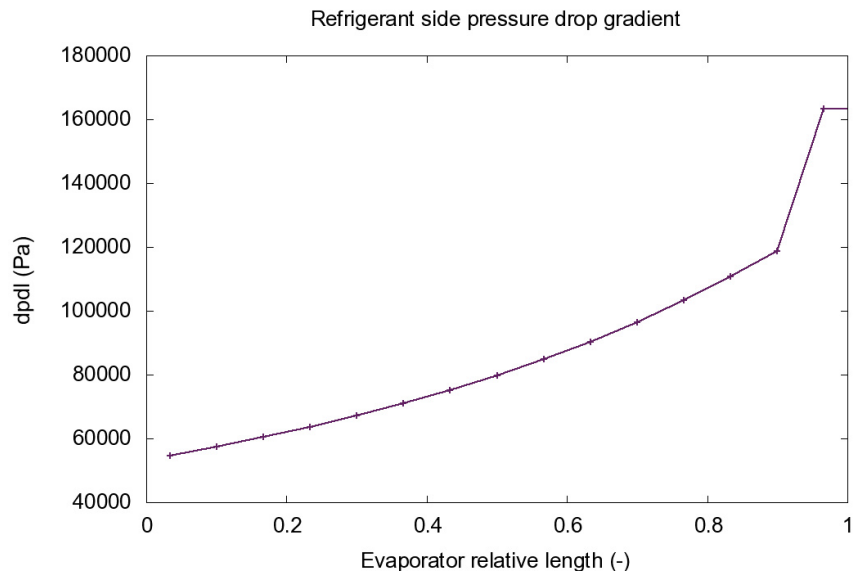
(b) Simulation with uniform heat exchanger models ("U/U")

Figure 4.13: Heat transfer coefficient profiles of the refrigerant side of the evaporator, comparison of case "U/U" and "A/A"

4. ADVANCED PLATE HEAT EXCHANGER MODEL (APEM)



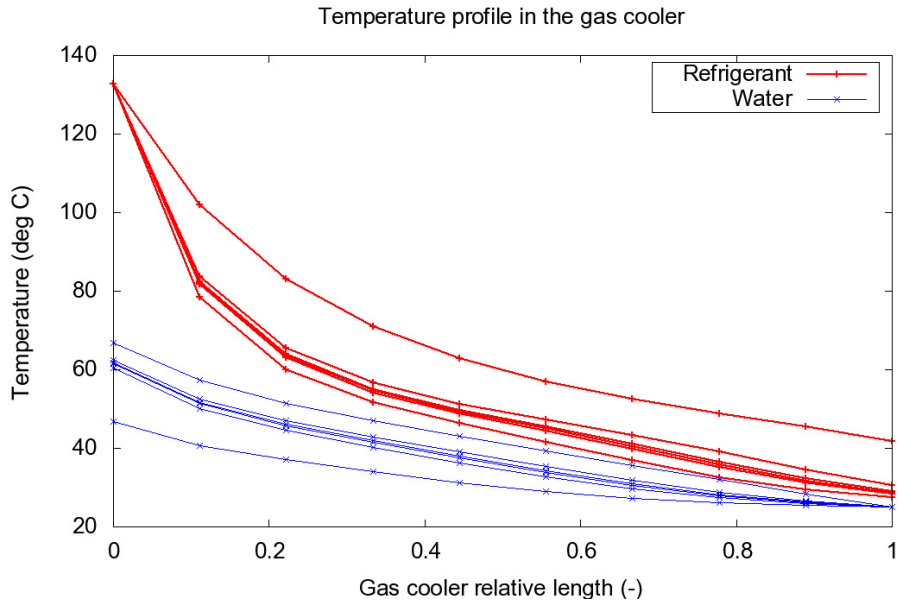
(a) Simulation with APEM heat exchanger models ("A/A")



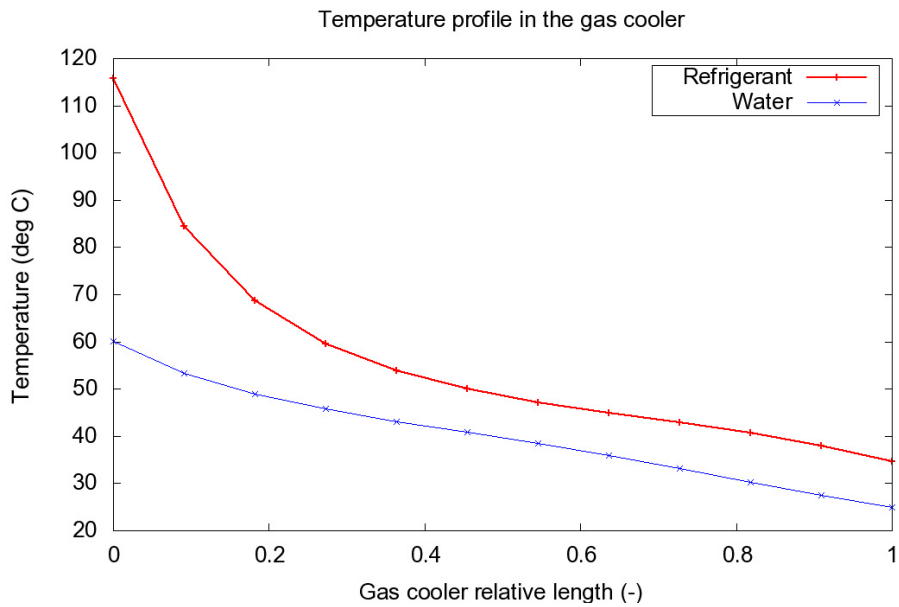
(b) Simulation with uniform heat exchanger models ("U/U")

Figure 4.14: Pressure gradient profiles of the refrigerant side of the evaporator, comparison of case "U/U" and "A/A"

4. ADVANCED PLATE HEAT EXCHANGER MODEL (APEM)



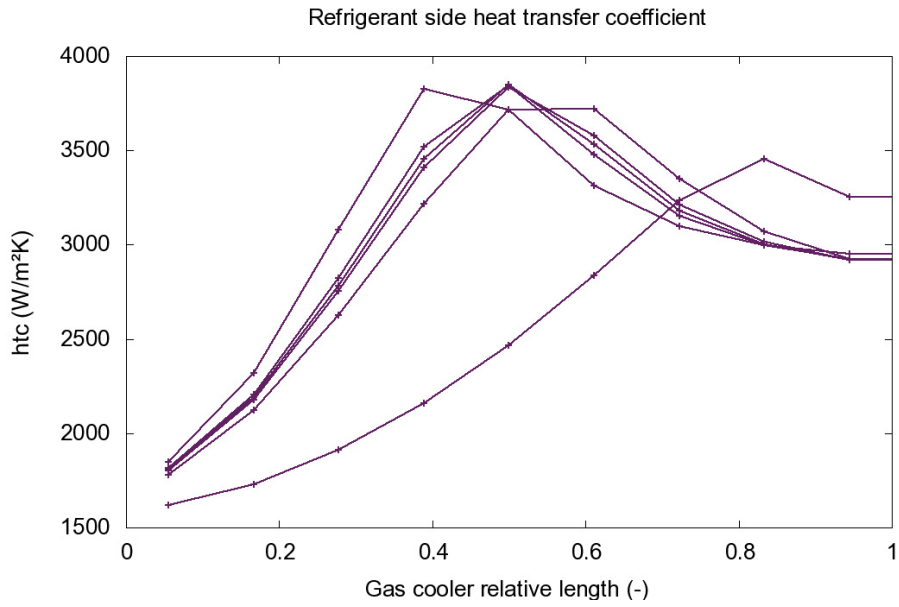
(a) Simulation with APEM heat exchanger models ("A/A")



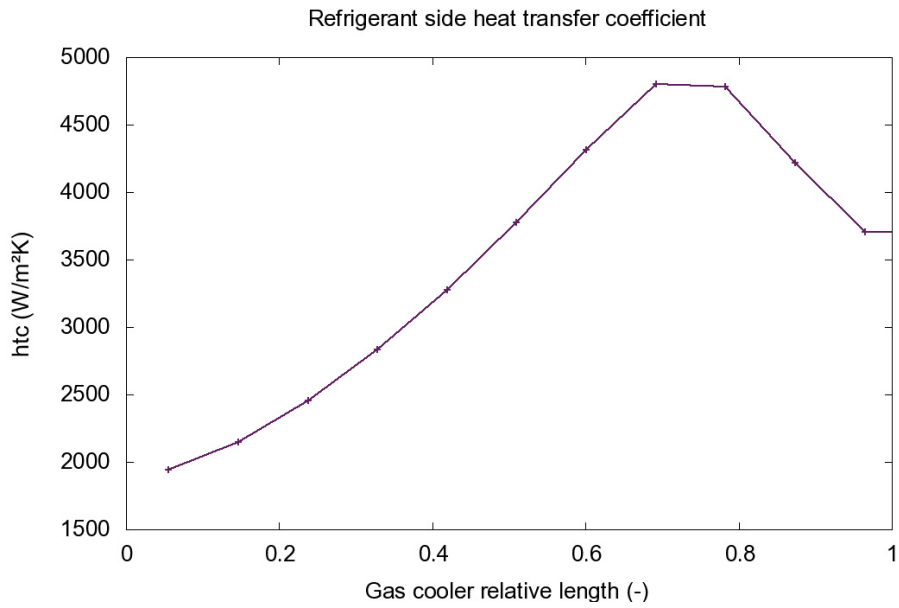
(b) Simulation with uniform heat exchanger models ("U/U")

Figure 4.15: Temperature profiles of the gas cooler, comparison of case "U/U" and "A/A"

4. ADVANCED PLATE HEAT EXCHANGER MODEL (APEM)



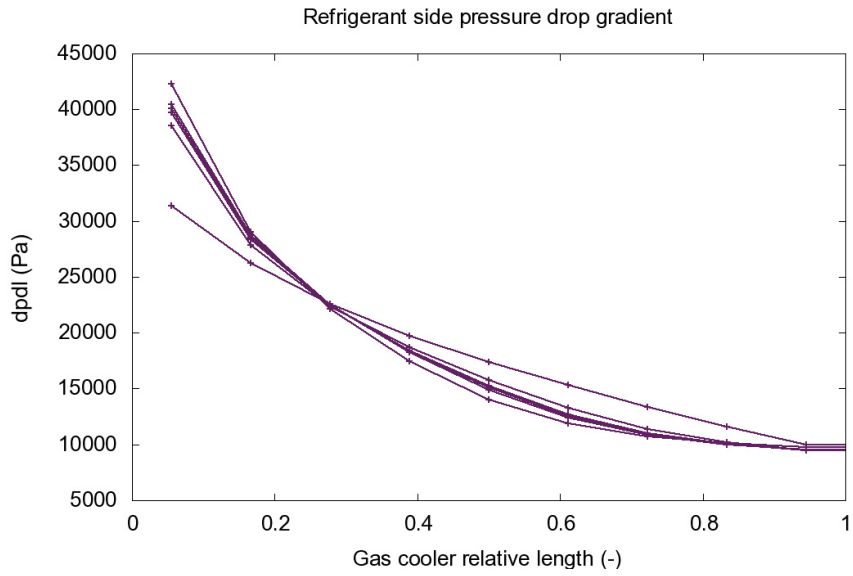
(a) Simulation with APEM heat exchanger models ("A/A")



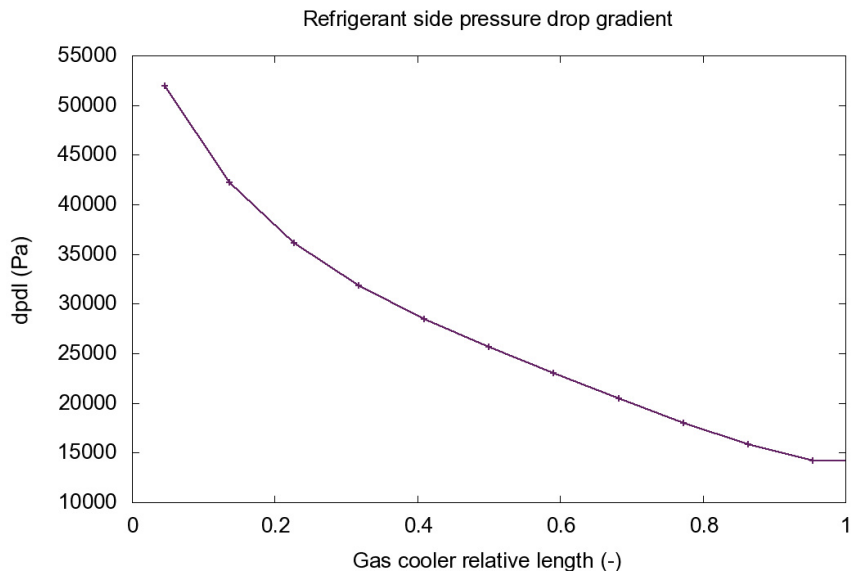
(b) Simulation with uniform heat exchanger models ("U/U")

Figure 4.16: Heat transfer coefficient profiles of the refrigerant side of the gas cooler, refrigerant side comparison of case "U/U" and "A/A"

4. ADVANCED PLATE HEAT EXCHANGER MODEL (APEM)



(a) Simulation with APEM heat exchanger models ("A/A")



(b) Simulation with uniform heat exchanger models ("U/U")

Figure 4.17: Pressure gradient profiles of the refrigerant side of the gas cooler, comparison of case "U/U" and "A/A"

4. ADVANCED PLATE HEAT EXCHANGER MODEL (APEM)

Table 4.3: Key values from output of circuit simulation with different plate heat exchanger models

Parameter	Unit	Case			
		U/U	A/U	U/A	A/A
COP	[-]	3.13	3.09	2.96	2.89
\dot{Q}_{gc}	[kW]	109	109	109	109
\dot{Q}_0	[kW]	75.9	75.1	73.6	72.8
\dot{W}_c	[kW]	35.0	35.4	36.9	37.8
T_0	[°C]	-7.9	-7.8	-11.2	-10.9
HTC_{ev}	[$Wm^{-2}K^{-1}$]	2864	2857	2261	2262
$\Delta p_{ev,refr}$	[kPa]	124	123	148	146
P_{high}	[bar]	95.2	96.3	102.0	104.4
HTC_{gc}	[$Wm^{-2}K^{-1}$]	2208	2105	1981	1886
η_{is}	[%]	79	78	74	74
λ	[%]	82	82	78	77
System \dot{m}	[kg/s]	0.46	0.46	0.40	0.40

The mass flow distribution between channels in the "A/A"-case can be seen in Figure 4.18 for the gas cooler and Figure 4.19 for the evaporator. The reduced mass flow is shown on the y-axis, which is the ratio between the individual channel mass flow and the average mass flows for all channels. For each channel "j":

$$\dot{m}_{j,red} = \frac{\dot{m}_j}{\dot{m}_{average}} \quad (4.26)$$

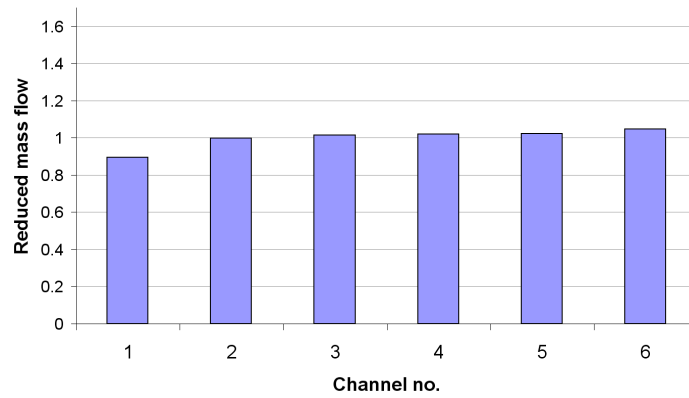


Figure 4.18: Refrigerant mass flow distribution between channels in the gas cooler for case "A/A"

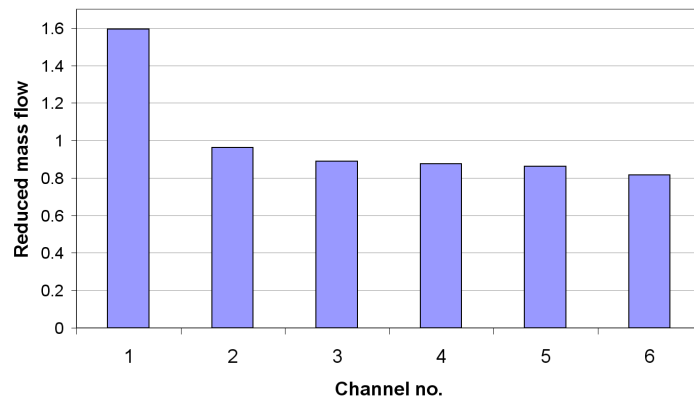


Figure 4.19: Refrigerant mass flow distribution between channels in the evaporator for case "A/A"

5. DISCUSSION

5.1 Main findings from the FTL test suite

5.1.1 Introduction

The design and development of FTL has been driven by the need for more rapid calculation of thermophysical properties for CO₂. FTL is based on linear interpolation in lookup tables, which represents a very low calculation load compared to the fundamental equations previously used in the in-house simulation tool, CSIM.

The following chapters discuss important aspects of FTL based on a test suite performed in Chapter 3.6.

5.1.2 Analysis of systematic error

As discussed in Chapter 3.2.2, the deviation from the full Span-Wagner EOS can be expected to be a systematic error rather than a random one. The results confirm this, the deviation in all tests increased significantly and abruptly in close proximity to the critical point. The systematic error seen in figures can be considered as a “worst-case” scenario, as the difference between the point on the secant and the real property line is at its largest.

The same phenomenon explains the white wedge of minuscule deviation appearing around the pseudo-critical line. In this region, properties as entropy and enthalpy reach an inflection point, meaning that the second order derivative changes sign. Thus, the property function is temporarily a relatively straight line, and linear interpolation has increased accuracy. See Figure 5.1 for a graphical map of over- and underestimation for enthalpy compared to TL_{Span} .

Other properties, e.g. specific isobaric heat capacity (c_p), are affected differently. The value of c_p spikes around the critical point and pseudocritical line, meaning that linear interpolation will over-estimate this property on both sides of the spike. Near the top of the spike itself, however, the lookup table implementation underestimates the function value, due to interpolation

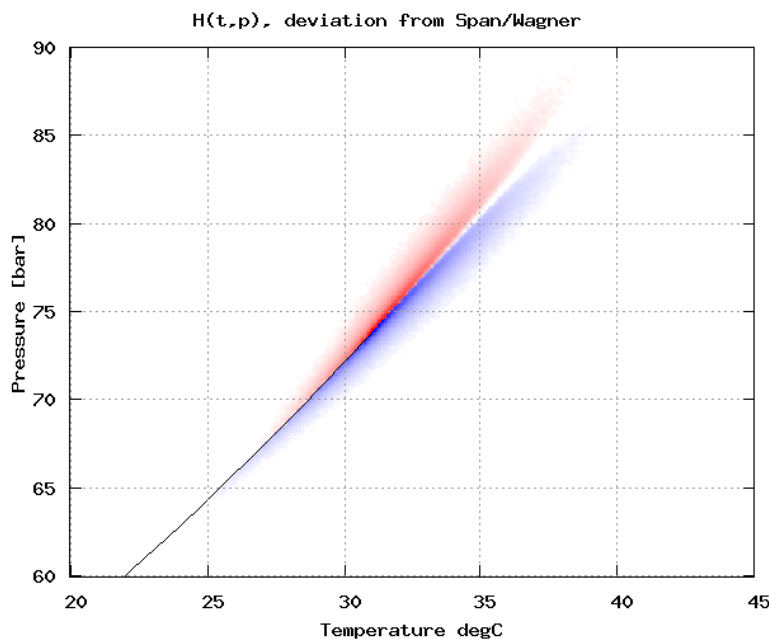


Figure 5.1: Map of systematic error for enthalpy. Red = over-estimate, blue = under-estimate.

across the summit of the spike or the inflection point of the peak. Figure 5.2 shows a graphical map of over- and underestimation for c_p compared to TL_{Span} .

Since the deviations from TL_{Span} are systematical and not random, higher-order interpolation can be expected to significantly increase accuracy. This could be a viable option for other applications with higher near-critical accuracy requirements.

When enlarging a small region just above the critical point, the pattern is better identified. In Figure 5.3, the relative deviation from SW-EOS has been plotted with 100x higher resolution. Between each table entry for both p and T , ten points are calculated and compared. For the lookup table implementation, these ten points will all be placed on a secant as shown earlier in Figure 3.3.

As expected, Figure 5.3 shows a pattern where deviation is small near the table grid (visible as lighter, or even white, squares), and largest between grid points. The jaggedness of the border between the red and blue areas is amplified by limitations in the plotting software. In reality, there will still

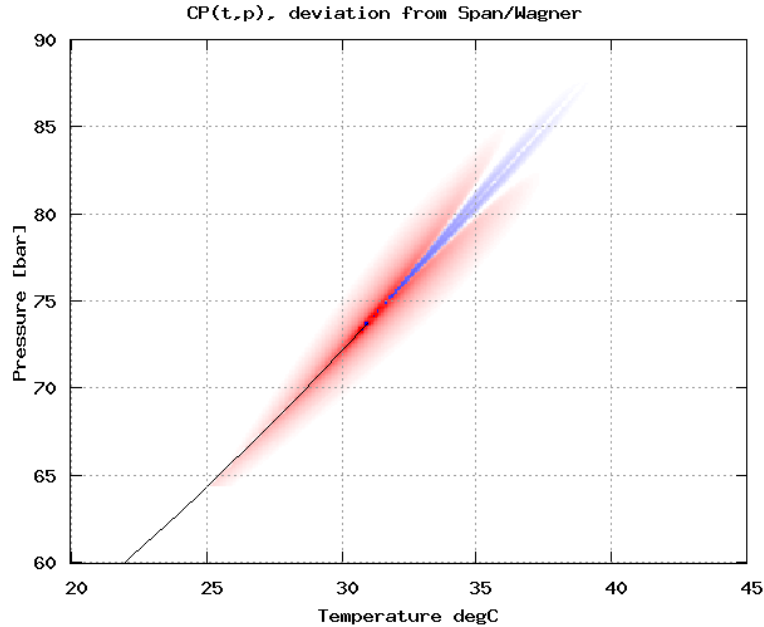


Figure 5.2: Map of systematic error for specific isobaric heat capacity. Red = over-estimate, blue = under-estimate.

exist some jaggedness due to interpolation data points spanning the pseudo-critical line. Property values could be either over- or under estimated in these cases.

5.1.3 Accuracy - saturated property data

From the comparison of saturated property data in Chapter 3.7.1, it is clear that the accuracy is predictably good for almost the entire range. Close to the critical point, deviations are significantly higher. As mentioned earlier, this does not necessarily affect the accuracy of simulation results to the same degree, even for a process that operates very close to the critical point. This is discussed further in Chapter 5.1.5.

$c'_{p,sat}(T)$ and $c''_{p,sat}(T)$ have, as expected, the highest deviations of all properties. The maximum deviation was 17.0% and 14.5% respectively, but only about 0.5% of the samples exceeded the $1\text{E-}3$ deviation threshold. About 1.6% of the sampled deviations exceeded $1\text{E-}4$. As all the high-deviation values came from the critical region, this corresponds to temperatures above

5. DISCUSSION

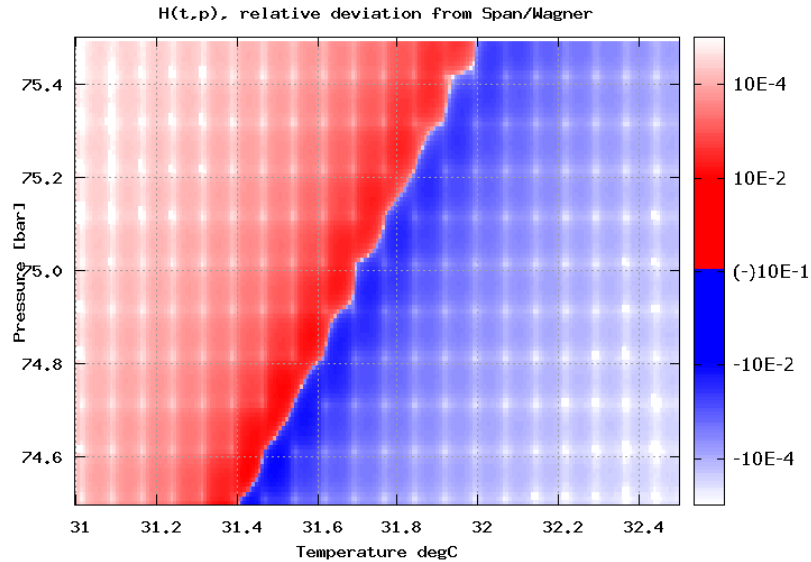


Figure 5.3: Close-up of systematic error for Enthalpy. Red = over-estimate, blue = under-estimate.

29.60°C, approximately 1.35°C from the critical point. All compared values from below this temperature had lower than 1E-4 deviation.

Two other properties with slightly higher deviations than average are the surface tension and thermal conductivity, but the deviations are also here within acceptable limits.

For the rest of the properties, the results are relatively homogeneous. Less than 0.03% of the temperature range had deviations larger than 1.0E-3, and less than 0.2% exceeded 1.0E-4.

For the current application (CSIM), the described level of deviation will not pose an issue for the reliability of simulation results. The overall level of accuracy is considered as satisfactory. If needed, a denser grid near the critical point can be used to further improve the accuracy.

5.1.4 Accuracy - continuous region

Common statistical parameters to describe average deviation are not enough to give a full picture of the accuracy and consistency for this work. Where deviation occur and in what pattern is equally important, because the errors are systematic rather than random.

The map plots in Chapter 3.7.2 show location and magnitude of the deviation in the T-p space. As expected, all properties had higher deviations around the critical point. In this region, properties have very abrupt variations in value. In the same region, isotherms and isobars are almost parallel. These two mechanisms both reduce the accuracy from linear interpolation in this region.

With the implementation of FTL, the region with significant deviations are limited to a narrow band that spans the saturation and pseudocritical lines, approximately 2°C or 5 bars wide.

The value of c_p deviated by as much as 300%, but that was adjacent to the critical point itself where the TL_{Span} function gradient is very steep. For the remaining 99% of the near-critical region¹ the deviation was less than 1.3E-02, which is acceptable for this value. The other properties had considerably smaller deviations. Typically, the 99% percentile deviation from TL_{Span} was in the order of 1E-04.

When examining the $T(h, p)$ plot in Figure 3.16, it first appears that FTL has intermittently failed to produce good values at the phase lines. At closer investigation of the data, it is clear that it is actually the TL_{Span} values that are wrong, occasionally failing to correctly calculate close to the saturation line. As this function is multiple-inverse in the Span-Wagner equation of state, it's probable that one or more iterative solving procedures have failed. FTL has a much simpler task calculating this function, as the additional h-p lookup table covers most of the two-phase region. Even outside the coverage of this lookup table, $T(h, p)$ is easily performed by iterative solving of the explicit function $h(T, p)$.

Based on the results, it is evident that linear interpolation in regularly gridded tables has some difficulties to accurately represent the highly non-linear properties for CO₂ in TL_{Span} in the critical region. For applications requiring higher accuracy in this region, one possibility is to replace linear interpolation with either higher-order interpolation or splines. Using a tighter grid to improve linear interpolation will make an improvement, but this is not nec-

¹ 26-40°C and 65-90 bar.

essarily a very efficient solution, as the table size will increase proportional to the grid density squared.

5.1.5 Impact of near-critical deviation on simulation results

The local systematical errors that occur around the critical point, even the relatively large deviations for c_p and λ , do not actually impact the simulation results to any significant extent. Both these functions have a strong peak value in this region.

c_p and λ are used for calculation of the Prandtl number, which again is used to calculate the Nusselt number.

$$Pr = \mu \cdot c_p \cdot \lambda \quad (5.1)$$

The Nusselt number is usually a function of Reynold's and Prandtl's numbers:

$$Nu = f(Re, Pr) \quad (5.2)$$

Nusselt's number is directly proportional to the heat transfer coefficient:

$$HTC = \frac{Nu \cdot \lambda}{d_{hyd}} \quad (5.3)$$

As c_p and λ abruptly peaks near the critical point, so does the local refrigerant-side heat transfer coefficient. Figure 5.4 shows a plot of local CO₂-side heat transfer coefficient in a gas cooler that operates very close to the critical point. The output is from a successfully converged CSIM simulation using TL_{Span} . Whether the huge, abrupt spike in heat transfer coefficient is realistic or not will not be discussed in this work. The high value for HTC is a consequence of very high local values for c_p and λ , resulting in a correspondingly high value for Prandtl's number.

Since the heat transferred is proportional to the U-value between the two fluids, the high local HTC for the CO₂ node only reduces the heat transfer *resistance* toward zero, effectively removing it from the equation (see Equation 4.9). All practical heat transfer resistance in effect is from the local heat transfer coefficient on the secondary fluid side. The *overall* U-value between the fluids in this case develops much less abruptly, as can be seen in Figure

5. DISCUSSION

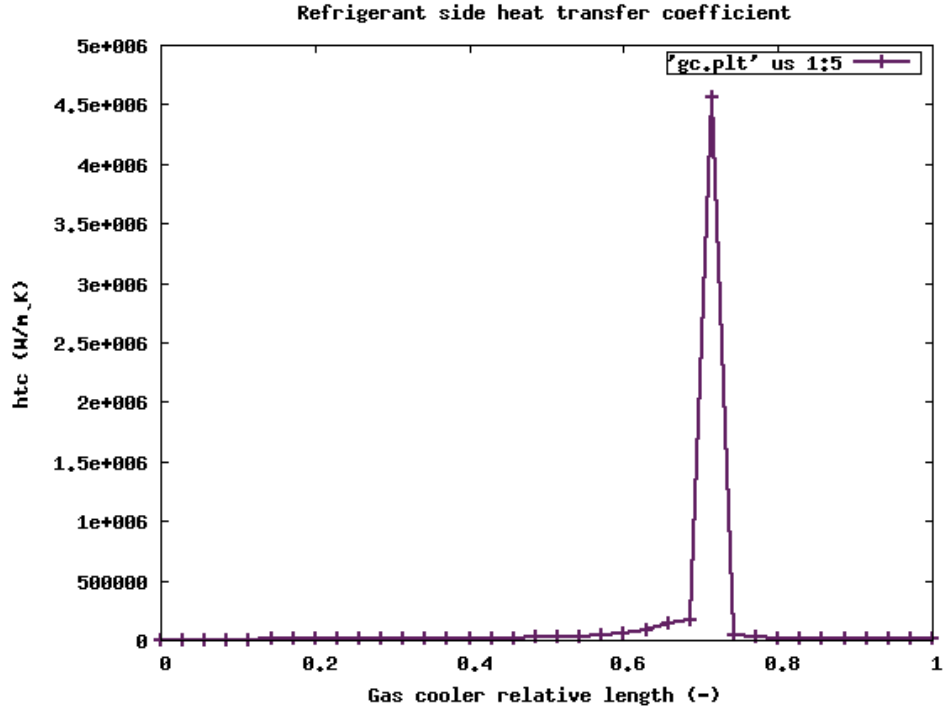


Figure 5.4: Local CO₂-side heat transfer coefficient in a gas cooler, near-critical operation

5.5.

Table 5.1 shows a simple comparison of local heat transfer coefficient and calculated U-value for the highest-deviating gas cooler subhx in test case 3. Here the refrigerant-side heat transfer coefficient deviates with 44%, but the U-value between fluids for the same subhx only deviates by 2%. The low deviation of local U-values is an important verification of adequate accuracy from FTL.

Table 5.1: Comparison of near-critical local heat transfer coefficients and U-values

	HTC_{refr}	HTC_{sec}	$U - value$
TL_{Span}	147527	9922	9089
FTL	212390	9920	8900
Deviation from TL_{Span}	44.0%	-	2.1%

To sum up; as FTL systematically over-estimates the values of c_p and λ , the

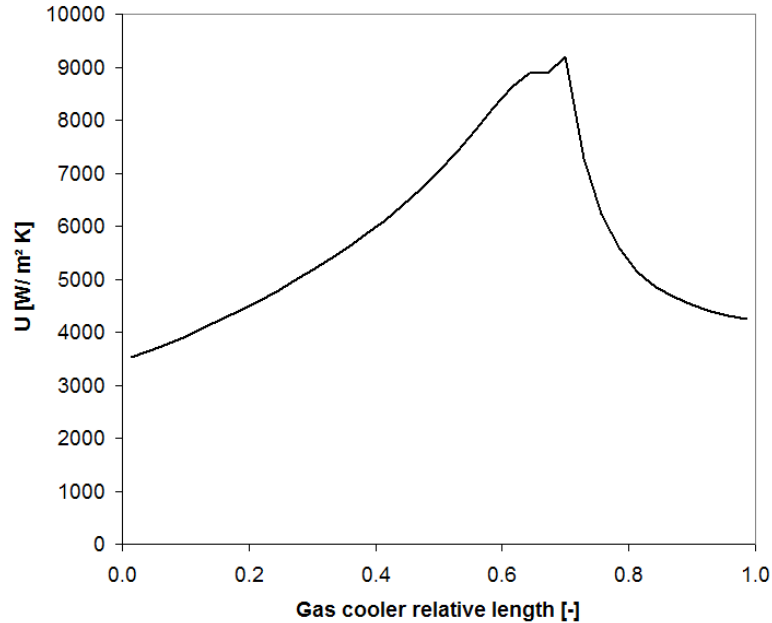


Figure 5.5: Example calculated local overall U-value in a gas cooler, near-critical operation

local value for heat transfer coefficient also gets over-estimated. However, the overall U-value is not strongly affected by this, because the higher deviation of FTL-values coincide with system states where the main thermal resistance are on the secondary fluid side.

5.1.6 Accuracy - simulation results

Based on the simulation results presented in Chapter 3.7.4 and Appendix C, it is clear that the simulation output is near identical as with TL_{Span} . Even Case 3 with the gas cooler outlet pressure of 73.6 bar, show minuscule deviations. This gas cooler process ran very close to the critical point, 0.06 bar above p_c at critical temperature.

Typical deviations in the simulation results were less than 0.5%. Simulations with TL_{Angus} converged at slightly different solutions, and the results usually deviated from TL_{Span} with 1-2%. This is all well within the uncertainty level that can be expected from CSIM.

5.1.7 Calculation performance

The calculation times are very significantly reduced compared to TL_{Span} . For a set of common functions, the calculation time was reduced from ≈ 6000 seconds to ≈ 2.0 seconds with FTL. This is an increase in calculation speed by a factor of approximately 3000. Compared to TL_{Angus} , the calculation performance increased by a factor of 50.

Calculation speed can be further improved by implementing similar property link features as in TL_{Angus} , where stored interpolation coefficients or internal solver results would save time in consecutive property calculations in the same system state. However, the effect on simulation times will be small.

Implemented into CSIM, the reduction in simulation time was on average approximately 99.77% compared to TL_{Span} , and 90.4% compared to TL_{Angus} . Based on the results in Table 3.21, this is quite near the theoretical maximum possible improvement of 99.85 %.

Compared to the results from the initial profiling of CSIM in chapter 2.3.6, the six test cases used for the main analysis differed slightly with respect to distribution of cpu time for calculation of CO₂ properties. This can be explained by a possible difference in the configuration and complexity of the test cases, or various forms of background noise from the operating system or other running programs interfering with the accuracy of logging cpu times during profiling.

Even if the CPU time of the calculation of thermophysical properties was reduced to zero, which naturally is impossible, the simulation time improvement compared to TL_{Span} would only increase from 99.77% to 99.85%.

Describing it in another way, FTL realizes 99.92% of the potential for reducing simulation time with faster calculation of thermophysical properties.

5.1.8 Usability and versatility

Although the lookup table implementation was adapted for CO₂ in a specific simulation tool, its usability extends beyond that. The adaptations made for CSIM were mostly with respect to total table size, expected accuracy and choice of the T-p space as main axis. Using the existing framework in FTL, a re-adaption for other applications with different requirements is a relatively small task.

One example could be CFD simulations, where common describing properties

are p and h . In this case, choosing pressure and enthalpy as the property space for the main tables could be very efficient. As seen in the results for the $T(h, p)$ function, this property space can also yield more accurate calculations than in the T- p space.

It is also possible to utilize the lookup table approach for other single-component fluids and refrigerants with complex equation of state and transport data correlations. As long as the fluid has a constant evaporation and condensation temperature, the transition should be quite trivial. For mixtures, some additional modifications are required.

5.2 Main findings from simulation with new heat exchanger model

5.2.1 Introduction

Based on the demonstration cases simulated, the advanced heat exchanger model (APEM) gives valuable information of the behavior of the component in different situations. The effect of asymmetric heat transfer and mal-distribution can be reduced with careful system and component design.

The demonstration case was deliberately set up to give some deviation between the different models, but it is not at all unreasonable for comparison. In real life, pinch points occurring in individual channels are likely to yield more extreme differences. Pinch issues are unfortunately particularly difficult to handle numerically in simulation tools like CSIM.

The results from the simulation test case depend to a large extent on the correlations for pressure drop and heat transfer coefficient. Different correlations could yield different results, but the basic mechanisms described in this work remain the same.

The plate heat exchangers in the test case had only 13 plates, considerably less than typical real-life models for this capacity. Heat exchangers with larger numbers of plates will be affected differently by the physical mechanisms described in this work. In short, the asymmetric heat transfer caused by end-plate effects, as described in Chapter 4.2.2, can be expected to have less impact. Other effects, e.g. mal-distribution due to pressure loss in headers and conduits or liquid-vapor separation, may have increased impact on performance. Experimental measurements and further development of APEM are needed to further investigate this topic.

5.2.2 Asymmetric heat transfer

From the results in Chapter 4.7, the effects of asymmetric heat transfer are well illustrated. In the evaporator temperature profile in Figure 4.12a, the secondary fluid outlet temperature over parallel channels differs by more than 4°C. That equals a spread in channel capacity of approximately $\pm 50\%$ of average capacity. The difference is particularly high due to the calculated mal-distribution of refrigerant flow, which to some extent is self-amplifying in evaporators.

The asymmetric behavior in this evaporator could be reduced by using an extra water-side channel, configuring a 6+7 channel heat exchanger. With the extra water channel, all refrigerant channels would be “boxed in”, reducing the level of asymmetric individual channel superheat. Instead, there would be two water channels with low thermal efficiency, impacting the overall performance of the evaporator.

In the gas cooler temperature profile in Figure 4.15a, the refrigerant temperature varies with as much as 20°C in parallel channels. As refrigerant mal-distribution was found to be a much smaller issue in the gas cooler, the temperature profile asymmetry is caused almost solely by the heat transfer asymmetry.

5.2.3 Distribution of mass flow in parallel channels

APEM includes the distribution of mass flows between parallel channels in the same pass. The distribution is calculated on the basis of the channel pressure drop, not including pressure loss in headers or ports. In the simulation test case this led to a large mal-distribution of refrigerant in the evaporator, with the first refrigerant channel receiving 60% more mass flow than average.

This high level of mal-distribution in the evaporator has several contributors:

- As seen in Figure 4.14a for the evaporator, the chosen correlations yield a higher pressure drop for superheated vapor than for two-phase flow.
- The refrigerant side heat transfer coefficient reduces for higher vapor qualities, as seen in Figure 4.13a.
- Asymmetric heat transfer causes asymmetric vapor qualities in the channels, and thus initiates the mal-distribution.

- The relationship between correlations further amplifies the mal-distribution.
- Lack of included port pressure loss that may counter-act some of the effect of mal-distribution.

Because port pressure loss also will be a function of, among other parameters, fluid velocity, that too can be expected to be higher for higher vapor fraction channels. Ideally, the inlet ports will have equal vapor fraction, but different mass flows, which in theory could help level out some of the differences.

$$\Delta p_{channel,tot} = \Delta p_{port,inlet} + \Delta p_{channel} + \Delta p_{port,outlet} \quad (5.4)$$

In real life, mal-distribution of liquid and vapor in headers and conduits further complicates the prediction of individual and overall channel pressure drop.

5.2.4 Simulation results

Based on the analysis of asymmetry heat transfer and mass flow in parallel channels, the results from the simulation test case presented in Chapter 4.7 are quite interesting.

In the test case, the system performance was affected considerably for different plate heat exchanger models. As can be seen from Table 4.3, it is clear that the evaporator model in particular has a great impact.

The asymmetric heat transfer and mass flow, discussed in earlier chapters, cause reduced thermal performance in the evaporator compared to the uniform model. The channels with higher vapor quality have higher nominal pressure gradients and lower refrigerant side HTC-values. This increases the total pressure drop in the heat exchanger, and forces the evaporation temperature down to reach the required refrigerant outlet state of 0.93 vapor fraction.

The lower evaporation temperature and vapor density result in a higher pressure ratio in the compressor, lower volumetric efficiency and reduced mass flow. With reduced global refrigerant flow, the deterioration in performance continues as the high-side pressure must increase to meet the heating capacity requirement with less circulated refrigerant.

An evaporator component simulation with the two models differ considerably

less in performance. Table 5.2 shows a comparison of APEM and the uniform model, ignoring the system performance deterioration. In this comparison, the mass flow and evaporator inlet conditions are identical for the two models, using the system state found in the “U/U” circuit simulation case, where both the gas cooler and evaporator were represented by uniform models.

Table 5.2: Comparison of evaporator component simulations with different plate heat exchanger models

Parameter	Unit	Case	
		Uniform	APEM
\dot{Q}_0	[kW]	75.9	76.0
T_0	[°C]	-7.9	-10.6
HTC_{ev}	[$Wm^{-2}K^{-1}$]	2864	2432
$\Delta p_{ev,refr}$	[kPa]	124	175

The results from the component simulation differ in evaporation temperature and pressure drop, but the calculated performance is practically equal. That is because this simulation assumed identical specific enthalpy at the evaporator inlet, which is directly related to the system state at the throttle valve.

The same component models made a much larger impact on performance, both component and flowsheet, in the full circuit simulation. Here, the cooling capacity was reduced by approximately 5%, and the COP by 8%. This is a good example of the importance of hardware based circuit simulation software such as CSIM.

5.2.5 Usability of model

The test case described in Chapter 4.6 is a good example of how component-level physical mechanisms can initiate self-amplifying deterioration of system performance. This kind of system behavior can only be discovered and investigated in circuit simulation tools with detailed component models.

A component model alone can not consider the widespread change in performance of the rest of the system, as could be seen in the component simulation results in Table 5.2.

The new plate heat exchanger model, APEM, can contribute to improve optimizations of CO₂ heat pumping system, and contribute to the design of

5. DISCUSSION

robust, efficient and environmentally friendly heat pumping systems. Validation of correlations for pressure drop and heat transfer coefficients is still needed to ensure more accurate predictions of behavior.

6. CONCLUSIONS AND SUGGESTIONS FOR FURTHER WORK

6.1 Conclusions

The in-house circuit simulation and optimization tool, CSIM, can be used to predict the behavior and performance of CO₂-based heat pumping systems for non-residential buildings, but has lacked a plate heat exchanger model and a general method to handle more complex fluid stream configurations.

Detailed circuit simulations with CO₂ are suffering from long simulation times, due to the high calculation load of CO₂ thermophysical property functions. An advanced plate heat exchanger model with a high level of discretization would further deteriorate the situation to that respect. Therefore, a method for reducing the calculation time of thermophysical properties has also been strongly needed.

This PhD work describes the development and implementation of a new plate heat exchanger model (APEM), and a fast thermophysical library (FTL). Together, FTL and APEM give the opportunity to improve the design and optimization of CO₂ heat pumping systems. The much faster calculations with FTL will allow a higher level of resolution in performance-critical components such as heat exchangers. The extra levels of discretization are needed to capture abrupt variations in local behavior, that can severely impact system performance.

APEM gives the ability to investigate many different configurations for using CO₂ as a working fluid in larger systems, aiding the optimal design of robust, high-efficiency refrigeration and heat pumping plants.

Both FTL and APEM are well suited for adaption or further extension for other applications.

6.1.1 The Fast Thermophysical Library (FTL)

The technique of using linear interpolation in lookup tables enhances simulation performance greatly. The implementation of FTL specifically designed for the in-house simulation tool, CSIM, reduces simulation times by

99.77% compared to simulations with the reference equation of state by Span-Wagner. This corresponds to an increase in performance by a factor of more than 400, which must be considered very substantial by any means.

In its current implementation, FTL realizes 99.92% of the maximum theoretical potential for reducing simulation time with faster calculation of thermophysical properties. In practical use, the reduction in simulation time is very noticeable, and is a real contribution to improved efficiency and work flow.

Based on the results from the CSIM test suite, the differences in simulation results compared to the Span-Wagner implementation are minuscule.

Linear interpolation in a regularly gridded lookup table is overall sufficiently accurate for replicating the high level of non-linearities in thermophysical properties for CO₂. However, in immediate proximity to the critical point, there is a small region where the deviation increases abruptly, particularly for c_p .

However, an analysis shows that these deviations does not impact the simulation results in CSIM. Even processes that runs very close to the critical point have near identical results. This implementation of FTL is therefore found to be accurate enough for circuit simulations.

All deviations between calculated properties in FTL and TL_{Span} are systematic, caused by the limitations of linear interpolation. Using higher-order interpolation or splines in the near-critical region for increased accuracy could be a good option for other applications.

The ability for simulation convergence is another area where FTL proved to perform well. It handles difficult regions and transitions equally well, occasionally even better, than both TL_{Span} and TL_{Angus} implementations.

6.1.2 Conclusions - Plate heat exchanger model for complex configurations

The new plate heat exchanger model (APEM) implemented into CSIM allows detailed investigations of both component and system performance. The test case demonstrates how the choice of component model can severely impact system performance. This system impact can not be predicted with component models alone.

The use of APEM can identify local asymmetric behavior in parallel channels,

with respect to temperature profiles, heat transfer and nominal pressure drop. This information could be used to design better, and more robust components and systems.

6.2 Suggestions for further work

6.2.1 The Fast Thermophysical Library (FTL)

To use FTL with other applications than CSIM, some modifications or further development may be needed. For increased accuracy in the T-p space, it may be beneficial to replace linear interpolation with other methods that have a smaller systematical deviations for large non-linearities. Some further work is also needed to adapt FTL to use with other refrigerants.

- Adaption for use with other refrigerants and refrigerant mixtures.
- Identify grid spacing and table sizes for use in other applications, using different main property space (e.g. Temperature - enthalpy).
- Increasing accuracy in the T-p space when required:
 - Generate irregularly gridded tables, where the local grid spacing is determined to yield a fixed maximum deviation.
 - Use higher-order interpolation to reduce the systematical deviation from linear interpolation.
 - Use an implementation of splines.
 - It could also be an option to combine linear interpolation and splines. Splines can be used in the near-critical region to better represent the abrupt changes in property values. Linear interpolation can be used in the more linear region for higher calculation performance.

6.2.2 Plate heat exchanger model

The new plate heat exchanger model (APEM) would benefit from further development. The following areas have been identified:

- Validate available plate heat exchanger correlations, preferably by experimental measurements. The values for heat transfer coefficient and pressure drop affect the simulation results greatly.

6. CONCLUSIONS AND SUGGESTIONS FOR FURTHER WORK

- Implement a better method for calculating pressure drop in inlet- and outlet ports.
- Investigate the possibilities to include a model for liquid and vapor mal-distribution in headers, plate-channels and ports.
- Develop a better method for calculating heat exchangers with pinch issues. The current method causes considerable convergence issues.

REFERENCES

- Angus, S., Armstrong, B., & et al. (1976). *Carbon Dioxide - International thermodynamic Tables of The Fluid State*. Pergamon Press.
- Bassiouny, H. M., & Martin, H. (1984a). Flow distribution and pressure drop in plate heat exchangers - i. *Chemical Engineering Science*, *39*, 693–700.
- Bassiouny, H. M., & Martin, H. (1984b). Flow distribution and pressure drop in plate heat exchangers - ii. *Chemical Engineering Science*, *39*, 701–704.
- Bassiouny, H. M., & Martin, H. (1985). Temperature distribution in a four channel plate heat exchanger. *Heat Transfer Engineering*, *6*(2), 58–72.
- Cavallini, A. (2004). Properties of co2 as a refrigerant. In *European Seminar, Carbon Dioxide as a Refrigerant: Theoretical and Design Aspects. November*.
- Ciofalo, M. (2007). Local effects of longitudinal heat conduction in plate heat exchangers. *International Journal of Heat and Mass Transfer*, *50*, 3019–3025.
- Cleland, A. C. (1986). Computer subroutines for rapid evaluation of refrigerant thermodynamic properties. *International Journal of Refrigeration*, *9*(8), 346–351.
- Corbern, J., Gonzlvez, J., & Fuentes, D. (2005). Calculation of refrigerant properties by linear interpolation of bidimensional meshes. In *Proceedings of IIR International Conference of Thermophysical Properties and Transport Process of Refrigerants, August 31September 2, Vicenza, Italy*. IIR.
- Danish Ministry of the Environment (2002). Announcement of regulation of certain industrial greenhouse gases (in danish). Accession number: B20020055205.
- Ding, G. (2007). Recent development in simulation techniques for vapour-compression refrigeration systems. *International Journal of Refrigeration*, *30*, 1119–1133.
- Ding, G., Wu, Z., Liu, J., Inagaki, T., Wang, K., & Fuyaka, M. (2005). An implicit curve-fitting method for fast calculation of thermal properties of

REFERENCES

- pure and mixed refrigerants. *International Journal of Refrigeration*, 28, 921–932.
- Fenghour, A., Wakeman, W., & Vesovic, V. (1998). The Viscosity of Carbon Dioxide. *J.Phys. Chem. Ref. Data*, 27(1), 31–44.
- Garcia-Cascales, J., Vera-Garcia, F., Corberan-Salvador, J., & Gonzalvez-Macia, J. (2007). Assessment of boiling and condensation heat transfer correlations in the modeling of plate heat exchangers. *International Journal of Refrigeration*, 30, 1029–1041.
- Giroto, S., Minetto, S., & Neksa, P. (2004). Commercial refrigeration system using co2 as the refrigerant. *International Journal of Refrigeration*, 27(7), 717 – 723.
- Gut, J. A. W., & Pinto, J. M. (2003). Modeling of plate heat exchangers with generalized configurations. *International Journal of Heat and Mass Transfer*, 46, 2571–2585.
- Han, D., Lee, K., & Kim, Y. (2003a). The characteristics of condensation in brazed plate heat exchangers with different chevron angles. *Journal of the Korean Physical Society*.
- Han, D., Lee, K., & Kim, Y. (2003b). Experiments on characteristics of evaporation of r410a in brazed plate heat exchangers with different geometric configuration. *Applied Thermal Engineering*.
- Kaka, S., & Liu, H. (2002). *Heat exchangers: selection, rating, and thermal design*. CRC Press, second ed.
- Kauffeld, M., Harnisch, M. J., & Rhiemeier, J. M. (2008). Environmental impact of various alternative supermarket refrigeration systems. In *Proceedings of the 8th IIR-Gustav Lorentzen Conference on Natural Working Fluids*. IIR.
- Klaus, R. L., & van Ness, H. C. (1967). An extension of the spline fit technique and applications to thermodynamic data. *AIChE Journal*, 13(6), 1132–1136.
- Kowalczewski, J. (1966). Vapor slip in two phase fluid flow. *ASHRAE Transactions*, 72(1), 115–129.
- Lemmon, E., Huber, M., & McLinden, M. (2007). Refprop 8, nist reference fluid thermodynamic and transport properties. NIST Standard Reference Database 23.

REFERENCES

- Li, D., & Groll, A. (2005). Transcritical CO₂ refrigeration cycle with ejector-expansion device. *International Journal of refrigeration*, *28*, 766–773.
- Lorentzen, G. (1994). Revival of carbon dioxide as a refrigerant. *International Journal of Refrigeration*, *17*(5), 292–301.
- Lyytikäinen, M., Hamalainen, T., & Hamalainen, J. (2009). A fast modeling tool for plate heat exchangers based on depth-averaged equations. *International Journal of Heat and Mass Transfer*, *55*, 1132–1137.
- Martin, H. (1996). A theoretical approach to predict the performance of chevron-type plate heat exchangers. *Chemical Engineering and Processing*.
- Martin, J. J., & Hou, Y. (1955). Pressure-volume-temperature behavior of pure gases and liquids. *AIChE Journal*, *1*(2), 145–151.
- Nekså, P. (2002). CO₂ heat pump systems. *International Journal of Refrigeration*, *25*, 421–427.
- Nekså, P., Zakeri, G. R., Aarlien, R., & Jakobsen, A. (1998). Carbon dioxide as working fluid in air conditioning and heat pump systems. In *The Earth Technologies Forum 1998*. Washington DC, USA.
- Pearson, A. (2005). Carbon dioxide new uses for an old refrigerant. *International Journal of Refrigeration*, *28*, 1140–1148.
- Pfafferoth, T., & Schmitz, G. (2004). Modeling and transient simulation of CO₂-refrigeration systems with modelica. *International Journal of Refrigeration*.
- Pitzer, K. S., & Schreiber, D. R. (1988). Improving equation-of-state accuracy in the critical region; equations for carbon dioxide and neopentane as examples. *Fluid Phase Equilibria*, *41*, 1–17.
- Rathjen, W., & Straub, J. (1977). *Temperature dependence of surface tension, coexisting curve, and vapor pressure of CO₂, CClF₃, CBrF₃, and SF₆*, chap. 18. Academic Press.
- Richardson, D. (2006). *An Object Oriented Simulation Framework For Steady-State Analysis Of Vapor Compression Refrigeration Systems And Components*. Ph.D. thesis, University of Maryland, College Park.
- Rieberer, R. (1999). Co₂ properties. In *IIR Workshop on CO₂ Technology in Refrigeration, Heat Pump and Air Conditioning Systems*. IIR.

REFERENCES

- Sarkar, J., Bhattacharyya, S., & Gopal, M. (2006). Simulation of a transcritical CO₂ heat pump cycle for simultaneous cooling and heating applications. *International Journal of Refrigeration*, *29*, 735–743.
- Schittkowski, K. (1985). Nlpql: A fortran subroutine solving constrained nonlinear programming problems. *Annals of Operations Research*, *5*, 485–500.
- Skaugen, G., Neksa, P., & Pettersen, J. (2002). Simulation of transcritical CO₂ vapour compression systems. In *Proceedings of the 5th IIR-Gustav Lorentzen Conference on Natural Working Fluids*. IIR.
- Span, R., & Wagner, W. (1996). A new equation of state for carbon dioxide covering the fluid region from the triple-point temperature to 1100 K at pressures up to 800 MPa. *Journal of Physical and Chemical Reference Data*, *25*, 1509–1596.
- Stene, J., Jakobsen, A., Andresen, T., Skiple, T., & Neksa, P. (2007). CO₂ heat pump system for combined heating and cooling of non-residential buildings. In *Proceedings of International Congress of Refrigeration, Beijing*. International Institute of Refrigeration.
- Svensson, M. C. (1994). *Studies on on-line optimizing control, with application to a heat pump*. Ph.D. thesis, Norwegian Institute of Technology, Trondheim.
- UNEP (1987). Montreal protocol on substances that deplete the ozone layer. United Nations Environment Programme.
- UNEP (2006). 2006 report of the refrigeration, air conditioning and heat pumps technical options committee - assessment of montreal protocol on substances that deplete the ozone layer. United Nations Environment Programme.
- UNFCCC (1997). Kyoto protocol. United Nations Convention on Climate Change.
- Vesovic, V., Wakeham, W., Olchowky, G., Sengers, J., Watson, J., & Millat, J. (1990). The transport properties of carbon dioxide. *J. Phys.Chem.Ref.Data*, *19*(3), 763–808.
- Winkler, J., Aute, V., & Radermacher, R. (2008). Comprehensive investigation of numerical methods in simulating a steady-state vapor compression system. *International Journal of Refrigeration*, *31*, 930–942.

Appendix A

RESULTS FROM CSIM FUNCTION PROFILE PERFORMANCE TEST

This appendix contains the complete results from the CSIM function profile performance test. Conditions are as described in chapter 3.6, with the addition that an implementation of Span-Wagner using non-consistent auxiliary functions is also included in the comparison.

**APPENDIX A. RESULTS FROM CSIM FUNCTION PROFILE
PERFORMANCE TEST**

Satcalc	No. Calls	Span-Wagner w/auxiliary [s]	Consistent [s]	FTL [s]	Angus et al. w/auxiliary [s]
Equation of state					
$f_{sat}(T)$ and $f_{sat}(p)$	4 435 000	2800.89	3885.74	0.50	15.98
$f(T, p)$	1 750 000	153.88	153.68	0.67	31.28
$f(T, h)$	363 000	10.17	334.72	0.14	3.40
$f(h, p)$	149 000	645.01	639.35	0.20	14.84
$f(s, p)$	3 000	2.11	2.12	0.00	0.25
Transport data					
$\lambda(T, p), \mu(T, p)$	990 000	95.33	94.5	0.31	16.09
$\lambda_{sat}(T), \mu_{sat}(T), \sigma_{sat}(T)$	2 310 000	63.24	1092.96	0.23	16.42
SUM	10 000 000				

Total calc time [s]		3770.63	6203.07	2.05	98.26
Relative calc time to $TL_{Spancons}$		60.8%	100.0%	0.03%	1.58%
Relative calc time to $TL_{Angusaux}$		3837%	6313%	2.09%	100.00%

Appendix B

DESCRIPTION OF CSIM CASES USED FOR VALIDATION OF LOOKUP TABLE IMPLEMENTATION

This appendix contains a description of all test cases used for validation of the lookup table implementation. The same test cases were used to validate both accuracy and calculation speed.

For each case, a range of characteristics are listed, as well as a description of the state of the initial values used. For instance, if the initial value field is marked " $P_{high} = 80\text{bar}$ ", it means that initial values are for an identical circuit and configuration, only at 80 bar high side pressure.

By using initial values slightly off, a better representation of a real simulation situation is achieved. It is also an advantage to have a simulation use a few iterations in order to better distinguish the various thermo physical libraries with respect to simulation time and the choice of system balance or optimum solution.

**APPENDIX B. DESCRIPTION OF CSIM CASES USED FOR
VALIDATION OF LOOKUP TABLE IMPLEMENTATION**

B.1 Case 1

Description: A water-to-water heat pump simulation with plate-type heat exchangers. Decreasing high side pressure and increasing GC heat exchanger area.

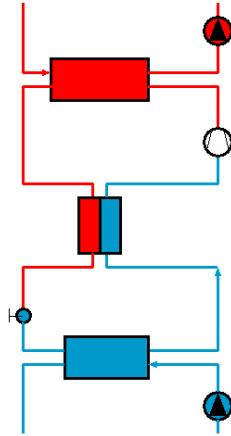


Figure B.1: Case 1 circuit layout

Table B.1: CSIM test case 1

Parameter	Value
Mode	Simulation
Gas cooler	Plate, 20 nsubhx
Evaporator	Plate, 48 nsubhx
Internal HX	Tube-in-tube, 5 nsubhx
Number of variables	153
P_{high} [bar]	85
T_0 [°C]	-0.9
EV outlet superheat/vapourfraction	1°C superheat
Heat sink inlet temp [°C]	25
Heat source inlet temp [°C]	8
Initial values	$P_{high} = 95$ bar 30% increase in GC HX area

**APPENDIX B. DESCRIPTION OF CSIM CASES USED FOR
VALIDATION OF LOOKUP TABLE IMPLEMENTATION**

B.2 Case 2

Description: A water-to-water heat pump with plate-type heat exchangers. Optimizing for max heating COP, with floating high side pressure and plate pitches in both EV and GC.

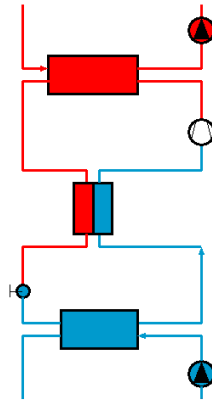


Figure B.2: Case 2 circuit layout

Table B.2: CSIM test case 2

Parameter	Value
Mode	Optimization
Extra optimization variables	P_{high} , CSA_{refr} for EV and GC
Optimization requirements	55kW heating capacity
Gas cooler	Plate, 28 nsubhx
Evaporator	Plate, 48 nsubhx
Internal HX	Tube-in-tube, 5 nsubhx
Number of variables	156
P_{high} [bar]	opt(93)
T_0 [°C]	-1.3
EV outlet superheat/vapourfraction	1°C superheat
Heat sink inlet temp [°C]	25
Heat source inlet temp [°C]	8
Initial values	$P_{high} = 100$ bar Fixed CSA for EV and GC No Q_{heat} requirement

**APPENDIX B. DESCRIPTION OF CSIM CASES USED FOR
VALIDATION OF LOOKUP TABLE IMPLEMENTATION**

B.3 Case 3

Description: Water-to-water heat pump, in a configuration that strifes very close to the critical point. As CO₂ is cooled in the gas cooler, the process passes about 0.06 bar over the critical point (calculated when the CO₂ temperature reaches the critical temperature).

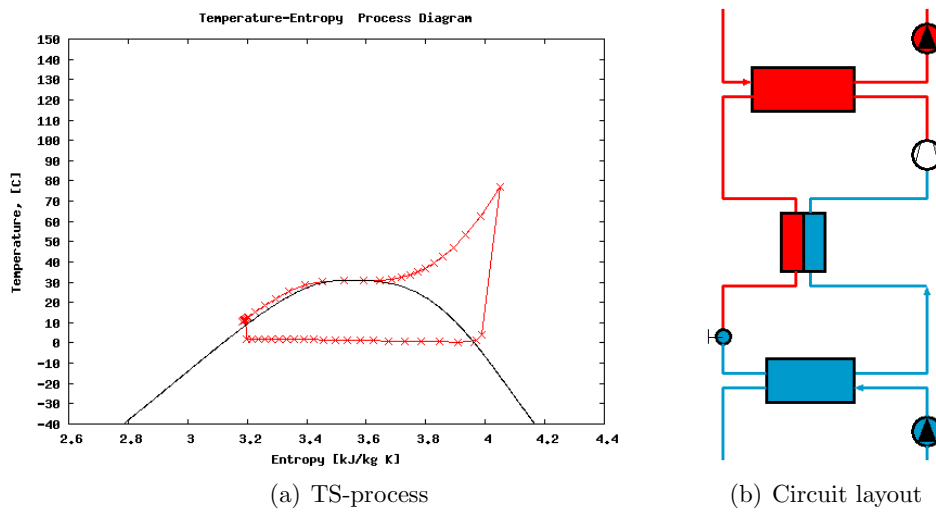


Figure B.3: CSIM test case 3, layout and TS-plot of process

Table B.3: CSIM test case 3

Parameter	Value
Mode	Simulation
Gas cooler	Tube-in-tube, 30 nsubhx
Evaporator	Tube-in-tube, 20 nsubhx
Internal HX	Tube-in-tube, 8 nsubhx
Number of variables	100
P_{high} [bar]	73.6
T_0 [°C]	0.27
EV outlet superheat/vapourfraction	1.0°C superheat
Heat sink inlet temp [°C]	5
Heat source inlet temp [°C]	12
Initial values	$P_{high} = 80\text{bar}$

**APPENDIX B. DESCRIPTION OF CSIM CASES USED FOR
VALIDATION OF LOOKUP TABLE IMPLEMENTATION**

Table B.4: CSIM test case 4

Parameter	Value
Mode	Optimization, 1 free
Optimization requirements	7000W cooling capacity
Gas cooler	Tube-in-fin, 22 nsubhx
Evaporator	Tube-in-fin, 12 nsubhx
Internal HX	Tube-in-tube, 10 nsubhx
Number of variables	90
P_{high} [bar]	opt(92)
T_0 [°C]	14.5
EV outlet superheat/vapourfraction	0.993 vaporfraction
Heat sink inlet temp [°C]	35
Heat source inlet temp [°C]	27
Initial values	$P_{high} = 105$ bar No Q_{cool} requirement

**APPENDIX B. DESCRIPTION OF CSIM CASES USED FOR
VALIDATION OF LOOKUP TABLE IMPLEMENTATION**

B.5 Case 5

Description: Air-to-air air conditioning unit with hot water heating. This case is an optimization at very high gas cooler pressure and temperature. The optimization temperature requirement is specified as a *minimum*, thus making it an un-equality constraint.

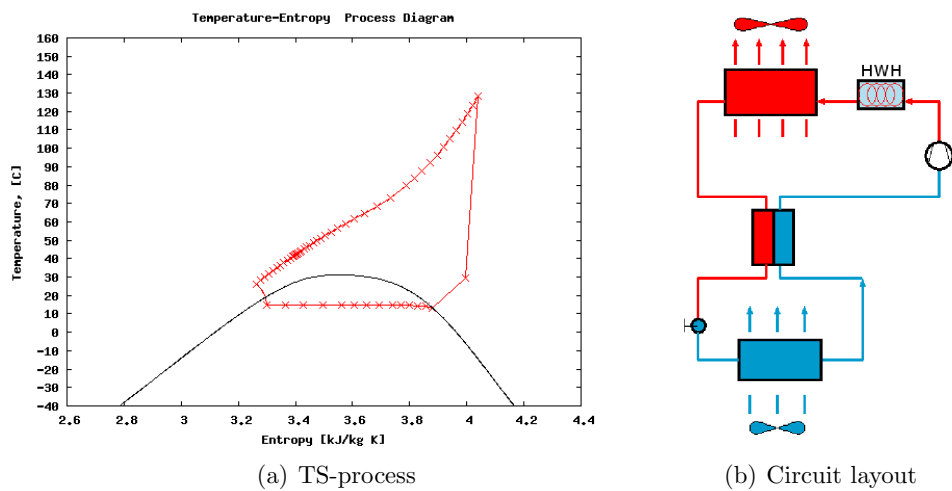


Figure B.5: CSIM test case 5, layout and TS-plot of process

**APPENDIX B. DESCRIPTION OF CSIM CASES USED FOR
VALIDATION OF LOOKUP TABLE IMPLEMENTATION**

Table B.5: CSIM test case 5

Parameter	Value
Mode	Optimization, 1 free
Optimization requirements	85°C hot water
Gas cooler	Tube-in-fin, 22 nsubhx
Evaporator	Tube-in-fin, 12 nsubhx
Internal HX	Tube-in-tube, 10 nsubhx
Number of variables	90
P_{high} [bar]	opt(137.6)
T_0 [°C]	14.4
EV outlet superheat/vapourfraction	0.975 vaporfraction
Heat sink inlet temp [°C]	40
Heat source inlet temp [°C]	27
Initial values	$Q_0 = 6500$ W (equals $P_{high} = 111$ bar) No hot water requirements

**APPENDIX B. DESCRIPTION OF CSIM CASES USED FOR
VALIDATION OF LOOKUP TABLE IMPLEMENTATION**

B.6 Case 6

Description: Water-to-water subcritical heat pump simulation. This case uses initial values for 65 bar and transfers to new solution at 60 bar.

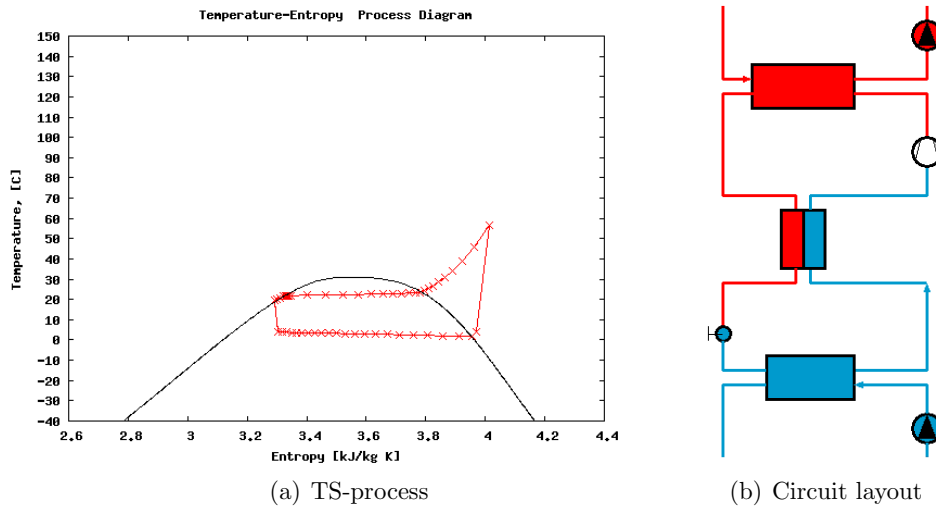


Figure B.6: CSIM test case 6, layout and TS-plot of process

Table B.6: CSIM test case 6

Parameter	Value
Mode	Simulation
Gas cooler	Tube-in-tube, 20 nsubhx
Evaporator	Tube-in-tube, 20 nsubhx
Internal HX	Tube-in-tube, 8 nsubhx
Number of variables	100
P_{high} [bar]	60
T_0 [°C]	1.9
EV outlet superheat/vapourfraction	0.95 vaporfraction
Heat sink inlet temp [°C]	5
Heat source inlet temp [°C]	12
Initial values	$P_{high} = 65$ bar

**APPENDIX B. DESCRIPTION OF CSIM CASES USED FOR
VALIDATION OF LOOKUP TABLE IMPLEMENTATION**

Appendix C

KEY SIMULATION RESULT VALUES FROM CSIM TEST SUITE

This appendix contains more output from CSIM test suite simulations.

**APPENDIX C. KEY SIMULATION RESULT VALUES FROM CSIM
TEST SUITE**

fileID	COP	\dot{Q}_{gc} [W]	\dot{Q}_{ev} [W]	\dot{W}_{co} [W]	\dot{m}_{co2} [kg/s]	$T_{sec,out}$ [C]	$T_{refr,out}$ [C]	$\Delta T_{gc,out}$ [C]	P_{high} [bar]	T_0 [C]	ΔP_{ev} [bar]	$CO_{T,out}$ [C]	CpuTime [s]
case1-TLSpan	3.46	49065	36101	14163	0.224	49.76	34.02	9.02	85	-0.94	0.06	103	1118.5
case2-TLSpan	3.74	54995	41388	14701	0.226	52.75	29.13	4.13	88.5	-1.69	0.21	102.9	1239.4
case3-TLSpan	4.8	194776	154914	40589	0.771	39.19	15.91	10.91	74	0.02	0.9	75.2	800.55
case4-TLSpan	3.63	8848	7000	1931	0.046	44.34	35.46	0.46	92.2	14.49	0.69	89	902.0
case5-TLSpan	2.25	5759	7025	3128	0.044	46.17	41.3	1.3	137.6	14.4	0.63	128.3	806.2
case6-TLSpan	5.37	169106	138184	31481	0.827	29.78	21.98	16.98	60	1.91	1.9	56.7	802.2
case1-FTL	3.47	49081	36116	14164	0.225	49.77	34.03	9.03	85	-0.9	0.06	102.9	2.45
case2-FTL	3.74	54995	41394	14694	0.227	52.75	29.16	4.16	88.5	-1.64	0.2	102.8	4.35
case3-FTL	4.81	194927	155085	40568	0.773	39.22	15.95	10.95	74	0.07	0.89	75.1	2.20
case4-FTL	3.63	8848	7000	1931	0.046	44.34	35.46	0.46	92.2	14.49	0.69	89	1.01
case5-FTL	2.25	5759	7025	3128	0.044	46.17	41.3	1.3	137.6	14.4	0.63	128.3	1.53
case6-FTL	5.37	168812	137949	31417	0.828	29.73	21.98	16.98	60	1.93	1.89	56.6	1.70
case1-TLAngus	3.41	49406	36166	14468	0.224	49.93	34.09	9.09	85	-0.95	0.06	104.6	29.44
case2-TLAngus	3.69	54995	41222	14891	0.226	52.75	29.41	4.41	87.8	-1.63	0.22	104	42.53
case3-TLAngus	4.77	195311	155115	40931	0.772	39.28	16.15	11.15	74	0.03	0.89	75.9	18.88
case4-TLAngus	3.55	8884	7000	1970	0.046	44.38	35.51	0.51	91.8	14.49	0.69	89.7	14.64
case5-TLAngus	2.22	5785	7018	3163	0.044	46.2	41.37	1.37	135.9	14.41	0.63	128.8	18.47
case6-TLAngus	5.34	168500	137519	31526	0.835	29.69	21.99	16.99	60	1.92	1.93	56	13.61